Design and validation of an ice adhesion set-up

Analysis of ice, surfaces and scatter

Ronan Connolly

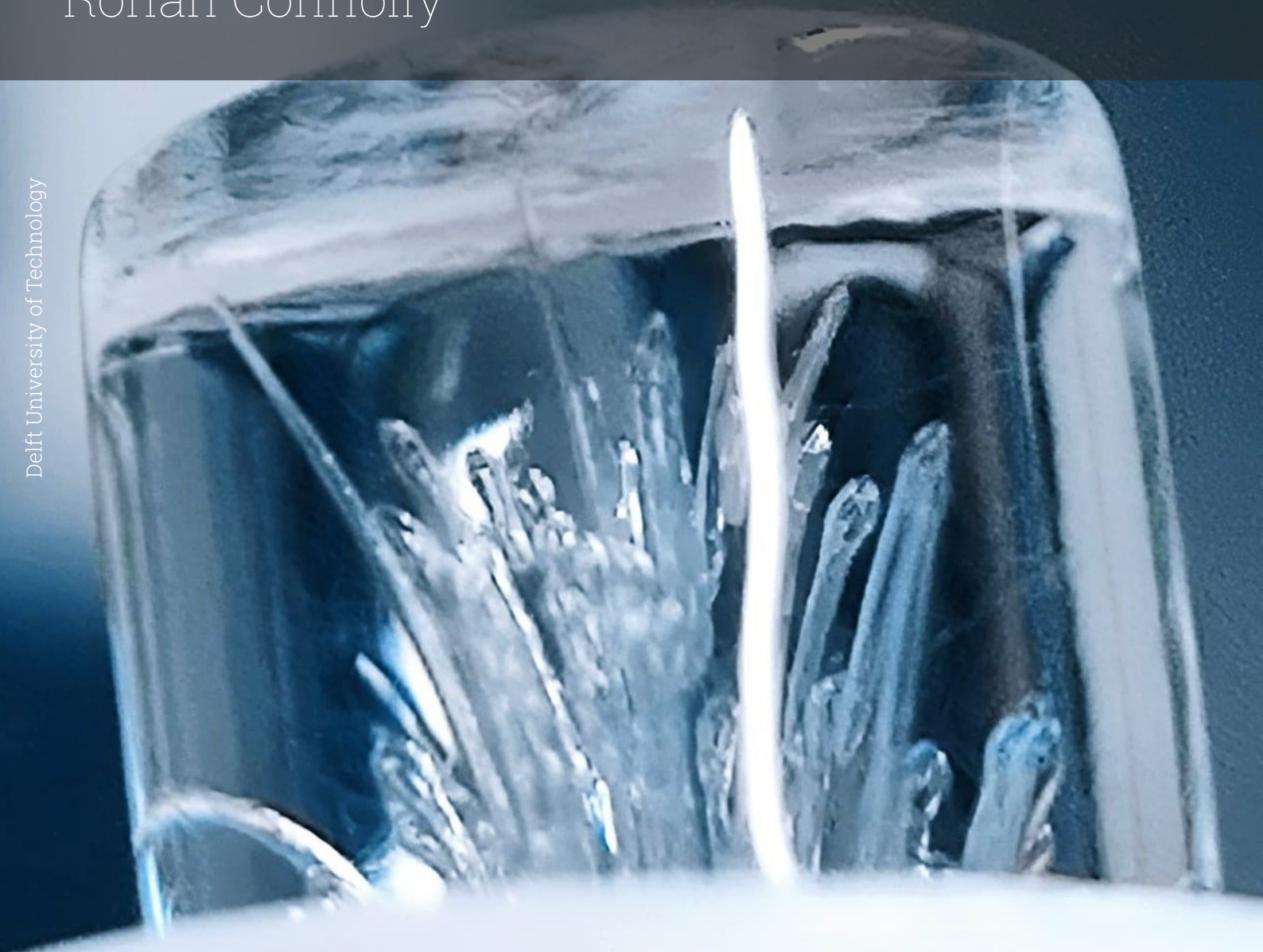

Delft University of Technology

TU Delft

Design and validation of an ice adhesion set-up

Analysis of ice, surfaces and scatter

by

Ronan Connolly

to obtain the degree of Master of Science in Aerospace Engineering,
at the Delft University of Technology,
to be defended publicly on Thursday March 21st, 2024 at 2:00 PM.

Supervisors:	Miisa J. Tavaststjerna	TU Delft, Aerospace Engineering
	Dr. Santiago J. Garcia Espallargas	TU Delft, Aerospace Engineering
Thesis committee:	Dr. ir. John-Alan Pascoe	TU Delft, Aerospace Engineering
	Dr. ir. Otto Bergsma	TU Delft, Aerospace Engineering

TU Delft

Acknowledgments

First and foremost, I would like to thank my family back home in Ireland, particularly my parents. Without your support, patience and love I would not be in the privileged position that I find myself in today. Thank you for always quietly encouraging me to aim as high as I could, and welcoming me home with open arms every time as if I had never left.

I would like to thank my daily supervisor Miisa, who has been a massive help to me in this project. I've really enjoyed the challenge of this project and getting to know you this past year or so, and your kind words and reassurances every time I thought my set-up was never going to materialize really helped me to push through. Thank you to Santiago, my main supervisor on this project, for providing the vision and encouragement for what's achievable in the scope of a masters thesis, and maybe at times for nudging me in the right direction when at times I felt was losing my way.

To all of the group at what was formerly NovAM, thank you for your help, feedback and encouragement which was available whenever I needed it. A big thanks goes to Dave and Alexander in the lab, and Ed and Rob at Demo for helping me to think through and implement all of the practical aspects of my design.

To my friends back in Ireland, especially Clíodhna and Tadhg, for pulling me through my bachelors at UCD, which allowed me to get to Delft in the first place. To the friends I've made in the Netherlands, especially Deniz, Zalán and Tom - you have made me feel at home here, and I will miss you dearly.

Lastly, a thank you to my girlfriend, Claire. Your unwavering love, support and laughter day-in, day-out have made taking the long way round that every bit easier - we got there in the end. It was a blast living here with you, and I can't wait to do it all again on our next adventure!

Ronan Connolly
March 2024, Delft

Abstract

Ice accumulation on aircraft surfaces is a prevalent issue, and passive anti-icing coating strategies can be implemented to assist in the removal of, or prevent the formation of, ice on an aircraft. Patterned anti-icing materials are an example of a novel strategy, where close control of the surface characteristics can lead to the ability to control and direct the ice-growth on a surface, or reduce the adhesion of the ice to the substrate. However, little is known regarding the effect of different novel materials and surfaces on ice adhesion strength, which is difficult to measure and quantify. Previous attempts at measuring and quantifying ice adhesion have typically led to high percentage standard deviations of σ = 15% to 40% and significant scatter in the data, due to variability in the approaches and the lack of standardisation in this field. Without a reliable and validated set-up which allows for analysis of results with confidence, reported values of ice adhesion strength for a novel coating will have little significance.

In this thesis, a robust and repeatable set-up for testing ice adhesion strength is designed, constructed, and validated. The set-up is specifically designed with validation as a priority and based on thorough research on other attempts at this problem, with the best elements of those designs integrated into an versatile horizontal shear set-up. With direct access to raw data and optimised testing parameters from a similar design with near identical conditions, the set-up was successfully validated with a percentage standard deviation with respect to the mean of σ = 11%. Additionally, each individual data point in the scatter can be cross referenced and analysed from various quantitative and quantitative data sources, which allows for the improved explanation of the results and outliers. In this work, the outliers provided interesting insights into ice adhesion and the sources of deviation in the set-up.

Using this set-up, it was possible to examine the relationships between various surface parameters and ice adhesion. The surface temperature and relative humidity were found to have a strong impact on the ice adhesion results. The ice adhesion failures can be categorised by their corresponding fracture surface, and in particular sorted by adhesive failure, cohesive failure, adhesive/cohesive mixed mode failure and sliding failure. For aluminium, adjusting surface characteristics such as grain direction and roughness did not have a significant effect on the ice adhesion results. For bare polymers samples such as polypropylene, polyvinyl chloride and Teflon, the ice adhesion mechanisms appear to be more significantly affected by surface chemistry as opposed to surface roughness. Failure of the ice substrate interface instantaneously in a stress dominated detachment was a common result, but slower toughness dominated detachment with crack propagation also occurred, despite the small interface length. To conclude, using this set-up is versatile, reliable method of analysing ice adhesion, and is an excellent platform for further research.

Contents

List of Figures

List of Tables

Nomenclature

Abbreviations

Abbreviation	Definition
PMMA	Polymethyl methacrylate
PVC	Polyviynl chloride
PP	Polypropylenene
SLIPS	Slippery liquid-infused porous surfaces
WCA	Water contact angle
DAQ	Data acquisition system
SEM	Scanning electron microscopy
Al	Aluminium
PDMS	Polydimethylsiloxane

Symbols

Symbol	Definition
θ	Contact angle
θ^*	Apparent contact angle
γ^{sv}	Solid surface free energy
γ^{lv}	Liquid surface free energy
γ^{sl}	Solid/liquid interface
r	Roughness factor
ΔG	Nucleation free energy barrier (condensation)
r*	Critical radius
$\sigma_l v$	Liquid-vapor surface energy
p	Vapour pressure
p_∞	Vapour pressure equilibrium
T	Temperature
n_l	Number of molecules per unit volume of liquid
k	Boltzmann constant
J	Nucleation rate (condensation)
t	Time
τ_{ave}	Average critical shear stress
τ_c	Critical shear stress
τ_{min}	Minimum shear stress
F	Force
A	Area
h	Ice pushing height
H	Ice column height
D	Ice mould diameter
Tg	Glass transition temperature
s	Probe speed
T_s	Surface Temperature
T_a	Air Temperature
t_f	Freeze time
σ	Standard deviation

Symbol	Definition
$\overline{x}$	Mean
N_v	Number of valid tests
S_a	Surface roughness

1

Introduction & Theory

Ice accretion on the surface of an aircraft is well established to have adverse affects both on flight performance and potentially the safety of the flight itself. Up until the 1980s, aircraft icing was deemed to be the cause of over 500 aviation accidents. Between 1982 and 2000 as volume of commercial flights increased, a further 583 airframe icing related accidents was reported in the U.S. alone, resulting in over 800 fatalities [1]. According to more recent analysis into the general aviation incidents from the last 15-20 years, it is clear aircraft icing is still a major external cause of accidents [2]. Icing can hinder and affect the safety of a flight in many ways. In terms of aerodynamics, airframe icing can lead to a loss of lift, increased drag and altered pressure distribution due to an unpredictable airflow pattern around airfoil surfaces. This has the potential to lead to accidents due to power stalls and subsequent loss of control. Critical instrumentation on aircraft can also be effected - ice accretion causing blockages in pitot static systems can produce errors in pressure instruments such as altimeters, airspeed indicators and vertical speed indicators [3].

There are many different strategies and techniques currently being developed to either prevent the ice formation on the aircraft surface in the first place (anti-icing), or to remove the ice which has built up by external means (de-icing). De-icing strategies such as mechanical vibration, pneumatic boots, and spraying of de-icing fluids are by nature a form of reactive maintenance, whilst anti-icing strategies such as permanent coatings are a form of preventative maintenance. Spraying of de-icing fluids such as propylene or ethelyne glycol to remove ice can be quite expensive, can have a severe environmental impact [4], and tally extra costs such as labor and equipment. Other approaches include fluid freeze point depressant systems and electrical/thermal heating systems. These methods often add extra weight and restrictive design requirements, making them difficult to implement into an efficient overall aircraft design. The development of anti-icing strategies, particularly those such as icephobic coatings which are passive as opposed to active, are therefore likely to be the future solution to the icing problem of this field in terms of sustainability and longevity. Icephobic coating strategies are passive in the sense that they do not require any extra energy or an active component within the coating itself to be effective once applied, and they are generally designed to prevent or delay ice growth, or significantly reduce the ice adhesion strength on the substrate. However, it is difficult to produce a passive anti-icing coating that repels ice formation and which is also durable and robust enough to survive the intense environmental conditions found during a flight cycle [4].

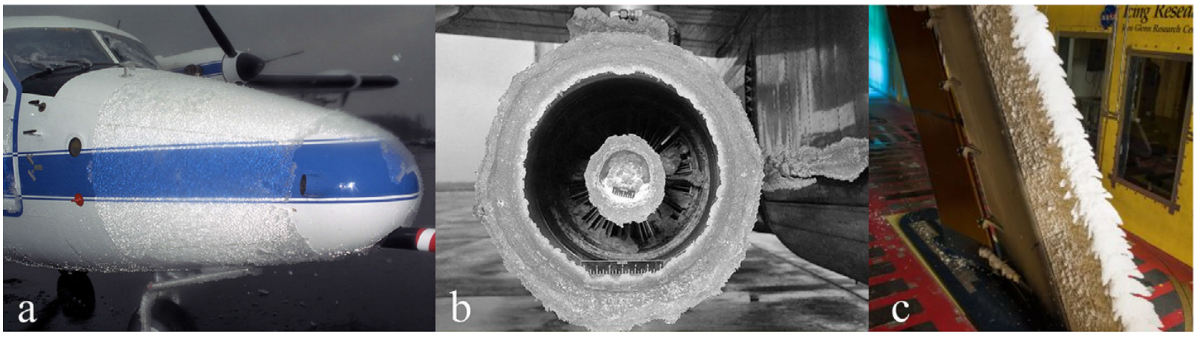

Figure 1.1: An example of hazardous icing accumulation on (a) aircraft fuselage, (b) engine inlet, (c) wing surface. Images supplied by NASA for Huang et al. [4].

The most popular methods to produce a passive 'icephobic' coating implement strategies which affect the wettability of a surface, the surface chemistry, or a combination of the two. These methods include strategies such as superhydrophobic topologies [5], slippery liquid infused porous surfaces (SLIPS) [6], and soft polymer surfaces [7], which all either reduce ice accretion and/or ice adhesion using different mechanisms. However, each of these methods have significant drawbacks, depending on the icing scenario. Novel strategies such as patterned coatings, have the potential to be very effective and not suffer from these same drawbacks, due to the different mechanisms by which they operate. Patterned coatings have shown to be able to control ice growth to some degree [8], in order to either prevent the formation of a thick ice-film, reduce ice adhesion, or keep parts of the surface dry.

However, testing the effectiveness of these coatings in a laboratory setting poses a significant challenge, due to difficulty in replicating and controlling the varied environmental conditions, and the sensitive nature of ice and low ice-adhesion coatings. Without a reliable method to test the existing coatings and surfaces and to compare them consistently against one and other, the development of new icephobic strategies is hindered. The most quantifiable and straightforward metric to compare coatings is an icing scenario is to test the ice adhesion strength of the coating. However, there is no standardized testing in this field, leading to an abundance of different attempts at the same issue, with varying degrees of success [9]. In this masters thesis, the objective will be to tackle this challenge by developing a home-built ice adhesion test-up. This project will be thoroughly researched, and the purpose and desired outcome of the testing will be reflected in the design methodology, with special consideration for validation of the set-up once built. From there, the results of testing will be analysed in order to compare various materials in terms of ice adhesion.

1.1. Icing and Surfaces

In this chapter, the physical characteristics of liquid-solid interactions and ice formation will be introduced, before further discussion on the merits and typical pitfalls of passive icephobic coatings. The focus will then shift to ice adhesion testing and ice adhesion mechanics, before finishing with a general discussion and a note on the overall scope and research objectives of this thesis.

1.1.1. Liquid-solid interactions

The physics of liquid-solid interactions were first modelled by Thomas Young in 1805 [10], and the primary term used to define this interaction is wettability. Wettability can be described as the ability of a liquid to maintain contact with a solid surface, and it is a balance between cohesive and adhesive forces at the interface. The degree of wettability is defined by the amount of surface free energy, and the surface roughness. It should be noted that the assumptions of this model were that the surface being wetted was completely smooth, flat, and isotropic. The contact angle, θ, is measure of the angle formed between the between the solid/liquid interface and the liquid/vapor interface, assuming stability of the gas, liquid and solid phases. Young's equation represents the surface energy equilibrium between the three phases in the system - solid surface free energy, γ^{sv}, liquid surface free energy, γ^{lv}, and solid/liquid interface γ^{sl}, - as tangents to the interfaces, as illustrated in Figure 1.2 below

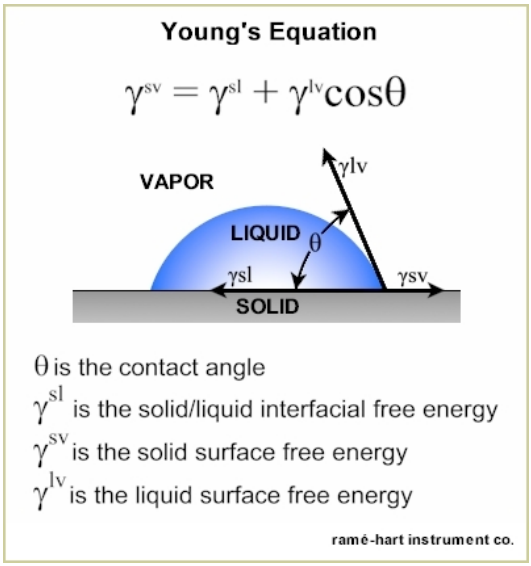

Figure 1.2: Young's Equation [11].

From Young's equation, parameters for hydrophilicity and hydrophobicity were defined. A contact angle of 0° indicates that a droplet will spread completely over the surface, remaining hydrophilic under 90°. A contact angle between 90° - 180° can be described as hydrophobic - the surface will be partially to fully wetted, with the droplet theoretically becoming spherical at 180°. A contact angle over 150° can be described as superhydrophobic. However, Young's model did not take into the account the reality of rough surfaces, and the significant effect surface topology has on liquid-solid interaction. Wenzel developed Young's Equation further, introducing an apparent contact angle θ^* and roughness factor r, to account for the roughness of a non-ideal surface. The roughness factor is the ratio between the area of the actual surface and the area of a smooth surface with the same shape and dimensions [12]. The relationship is as follows:

$$cos\ \theta^* = r\ cos\ \theta \tag{1.1}$$

The assumption in this case is that the liquid droplet completely penetrates the rough area as shown in Figure 1.3. It was found through experimentation that under hydrophilic conditions, the apparent contact angle θ^* decreases with the increased roughness of the surface, and the hydrophilicity increases. However, under hydrophobic conditions, the apparent contact angle increases with surface roughness, and surface becomes more hydrophobic. This model directly correlates the effect that roughness has on the wettability of the surface.

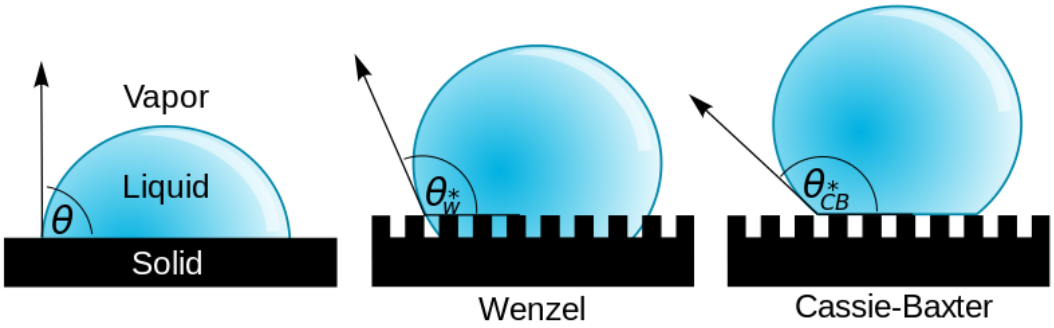

Figure 1.3: The fundamental models of surface wettability [13].

The Cassie-Baxter Model takes into account other instances of wettability that the Wenzel model cannot fully explain. Wetting phenomena such as the naturally superhydrophobic lotus leaf surfaces do not fit into the Wenzel's modification of Young's equation for rough surfaces. For example, according to Wenzel's model in order to achieve apparent contact angles over 150°, an extremely rough surface would be required when in reality this isn't true in the case of the lotus Leaf. Therefore, Cassie and Baxter modelled the additional effect of the air entrapped in the structure as a result of the increasing roughness using a composite phase concept. It takes into account both the solid-liquid contact interface and the gas-liquid contact interface. The relationship between the apparent contact angle and these interfaces are as follows:

$$cos\ \theta^* = f_1\ cos\ \theta_1 + f_2\ cos\ \theta_2 \tag{1.2}$$

θ_1 and θ_2 are the contact angles of the liquid droplet on the solid and gas respectively, whilst f_1 and f_2 are the percentage of the solid-liquid area and the gas-liquid area respectively. As one of the components is air, the contact angle θ_2 is equal to 180°. The equation becomes:

$$cos\ \theta^* = f_1\ cos\ \theta_1 + f_1 - 1 \tag{1.3}$$

This equation explains superhydrophobic non-wetting surfaces, as it implies that surfaces with a low percentage of solid-liquid area and a high contact angle, can have a very high apparent contact angle. The air-pockets which are trapped beneath the surface are essentially suspending the liquid droplet on the top of the surface, and it is unable to wet the surface and spread further, as illustrated in Figure 1.3

To summarize, hydrophobicity and hydrophilicity are defined by the contact angle, which is heavily influenced by the surface topology. The Wenzel model observes increasing hydrophobicity by increasing the contact area (roughness) up to an apparent contact angle of 150°. The Cassie-Baxter model is reliant on a specific surface structure with composite interface contact, which traps air pockets beneath the surface and repels the water due to the low solid-liquid contact area. It is apparent that the Wenzel model is more relevant when the rough surface has a microscale structure, and the Cassie-Baxter Model of a composite contact nature becomes more suitable as the surface gets closer to a nanoscale structure [14]. Now that the basics of liquid-solid interaction have been outlined, the progression from condensation frosting to ice accretion can be studied.

1.1.2. Types of icing

Aircraft icing is often classified into three types - rime ice, glaze ice and mixed ice. Rime ice is typically formed at temperatures where there is a low liquid water content, and is the result of smaller supercooled water droplets striking the aircraft surface and freezing immediately, building a hemispherical icing shape on the wing surface over time. These supercooled droplets are typically found in the cloud formations that a commercial aircraft may encounter whilst operating at high altitudes, and ice can form when an aircraft strikes through a cloud, usually in the temperature range of -20°C and -40°C [2]. In this process the supercooled water droplets hit the aircraft surface, where the phase transition occurs and creates high adhesion to the substrate. Supercooled water droplets have a tendency to be very unstable, and are easily dispersed under a strong airflow. Therefore, when an aircraft flies through a supercooled region of cloud, the water droplets strike the surface of the aircraft, breaking and spreading along the surface. The surface curvature of the water droplet is suddenly decreased, rapidly reducing the liquid water pressure and therefore the temperature decreases and the relative freezing point is increased [14]. Supercooled water droplets freeze rapidly when they come into contact with the aircraft surface.

Glaze ice is formed at slightly higher temperatures above -10°C, with larger water droplets and higher liquid water content [2]. As a result, the droplets do not freeze immediately, and flow along the surface of the wing until they do. This results in a dense layer of ice in irregular shapes, with high adhesion to the substrate. In many cases, the icing conditions found in reality are a mixture of these two icing types, leading to the classification of mixed ice. Mixed ice will have the characteristics of both rime and glaze ice, owing to the varying sizes of supercooled water droplets and degree of liquid water content in flight conditions. Cao et. al [2] discusses the detrimental effects of aircraft icing in greater

detail, along with exploring the effect of the various environmental and aircraft related conditions that contribute to ice accretion in flight.

However, these icing types are not the only that are defined, and nor are the descriptions from various sources exactly agreed upon. For example, glaze ice which is described in power lining icing or affecting marine applications phenomenon may not be comparable to glaze ice for aircraft applications, and even from study to study in aviation the definition may be different [15]. This is highlighted by the study Rønneberg et al. discussing the needs for standardization in this field, by the table plethora of similar icing types with differing descriptions which is reproduced in Figure 1.4. For the purposes of this thesis, the classifications proposed by Rønneberg et al. will be followed to avoid introducing extra definitions where it is not necessary.

An important classification can be made between impact ice and non-impact ice when considering ice adhesion testing, as the method for the ice generation will need to be considered. Impact ice and non-impact ice are inherently different, as impact ice can be defined as having a non-zero initial velocity at impact [9], which is akin to how supercooled water droplets from a cloud strike a surface during flight. This icing type would be the the most realistic to test, however perhaps the most logistically challenging, due to the requirements of a wind tunnel and the difficultly in quantify the adhesion mechanics when scraping a layered ice film [16]. Non-impact ice is a static ice, often also described as bulk ice, which is operationally much easier to test and control. This is typically generated using moulds, where the water is injected and frozen onto a chilled substrate [17–19]. An alternative ice generation technique which sits somewhere between the other two is employed by the Anti-icing Materials International Laboratory in Canada, where precipitation ice in generated on a centrifugal ice adhesion set-up using a spray nozzle [20]. This is best described as a freezing drizzle, and is classified as impact ice, albeit at a much slower impact velocity.

Figure 1.4: Table of ice types, reproduced from study by Rønneberg et al., relevant references can be found here: [21]

Ice type	Definition	References
Atmospheric icing	Any process of ice build-up and snow accretion on the surface of an object exposed to the atmosphere (ISO 12494)	CIGRE TB 631 [27]
Bulk water ice	Water frozen in freezer or on a Peltier plate at constant temperature, which may vary from freezer to freezer. Results in a clear and mostly bubble-free ice	Rønneberg et al. [54]
Dry snow	A type of precipitation icing that accretes at subfreezing temperatures. Low density and low adhesion, and appears rarely when wind speed is below 2 ms^{-1}	CIGRE TB 631 [27]
Freezing drizzle	Water droplets that freeze on impact with the ground or with objects on the earth's surface or with aircraft in flight	Armstrong et al. [59]
Freezing rain	A type of precipitation icing that falls in liquid form but freezes on impact to form a coating of glaze ice upon the ground and on exposed objects	CIGRE TB 631 [27]
Glaze	A generally homogeneous and transparent deposit of ice formed by the freezing of supercooled drizzle droplets or raindrops on objects the surface temperature of which is below of slightly above 0°C. It may also be produced by the freezing of non-supercooled drizzle droplets or raindrops immediately after impact with surfaces the temperature of which is well below 0 °C	Armstrong et al. [59]
Glaze ice	Temperatures over −10 °C, freeze from water film after droplets have spread out. Has the highest possible ice density	Fortin and Perron [60]
Glaze ice	Hard, bubble-free and clear ice, generated under wet growth conditions and where surface temperature is above 0 °C	Makkonen [61]
Glaze ice	Ice frozen in silicone mold at −5 °C for 24 h, resulting in a smooth clear structure. Ice that does not freeze on impact on aircrafts	Janjua et al. [52]
Glaze ice	A type of precipitation icing resulting in transparent ice accretion of density 700–900 kg m^{-3}, sometimes with the presence of icicles under the conductors. It very strongly adheres to objects, and is difficult to knock off	CIGRE TB 631 [27]
Glaze ice	Ice formed under glaze conditions, where the impinging droplets form a liquid film that freezes to form the ice. Latent heat release from formation is not sufficient to completely freeze the water on impact	Work et al. [62]
Hoarfrost	A deposit of ice having a crystalline appearance, generally assuming the form of scales, needles, feathers, or fans; produced in a manner similar to dew but at temperatures below 0 °C	Armstrong et al. [59]
In-cloud ice	Spraying supercooled micro droplets of MVD 27 μm and LWC 2.5 gm^{-3} in a wind tunnel of wind speed typically 15 ms^{-1} at temperatures of −10 °C	Rønneberg et al. [54]
Precipitation icing	A type of atmospheric icing which is caused by rain droplets or snowflakes that freeze or stick to the icing body	CIGRE TB 631 [27]
Precipitation ice	Supercooled droplets of MVD 324 μm as precipitation in a cold room with temperature typically −10° C, impact velocity calculated to 5.6 ms^{-1}	Rønneberg et al. [54]
Rime	A deposit of ice composed of grains more or less separated by trapped air, sometimes adorned with crystalline branches, produced by the rapid freezing of supercooled and very small water droplets	Armstrong et al. [59]
Rime icing/ in-cloud icing	A porous, opaque ice deposit which is formed by the impaction and freezing of supercooled water droplets on a substrate. The density of rime can vary from 150 to 700 kg m^{-3}	CIGRE TB 631 [27]
Wet snow	A type of precipitation icing which is observed when the air temperature is just above freezing point, usually between 0.5°C and 2°C	CIGRE TB 631 [27]

Figure 1.5: Table of ice categorised by ice type and density, reproduced from study by Rønneberg et al., relevant references can be found here: [21]

Category	Description	Density ρ (average) (g cm^{-3})
Clear ice	Virtually no air entrapped	>0.86 (0.906)
Transparent ice	Moderate amounts of air entrapped in fairly large bubbles	>0.86 (0.906)
Milky ice	Considerable amounts of air enclosed as small bubbles	>0.80 (0.876)
Opaque rime	Dull and white, crumbles rather than cracks	0.40–0.90
Kernel rime	Similar in appearance to kernels of corn on a cob	0.33–0.61
Feathery rime	More open and fragile than kernel rime	0.08–0.40

The top three ices are in the glaze family, while the bottom three are in the rime family.

1.1.3. Condensation frosting phenomena

Condensation frosting is a prominent pathway for ice formation, and until relatively recently this phenomenon was assumed to have similar physics to direct ice formation, where supercooled droplets are frozen spontaneously due to heterogeneous nucleation at the solid-liquid interface [22]. However, in the case of condensation frosting for hydrophobic and slightly hydrophilic surfaces, the underlying mechanisms and physics for frost growth and ice growth are fundamentally different, and revolve around characteristics such as interdroplet ice bridging, frost halos and dry zones [23]. Controlling the development of frost formation by preventing condensation with patterned coatings is a viable strategy for anti-icing [8, 24], and the understanding of this mechanism begins with exploring what drives condensation and subsequent frosting.

In order for condensation frosting to take place, heterogeneous nucleation of water must occur on a substrate where the bulk temperature is below the dew point. The dew point temperature is defined as the saturation temperature corresponding to the partial pressure of ambient water vapour [23]. Heterogeneous nucleation of water refers to the phase transition from supersaturated water vapor to the nucleation of a water droplet, which is facilitated by an external surface [25]. In the case of homogeneous nucleation, the water droplet nucleates in the bulk as opposed to the surface, so this is less relevant when observing liquid-solid interactions. According to classic nucleation theory, Heterogeneous nucleation occurs when there is a shift in thermodynamic equilibrium. Volmer et al. [26] proposed that the free energy barrier ΔG for the formation of a liquid nucleus on a flat surface is dependent on the wettability of the surface via the contact angle θ, the critical radius r* and the liquid-vapor surface energy, $\sigma_l v$.

$$\Delta G = \pi \sigma_l v r^* (2 - 3cos\theta + cos^3\theta)/3 \tag{1.4}$$

The critical radius is derived from Kelvin's classical equation, which is given by

$$ln(p/p_\infty) = 2\sigma_l v / n_l k T r^* \tag{1.5}$$

where p is the vapour pressure over a curved interface of radius $r*$, p_∞ is the vapour pressure equilibrium above a flat surface at temperature T, n_l is the number of molecules per unit volume of liquid, and k is the Boltzmann constant [27]. The nucleation rate J, is very much dependent on the wettability of the surface, due to its inverse exponential relationship with ΔG.

$$J = J_o exp(-\Delta G/kT) = J_o exp[\pi \sigma_l v r^* (2 - 3cos\theta + cos^3\theta)/3kT] \tag{1.6}$$

As discussed by Varanasi et al., this implies that a surface with spatially uniform intrinsic wettability will experience heterogeneous nucleation as a random process, with no preference for one area over another. This phenomenon can also account for the loss of hydrophobic properties on naturally hydrophobic surfaces such as lotus leaves when exposed to condensation [27]. Similarly in freezing conditions, a hydrophobic surface will experience frost formation and growth leading to ice formation. The effects of random frost nucleation on a hydrophobic surface are illustrated in Figure 1.6.

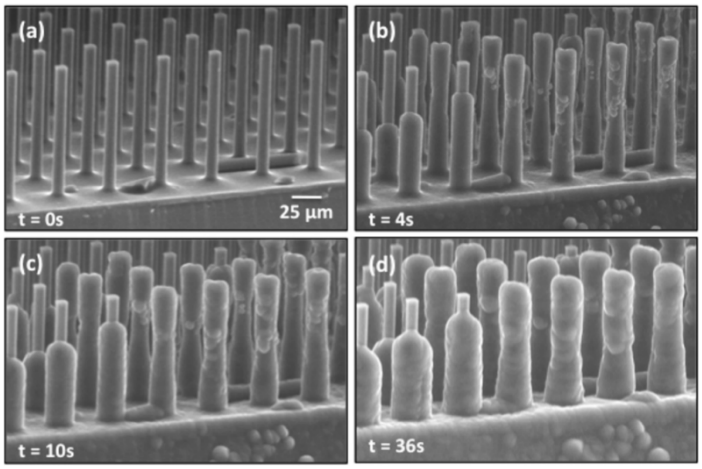

Figure 1.6: ESEM images of frost formation on a superhydrophobic surface comprising of an array of hydrophobic square posts with width, edge-to-edge spacing, and aspect ratio of 15 μm, 30 μm, and 7 μm, respectively. (a) Dry surface. [b–d] Snapshot images of frost formation on the surface.The intrinsic water contact angle of the hydrophobic coating on the posts is 110°. Frost nucleation and growth occurs without any particular spatial preference due to uniform intrinsic wettability of the surface [28].

In the past, superhydrophobic surfaces modelled on lotus leaf structures had been presented as a method of reducing ice adhesion [29], due to their innate ability to repel water and therefore delay ice formation. Lotus leaves are naturally superhydrophobic, but when exposed to condensation conditions they experience random heterogeneous nucleation of water droplets. The surface roughness, in particular the pitch distance between the individual lotus 'fibres', can often be bigger than the critical radius r^*. Therefore, water droplets in this case begin to nucleate inside the rough topology, nullifying the feature which is providing the superhydrophobic effect. In the case of freezing conditions, the superhydrophobicsurface begins to accumulate ice across the rough surface due to the freezing of the condensation droplets. The pitfalls of this method were outlined by Chen et al. [30], where it was found that superhydrophobicsurfaces in fact tended to increase ice adhesion compared to hydrophilic surfaces over several freezing cycles, due to mechanical interlocking on the textured surface. In certain experiments it has been shown that well-designed superhydrophobicsurface can suspend supercooled condensate in a Cassie state [31], however such finely coated nanotextures are likely too fragile for aerospace applications.

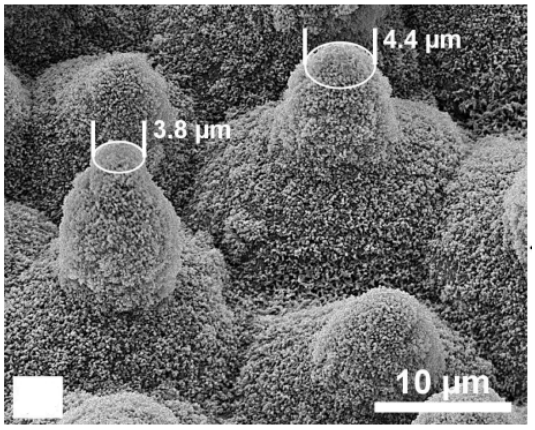

Figure 1.7: SEM image of lotus leaf papillae structure covered with wax tubles, two properties which make the leaf superhydrophobic. Under condensation frosting conditions, water droplets can nucleate and freeze, nullifying the superhydrophobiceffect [32].

The key takeaway from these studies is that spatial control in the heterogeneous nucleation of water is possible, by manipulating the wettability of the substrate beneath. The energy barrier for nucleation

increases with increasing contact angle, which implies that nucleating water droplets will preferentially settle on a hydrophilic surface in a hydrophobic-hydrophilic patterned surface, due to the lower ΔG and higher J value. The large contrast in nucleation rate and nucleation energy barrier values in the hydrophilic and hydrophobic phases highlights the potential to achieve spatial control through surface patterning. If spatial control is achieved, ice growth should become more predictable as the patterning parameters will directly influence the preferential areas of ice formation on a surface. This could an incredibly powerful tool, as specific patterns could potentially be used to reduce overall ice adhesion.

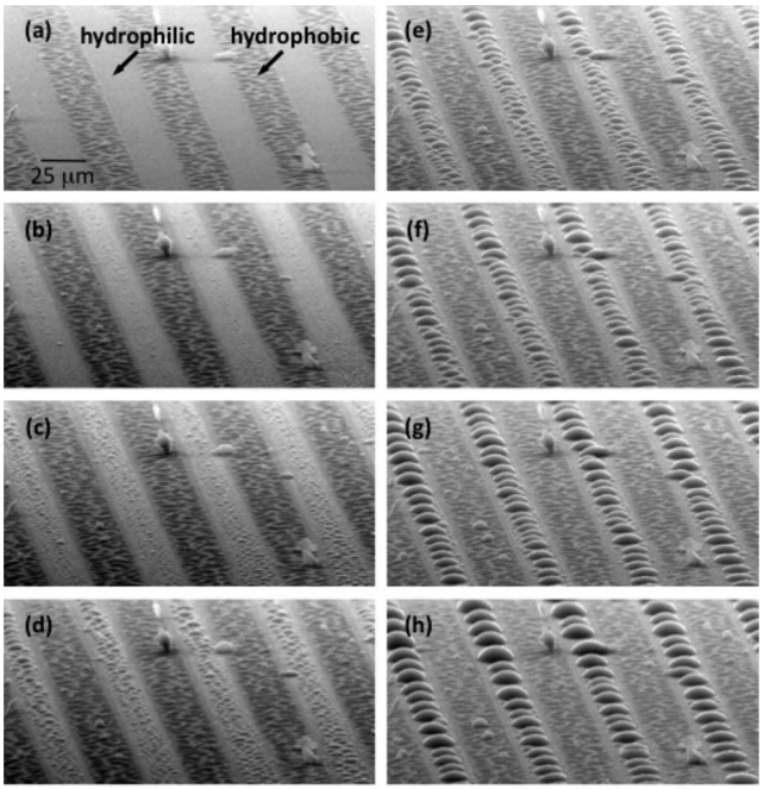

Figure 1.8: Condensation of water vapour on surface with alternating hydrophilic and hydrophobic segments (size 25μm). Approximate contact angle of hydrophobic,hydrophilic regions respectively: 110°, 25°. (a) is the dry surface, (b)-(h) is the preferential condensation phenomenon over time. [27]

Once heterogeneous nucleation of water has occurred on a substrate, the supercooled water droplets will continue to grow from the vapor present. This growth is initially in isolation, and as the droplets are spaced out sufficiently, the pressure gradient about each droplet does not overlap. As the distance decreases between droplets due to the individual droplets growing in diameter, the pressure profiles for each droplet now begin to overlap [23]. Soon the droplet coverage of the substrate can be treated as a homogeneous film, as opposed to individual droplets. The pressure gradients about condensate droplets and their interaction with one another have a significant effect on the aforementioned mechanisms of condensation frosting, namely interdroplet ice bridging, frost halos and dry zones. These mechanisms will now be discussed in more detail considering a case of condensation on a chilled substrate, in order to understand how one could potentially utilize these phenomena when creating patterned surfaces.

Frost halos: The first feature of condensation frosting on a chilled substrate to consider are frost halos. Frost halos occur as a result of recalescence during the onset of freezing, which is a temporary increase in temperature of a supercooled water droplet. This results in a change in pressure at the ice interface as the droplet begins to freeze, and a release of vapor from the ice interface which deposits in a ring or halo pattern around the droplet [23]. These droplets quickly freeze, leading to a frost halo such as those pictured in Figure 1.9.

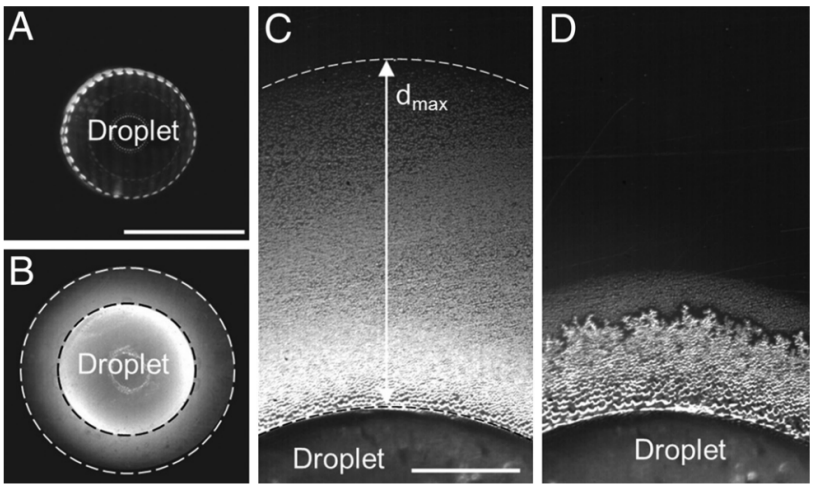

Figure 1.9: Optical microscope images of a condensation halo around a freezing 5-µl droplet on PMMA[33]. (A) Water droplet in supercooled liquid state. (B) Condensation halo during freezing. (C) Magnified region of condensate. d_max indicates maximum expanse of halo. (D) Partial freezing of condensate halo.

Interdroplet Ice Bridging: The chilled substrate in question is now populated with supercooled droplets. When a single droplet freezes due to heterogeneous nucleation at the solid-liquid interface, this will trigger interdroplet condensation frosting, whereby the freezing supercooled droplets interact with each other and influence the surface phenomena [34]. Interdroplet ice bridging, which in turn creates dry zones, occurs as a result of the droplets freezing and exhibiting localized humidity sink behavior because of localized vapor pressure gradients now in the system [23]. This localized pressure drop due to the freezing droplet coming into temperature equilibrium with the chilled substrate has an immediate effect, evaporating condensate droplets in the annular vicinity of the now frozen droplet [33, 35]. If there is no condensation halo present around the frozen droplet, the droplet will begin to harvest water from neighboring droplets. When the harvested water which has evaporated from another droplet, comes into contact with the frozen droplet, the vapor freezes, growing ice bridges toward the affected water droplet and other neighboring droplets. When neighboring droplets freeze, they in turn behave as localized humidity sinks, and the process repeats. This phenomenon was first reported by J. B. Dooley in 2010 [36]. The initial probabilistic freezing event is described as a trigger, because of the chain reaction which ensues and the network of interconnected of ice bridges which are formed.

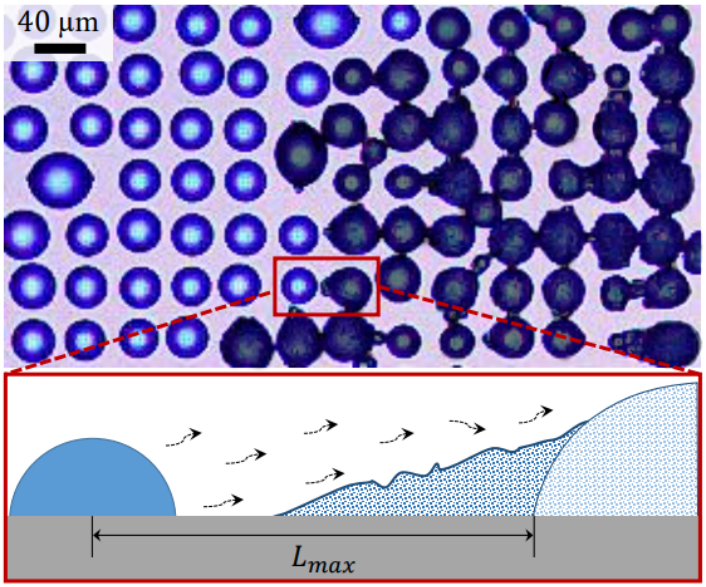

Figure 1.10: Frost percolating across a supercooled (-10°C) condensate population, frozen droplets and connecting ice bridges are colored false-black. Inset with red outline: Illustration of the diffusive vapor exchange between a frozen droplet and a liquid droplet, leading to the formation of an interdroplet ice bridge [37].

Dry Zones: In the scenario above, there is no guarantee that the frozen droplet which is harvesting water vapor from nearby droplets will connect with the droplet via an ice bridge. If the there is sufficient distance between both the frozen droplet and liquid droplet, the liquid droplet may evaporate fully before that ice bridged connection is made. This halts the network of interdroplet ice bridges. If there is a series of liquid droplets which are outside the critical distance required to form an ice bridge, a stable dry zone can form around the frozen droplet [23]. Examples of dry zone formation can be seen in Figure 1.12. Nath et al. found that for droplet sizes in the range of 1µm - 10µm on a superchilled substrate, the criterion for an ice-bridge connection to a neighboring droplet were primarily dependent on the droplet size, the interdroplet distance and the ratio of sizes for the the liquid and frozen droplets [37]. The formation of dry zones by creating scenarios where interdroplet ice bridging fails in condensation frosting conditions, have the potential to slow the progress of global freeze fronts depending on the surface conditions. Therefore, by manipulating the surface characteristics such as wettability, to achieve spatial control in different regions through surface patterning, one can expect that the kinetics of interdroplet ice bridging and dry zone formation can be somewhat controlled.

As mentioned, the initial freezing event will lead to the formation a network of interconnected ice bridges, which percolates globally in a freeze front. This provides the platform for out-of plane frost growth and further frost densification, leading to a easy platform for ice accumulation. As outlined in the introduction and shown in Figure 1.1, significant ice accumulation can be harmful in many engineering applications. A illustrative summary of the condensation frosting process and mechanisms is shown in Figure 1.13.

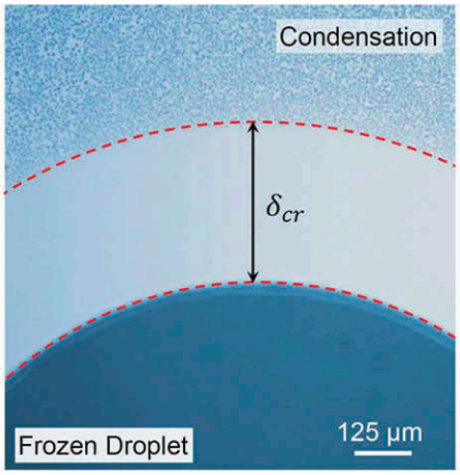

Figure 1.11: Dry zone formation surrounding a frozen droplet. [38]

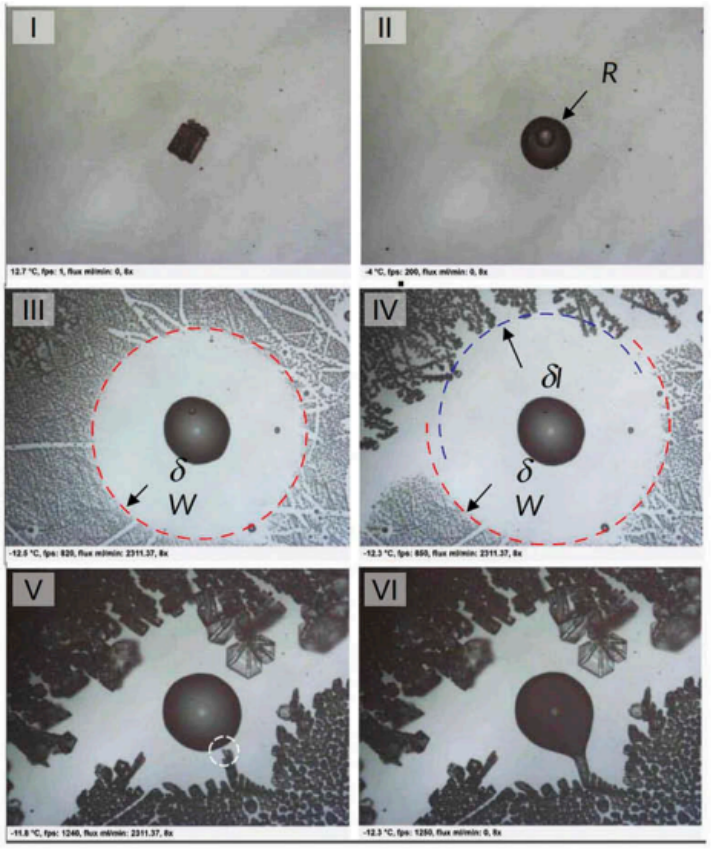

Figure 1.12: Salty water droplet exhibiting dry zone formation during condensation frosting (I) Salt crystal just after deposition (t = 0). (II) Partial crystal dissolution, (t = 8 s). (III) Condensation under humid air (t = 30 s). Ice is beginning to percolate from top left corner. (IV) Dry zone formation, halting ice percolation. (V)-(VI) Ice dendrite hits the drop. When hit, the salty drop immediately freezes and forms an ice bridge .[39].

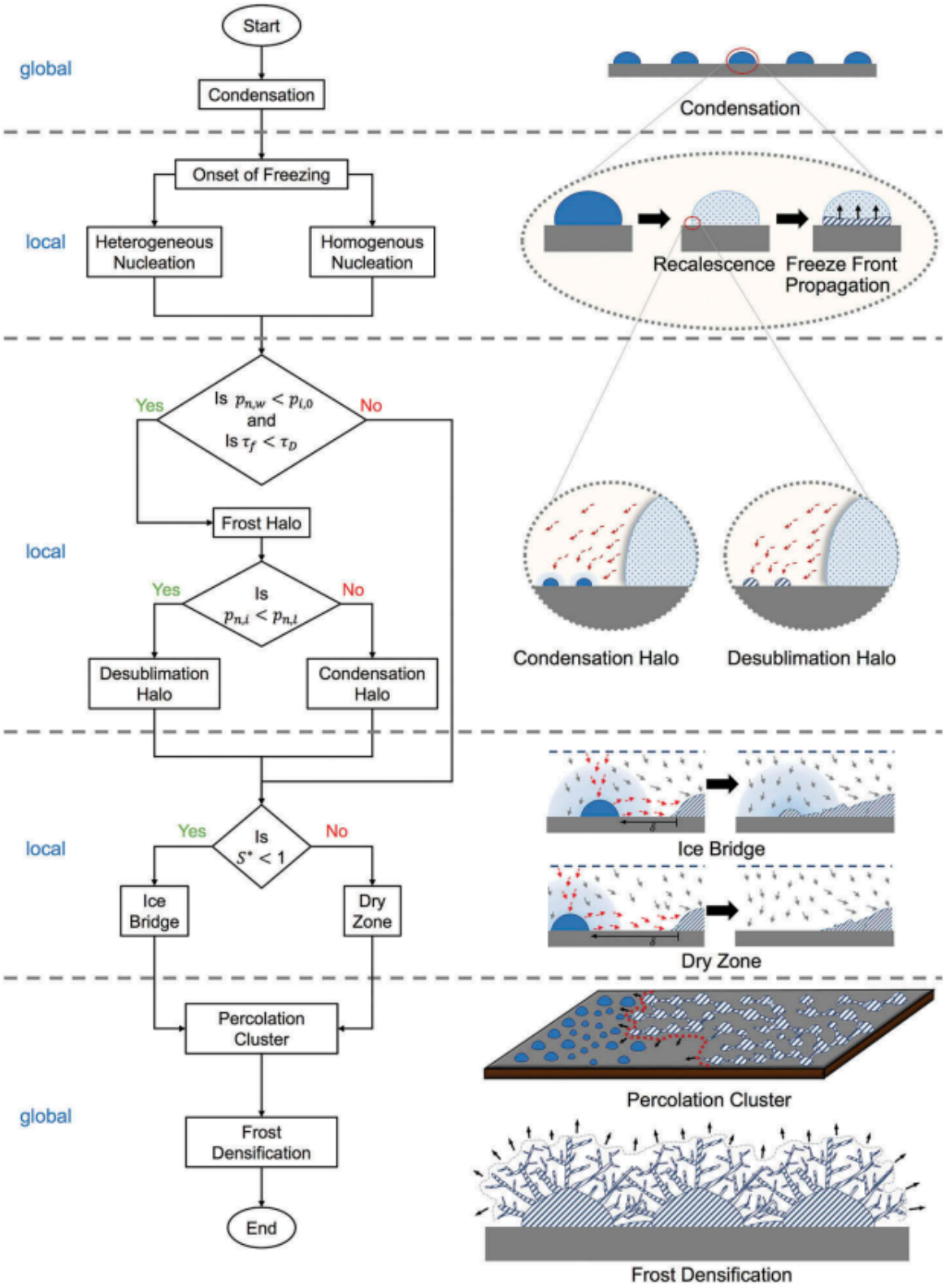

Figure 1.13: Condensation Frosting process and mechanisms, from condensation to frost densification. The parameters for the process diagram decision points are further discussed in the review by Nath et al. [23].

1.2. Passive anti-icing strategies

As discussed, the process of frost and ice formation and subsequent accretion on a surface is quite complex, and heavily dependent on a number of environmental factors and surface conditions. Therefore, it is difficult to design, produce and apply an icephobic coating that repels ice formation and is also durable enough for the variety of icing conditions found during a flight cycle[4]. However, many attempts have been made in the past 15-20 years, and the mechanisms by which these coatings work and the problems that arise will now be briefly discussed. In all of the mechanisms discussed, it should be noted that surface chemistry will always be an important factor to be consider and potentially utilise. Fluoropolymers and their use in coating applications across many industries are a typical example of using powerful surface chemistries to achieve desired surface energies and water contact angles. They are a very effective form of water repellency, and have been shown to significantly decreased ice adhesion strength in certain icing conditions [40], due to the extremely low surface energy caused by fluorine groups. However, fluorinated materials and coatings have come with the major drawback of a potentially harmful impact on environmental and human health [41], and their use therefore are recommended to be restricted to essential use cases, laboratory environments and closed-loop systems.

The key factors which affect the hydrophobicity of a surface and its ability to effectively repel water are the degree of surface free energy and the structure of the surface at the micro and nano level. Surface free energy is decided by the chemical composition at the surface, and this can be manipulated to a significant degree in order to reduce the apparent contact angle and therefore decreasing the surface free energy [42]. Combining this with the effect of well-designed micro and nanostructures, which are often bio-inspired [43–46] can be a powerful tool in designing icephobic materials that repel water using superhydrophobicity, and thus delay ice formation. Man-made topology modifications designed to manipulate the mode of solid-liquid behavior are also well established [47–49], however long-term they may not be best suited for icephobic applications, especially if the mechanism is to make the structure as superhydrophobic as possible. This is best highlighted by Bharathidasan et al., who investigated the effect of surface roughness and wettability on the ice-adhesion strength of various elastomer hydrophilic, hydrophobic and superhydrophobic surfaces [5]. It was found that hydrophobic coatings outperformed superhydrophobic coatings and reduced ice-adhesion to a greater degree. The modified elastomer which was superhydrophobic had significantly higher ice-adhesion, which is likely due to the mechanical interlocking effect when smaller droplets condensate and freeze within the additional faces of the nanostructure. This phenomenon nullifies the icephobic effect of the surface, and reinforces the notion that high water repellency does not necessarily equate to icephobic performance. This experimental work is in agreement with observations by Chen et al. [30], and also Cui et al., where it was verified that smoother hydrophobic surfaces were more effective against ice adhesion as opposed to rougher surfaces [50].

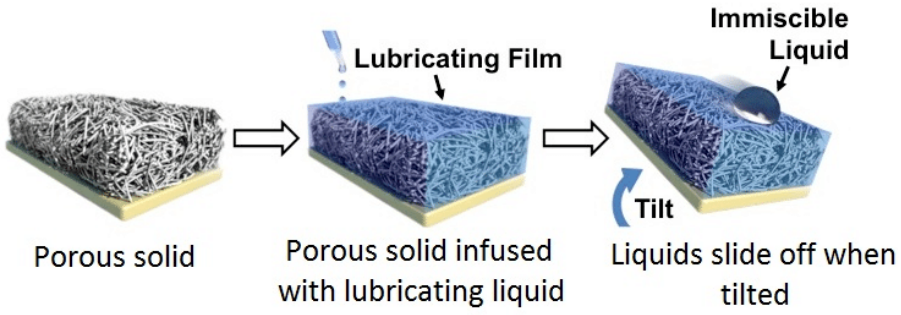

Figure 1.14: Slippery-liquid infused porous surfaces. [51]

Slippery-liquid infused porous surfaces or SLIPS are a relatively new technology that has emerged in the last decade or so, coming to the fore as a coating technology with some excellent results when it comes to icephobicity, along with anti-soiling, self-cleaning and anti-fouling applications. The first of SLIPS was originally fabricated by Aizenberg et al. [51], and once again bio-mimicry was a key component here as the coating structure is inspired by the *Nepenthes* pitcher plant. This plant uses a solid micro-textured surface which is filled with a lubricating liquid phase, where the combination of

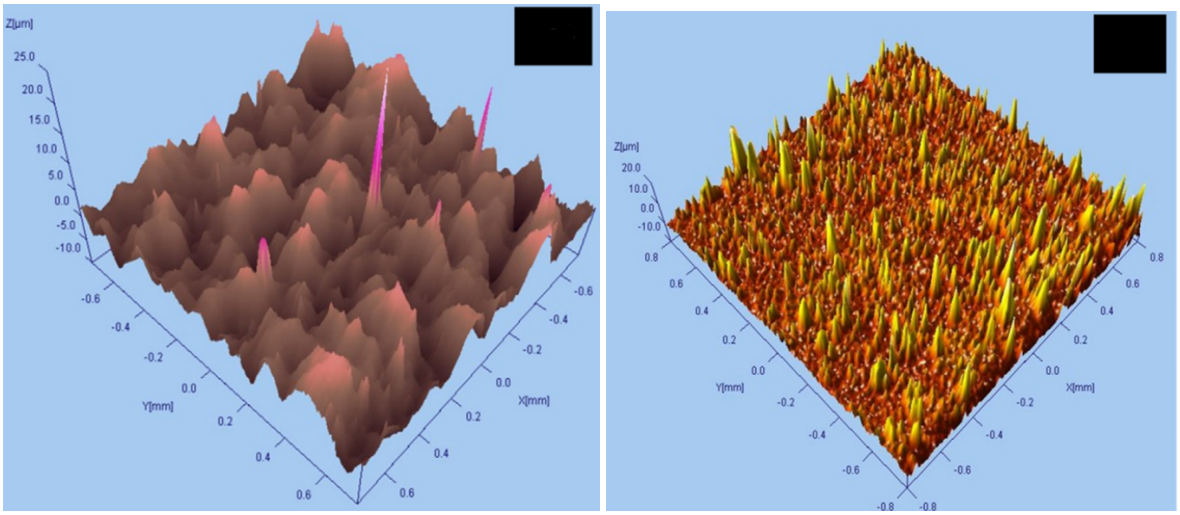

(a) 3-D roughness profile of hydrophobic elastomer

(b) 3-D roughness profile of modified superhydrophobic elastomer

Figure 1.15: 3-D roughness profile of (a) hydrophobic elastomer, and (b) modified superhydrophobic elastomer. The increased roughness allows smaller droplets to condensate and freeze within the structure, leading to increased ice adhesion due to a mechanical interlocking effect of the structure and the ice [5].

surface energies creates a stable film which creates a 'slippery' surface which highly liquid repellent. This concept was then artificially reproduced in a laboratory environment, with a microstructure solid phase and a stable liquid matrix. It works in terms of icephobicity in a similar fashion to superhydrophobic surfaces, by creating a low contact angle hysteresis, low sliding angles, and thus repellency and delayed ice nucleation in the water-surface interaction [6]. SLIPS does not suffer from the issue of increased ice adhesion in conditions of high humidity, which is a significant advantage. Other examples include oil infusion into softer surfaces [52, 53], and similarly designed water-based hydrophilic surfaces with added solutes [54, 55] which can improve anti-icing performance by the introduction of a lubricating layer. However, liquid-infused surfaces come with a significant number of disadvantages, especially when it comes to the case of icephobic materials for aircraft. The mechanism itself relies on delaying the ice nucleation at the material surface, and the functionality of SLIPS relies heavily on the performance and availability of the the lubricating liquid at the surface - this is a finite resource which is next to impossible to replenish during practical use cases. In these practical cases, the lubricant can be diminished and stripped by a number of different factors - icing/deicing cycles, aerodynamic stress and shear flow, evaporation, abrasion, contact with surrounding surfaces [56].

Icephobic strategies which focus on utilising the stiffness of materials to reduce the ice adhesion strength have been explored in recent years. The interaction energy between a softer material such as silicone and water is approximately three times less than the interaction between flouropolymers and water [57], meaning from a surface energy point of view the silicone is will have less of an effect. However it exhibits low anti-icing properties also by a different mechanism, due to the 'soft' surface of the elastomer. Polysiloxane has a relatively low glass transition temperature (Tg), which causes the polymer chains in interaction at the surface to be softer. The mismatch in mechanical and rheological properties between ice and silicone polymers is what what results in the low ice adhesion strength. On a softer surface, the coating stress cannot be distributed over the surface as evenly, so this builds up at the interface. When a force acts to remove the ice, the concentrated stress at the interface results in a favorable route for easier ice release [58].This mechanism is effectively a manipulation of matrix stiffness, and this can be executed over an interface. Wang et al. demonstrated this by directly comparing the ice-adhesion of the rigid polymethyl methacrylate (PMMA) versus a standard silicone elastomer (Sylgard 184), using a push ice adhesion test based on the peak removal stress. The other significant finding of this study was the thickness of the elastomer coating had a significant effect on the ice-adhesion strength, with peak removal stress values ranging from approximately 460kPa for a thinner 18μm, and decreasing to 120kPa for the thicker 533μm coating. This large disparity is explained well by the schematic in Figure 1.16. With a thicker coating, the build up of stress is not only at the interface plane, but it is now also more biased to be concentrated at the front of the ice block

where the force is applied due to the larger vertical displacements that take place. Golovin et al. [59] developed many 'durable' icephobic elastomer coatings by building on this principle, but increased the icephobicity by reducing the cross-link density to create a material with a lower modulus, essentially amplifying the effect of the rheological mismatch.

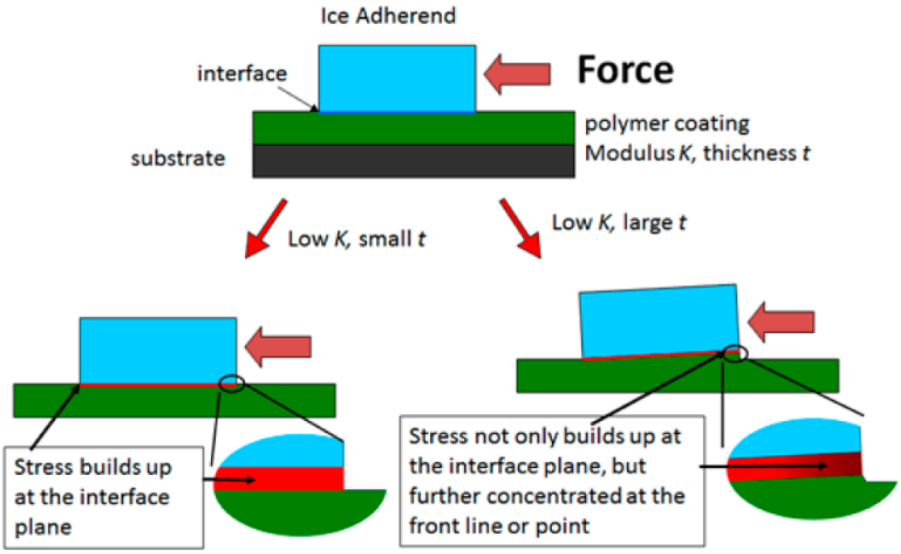

Figure 1.16: Schematic diagram demonstration of stress building up at the interface plane and/or the front line or point during removal of a rigid, bonded object (ice) from a soft coating. [58]

The stiffness properties of elastomers can also be utilised to good effect on a localized scale. Irajizad et al. also used the elastic instability at the interface and other fracture mechanics outlined by Chuadhury et al. [60] to drive his novel approach in developing an elastomeric icephobic coating [7]. The coating developed introduced local phases with low shear modulus into a elastomeric matrix with high shear modulus, at the ice-material interface. As force is applied to the ice, these local phases are the first regions to detach from the ice, but the ice is for the most part still adhered to the surface. The initial detachment actions causes multiple local cavities, which in turn cause local stress phases and small cracks. Under increasing force, this local effect spreads across the interface quickly and transitions to a global effect, and the induced local stress leads to larger crack propagation and ultimately failure. The higher modulus material was a silicon elastomer, and the lower shear modulus material was a silicon based organogel. Choosing a higher modulus material as the wider matrix increases the durability of this coating, whilst still remaining a very low-ice adhesion material. Although softer materials such as these are unlikely to be the final solution for an icephobic coating in aerospace due to their durability and unsuitable mechanical properties, they present an accessible route for laboratory work testing new methods, patterns and chemistries for icephobic coatings, and interesting insight into proposed ice adhesion mechanics.

From the above analysis, the approaches that appear to be the most effective are those which combine certain elements of different techniques, creating a synergistic effect from these elements to obtain an icephobic surface. In ice growth conditions, ice accumulation is not something which can inherently be prevented. Therefore, to deal with the issue using a passive coating strategy, the coating will have either remove the ice or to try and control how it forms and grows on the surface. To remove the ice without active de-icing strategies, the coating needs to have low adhesion to the ice accumulating. Attempting to influence and control the nature and type of ice growth on the surface may be an alternative solution with many possible avenues. Control of the ice shape, type, amount and/or growth direction could have many possible benefits such as reduced drag and reduced ice adhesion, and this is where the potential of patterned materials and coatings comes to the fore. Patterns have already shown the ability to change surface characteristics. A superhydrophobic/superhydrophilic bump pattern inspired by the Stenocara beetle was manufactured via a coated steel mesh by Zeng et al. [61], to separate

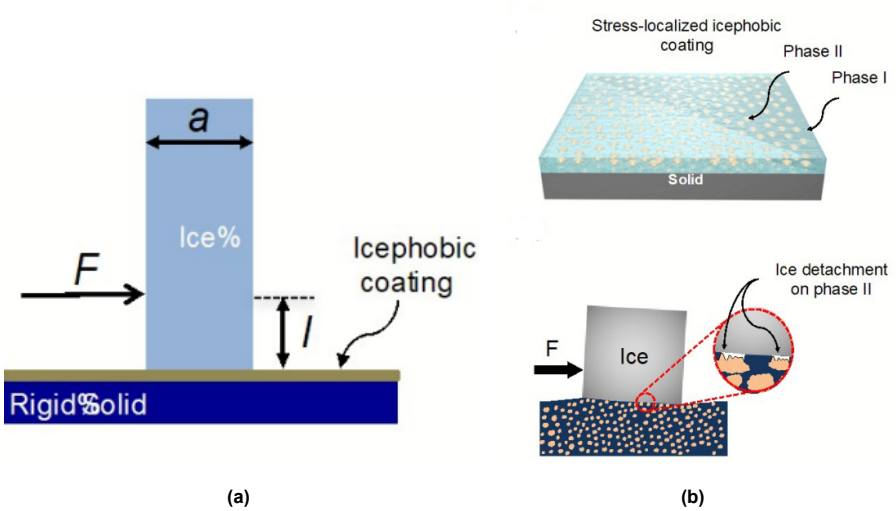

Figure 1.17: (a) Ice-adhesion push test on a stress-localized icephobic coating, with a rigid silicone matrix (phase 1) and a softer, second phase at the interface. (b) The lower shear modulus (phase 2) leads to local detachment points at low forces, local stress concentrations and ultimately crack propagation and failure [7].

water and oil in a mixture. Boreyko et al. were one of the first to examine the wettability contrast by exploring the effect of chemical micropatterns on condensation and frost growth [8]. In this study, the author exhibits and utilizes an understanding of the condensation frost phenomena which were already discussed, targeting the prevention of interdroplet ice-bridging and the subsequent ice growth chain reaction by carefully controlling the distances between nearby nucleation sites for supercooled condensate. The patterns worked (albeit on not very durable silicon wafers), and the condensate at both testing temperatures of 5°C and -10°C preferentially grew on the hydrophilic regions for the majority of cases. Whether there was any growth on the hydrophobic regions depended on the pitch distance between features and the degree of supersaturation. In order to stop the frost front becoming a film of frost and then ice, it is required to stop halt inter-droplet ice bridging. Boreyko et al. found that freezing as quickly as possible is the best way to utilise the patterning and local pressure gradients, as the water droplets on the surface evaporated or were harvested by the hydrophilic regions before they were able to undergo inter-droplet ice bridging. This results in a stable dry zone for at least 5 minutes, which is an excellent result.

Further developments on this work by many of the same researchers have led to developments in not only chemical micropatterns, but also physical micropatterns on more robust materials which also exhibit a similar effect. To this effect, an anti-frosting aluminium surface was developed by patterning the material using with microgrooves using laser-cutting [62], as seen in Figure 1.19 .The microgrooves were also 'wicked' with an inner groove on the top of the fins, in order to encourage the water to freeze in these channels, and reduce the probability of interaction with the dry zones below. These fins have a significant advantage as being purely physical, they are not susceptible to degradation or contamination. interestingly, Zuo et al. created the inverse of these passive anti-frosting fins for a similar effect. In this study, well-designed micropatterned ice walls were intentionally frozen onto the surface, and were placed in specific positions in order to manipulate the dry zone formation and suppress the condensation frosting [63].

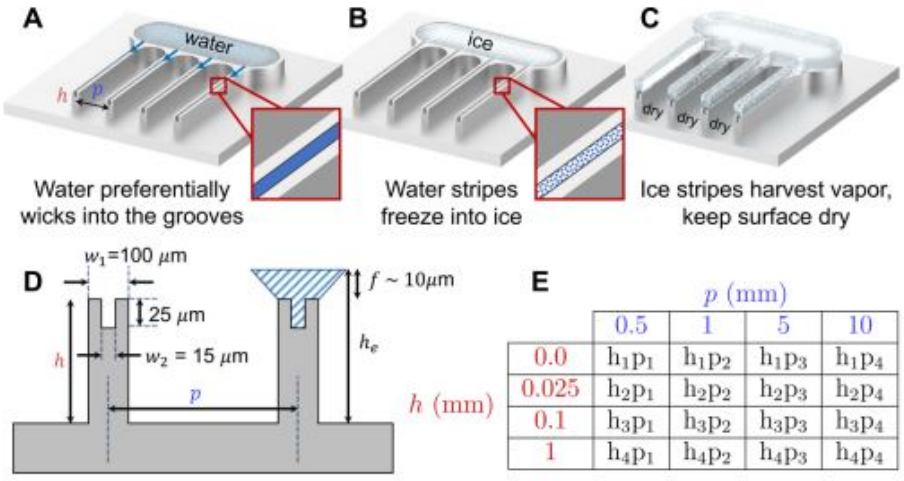

Figure 1.18: Schematic demonstrating how wicked aluminium fins can be used to help control ice growth [62].

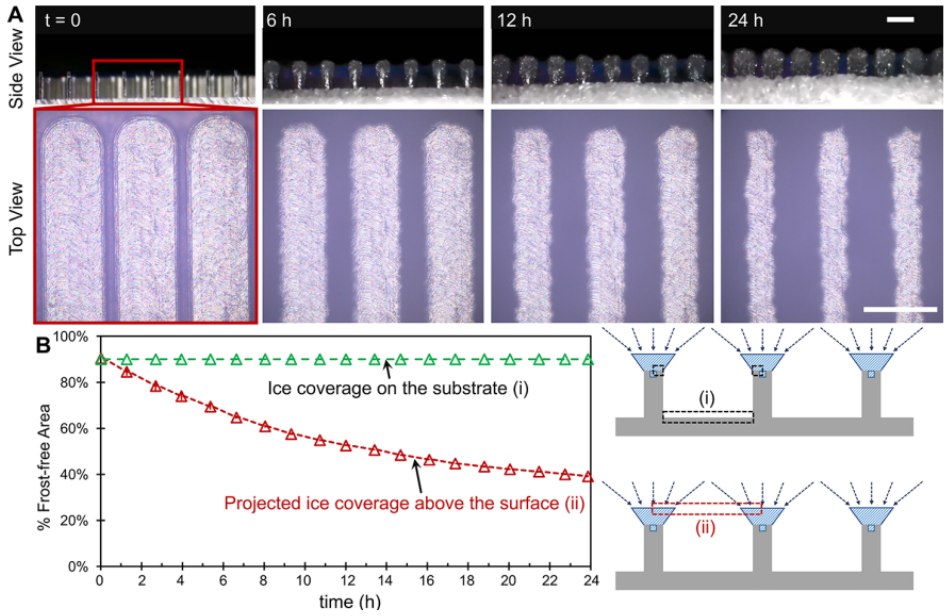

Figure 1.19: A 24h experiment on the antifrosting aluminium wicked surface at -10°C. (A) The white regions represent dry zones, while the purple zones are the sacrificial ice stripes. (B) Line (i) represents the 'direct solid-ice contact' definition of ice coverage on the horizontal surface, whilst line (ii) represents the projected ice coverage, taking into account the coarsening frost elevated on the fins above the base surface [62].

In summary, there are many exciting developments in the field of passive anti-icing coatings and materials. However, in order to develop emerging strategies such as patterned materials further and apply them to practical use cases, the ability to quantify their effectiveness and durability in an icing environment becomes critical. The mechanisms at play are clearly quite complex and sensitive, which implies that their may be an element of fragility when they are scaled upwards. This highlights the need to investigate how these differing strategies react under known, controlled environmental conditions and testing parameters, so they can be compared by fundamental metrics, such as ice adhesion strength. Starting from this base level of understanding, the efficacy of the strategies can be further analysed and tuned before scaling further.

1.3. Ice adhesion testing

As discussed, an important component of developing novel anti-icing coatings and materials is the ability to test their effectiveness in comparison to bare surfaces, and also in comparison for one another. This requires a precise, controlled testing procedure in which the degree of ice adhesion to a surface can be quantified in some manner. This section will briefly discuss various approaches to this problem that have been attempted in the past, along with some key points on ice adhesion mechanics.

1.3.1. Existing techniques

Ice adhesion testing set-ups can divided be into three main categories: shear testing (both vertical and horizontal), tensile testing and centrifugal adhesion tests (CAT). The design of the set-ups typically differ in the details, but loading mechanism or force application is usually what defines the experiment. The type of ice tested, along with various other parameters, will also have a large influence on the results, as explored by Rønneberg in their inter-laboratory investigation into ice adhesion across different techniques [15]. There have also been several critical reviews outlining the adhesion methodologies, the most recent of which by Work and Lian [9]. The two most relevant methods, which could be implemented considering the time constraints of masters thesis are discussed.

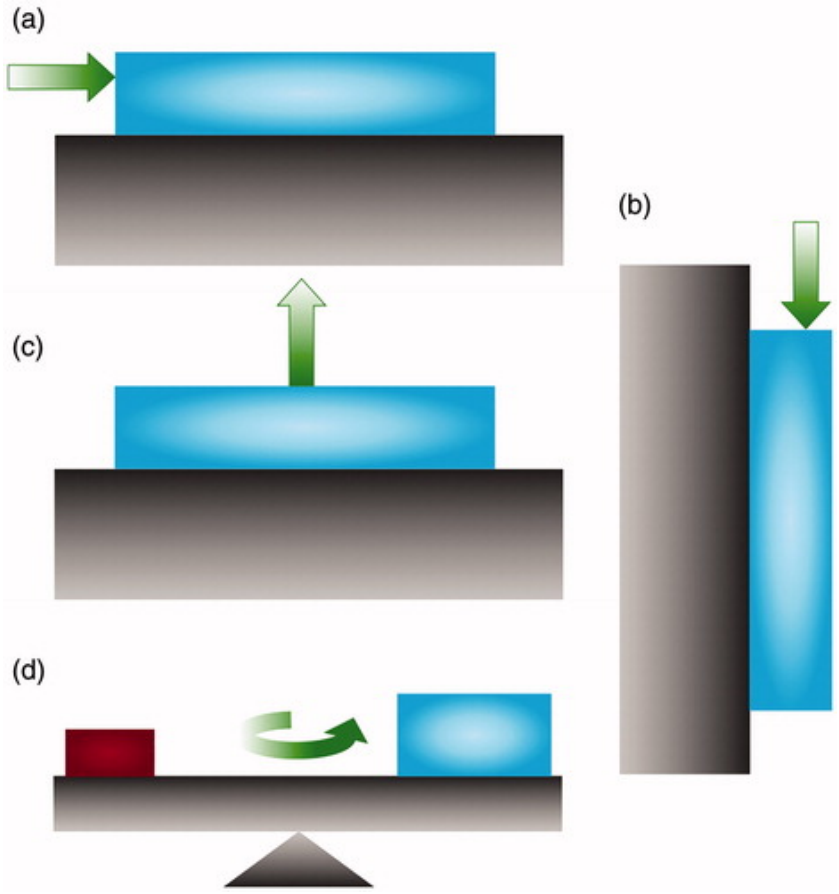

Figure 1.20: Schematic illustration of four typical tests methods for ice adhesion strength measurements: (a) horizontal shear test, (b) vertical shear test, (c) tensile test, and (d) centrifugal adhesion test. The green arrow indicates the application of the force [21].

The most prominent example of centrifugal adhesion tests in literature is the set-up developed by Laforte et al. at the Anti-icing Materials International Laboratory [20]. This method utilises a beam with the icing sample in question and a counterweight for balance, as seen in Figure 1.21, which is rapidly accelerated until the ice detaches from the beam in shear. The velocity of the beam in the moment is recorded from the moment the ice detaches, which is measured by a change in vibrations in centrifuge by piezoelectric cells. The advantage of this set-up is that it can measure the ice adhesion strength

of coatings with accreted impact ice, as a spray nozzle directs the freezing drizzle onto the sample. However, the set-up can only test one coupon at a time is more difficult to replicate between laboratories, as the set-up and analysis is more complex that other methods. Additionally, force curves are not captured which provides little information about failure, and cohesive failures cannot be analysed, as the test stops when it senses the first piece of ice striking the wall of the centrifuge. The spread of the filtered data from this set-up and its improved iteration looks promising, as for a relatively high sample size, the reported standard deviations for ice adhesion strength with adhesive failure is close to 10% [64]. Other attempts at using centrifugal tests have similar deigns, and run into similar issues as outlined by Work and Lian in their review [9]

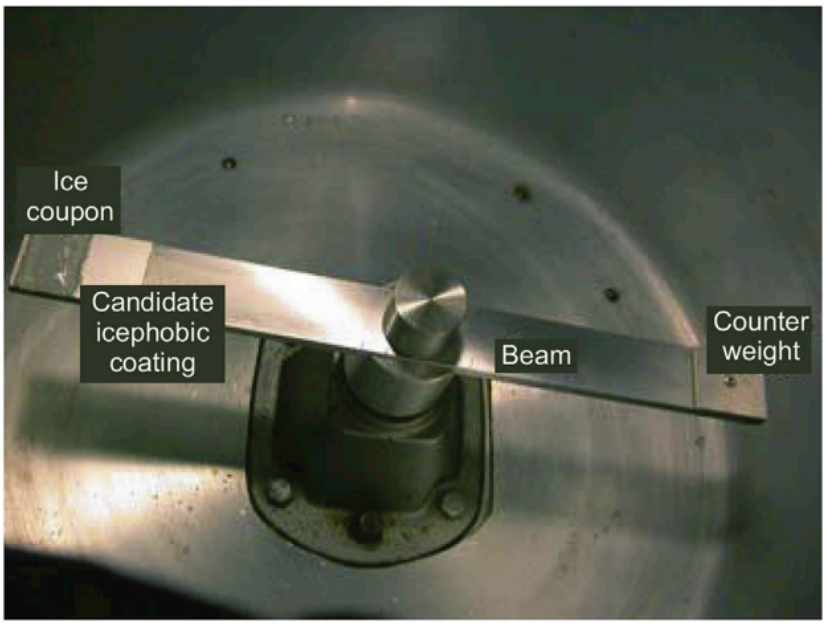

Figure 1.21: Centrifugal adhesion test set-up developed at AMIL. [20]

By far the most researched and utilised testing method is that of the shear test, in either the horizontal or vertical orientation, also known as a push test. In these tests, the water is typically frozen in a mould, and then the average stress required to remove the ice from the test substrate is recorded. The vertical shear test is almost identical in its operation to the horizontal shear test, but with the perhaps unnecessary added layer of complexity of dealing with gravity, so horizontal set-ups will be highlighted. In the last 15 years the design which many other set-ups have subsequently been based on is that of Meuler et al. [19]. In this set-up, water is poured into surface modified glass cuvettes, which are on top of the samples in question as seen in Figure 1.22. The samples are held in a sample holder, which is attached to a peltier plate at -10° C and thus the ice is frozen in a column of chosen height. The force is applied using a probe attached to a force transducer on top of a motion stage, which is applied at a constant velocity of 0.5mm/s until the ice column breaks. The test takes place in a cold room under a nitrogen atmosphere. This is a simple yet effective design, which allows for direct comparison of ice adhesion strength between substrates, with relatively low standard deviations of between 15-20%, with respect to the mean value. Similar projects have also implemented similar designs with similar degrees of success and accuracy [17, 65, 66], pointing to the efficiency of the design. However, it should be noted that the direct mechanical contact with the moulds will lead to stress concentrations at the ice and substrate interface, which may influence the failure mechanism. Additional detail will be given to ice adhesion testing in the following sections and chapters, however an initial analysis can be made between the techniques discussed, outlined in Table 1.1

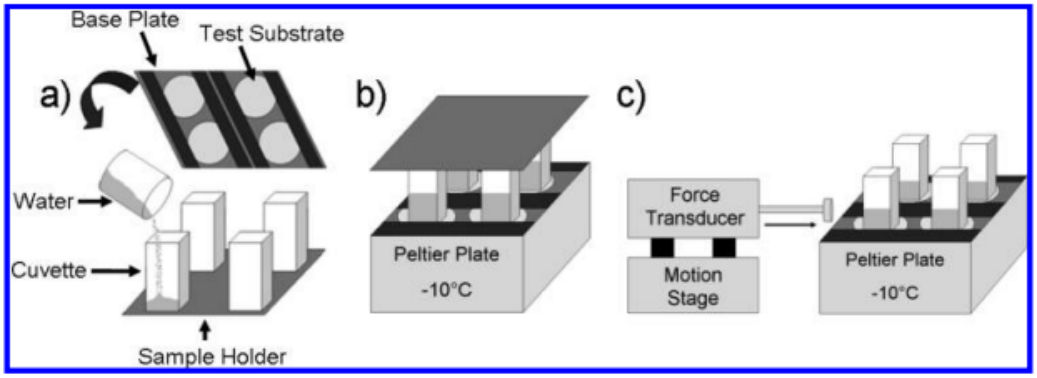

Figure 1.22: Horizontal shear ice adhesion test developed by Meuler et al.

Table 1.1: Comparative table of key testing parameters between shear and centrifugal designs

Test parameter	*Shear*	*Centrifugal*
Speed of testing	Fast	Fast
Cost	Moderate	High
Complexity	Low	High
Multiple samples?	Yes	No
Impact ice?	No	Yes
Cohesive failures analysis?	Yes	No
Standard deviation	≈ 15-20%	≈ 10%
Validation	Easier, more sources	Difficult
Force curve?	Yes	No
Stress concentrations?	Yes	No

Ice adhesion testing follows no set standard, and this is a significant problem in this field. Without standardization, it becomes difficult to accurately compare results, as each different ice adhesion set-up will have differences which can have a significant impact on the results. Both Wang et al. and Stendardo et al. has shown in their horizontal shear adhesion tests the strong influence that different testing geometries can have on ice adhesion strength [17, 18], highlighting the problematic nature of comparing data between tests without full transparency on the nature of the testing conditions. Any potential standard such as those proposed by has not to date been followed exactly, however it should be noted that they are both horizontal shear adhesion tests. Rønneberg et al. proposed the test design shown in Figure 1.23, which has many strong elements [21]. It is a simplistic, easily reproducible design, which outlines set values for key parameter such as the probe distance, speed, ice height and temperature. However, the bare contact with the ice will likely induce contact errors, and the humidity value at 80% is a significant flaw. It has already been discussed the effect that condensation frosting phenomena can have on ice nucleation and growth, and a humid environment at 80% relative humidity is primed for heterogeneous nucleation. The more recent proposal from Bleszynski et al. is an interesting concept, with the addition of a removal mould with a pull tab as seen in Figure 1.24 [67]. However, how user-friendly and useful this feature is in practice remains to be seen, and once again it introduces an unknown with the contact of bare ice against a probe may be problematic. There are no specific values set for humidity and temperature in the proposal, and are only mentioned saying that they 'should be controlled' - this vagueness and lack of precision is the exact opposite of what is required in a standard.

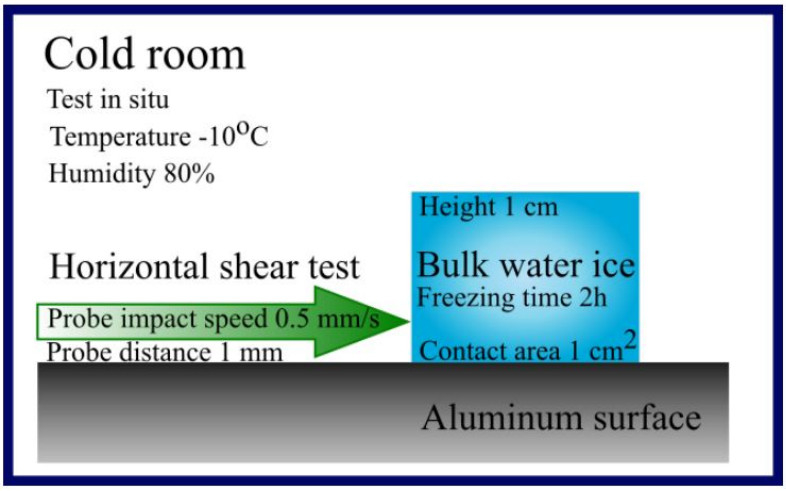

Figure 1.23: Proposal for an ice adhesion testing standard by Rønneberg et al.[21].

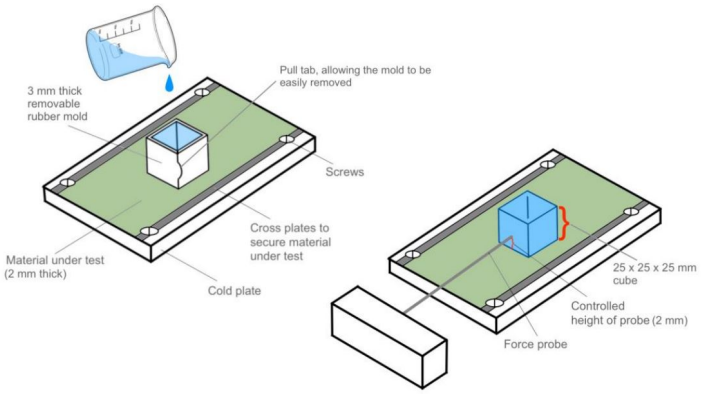

Figure 1.24: Proposal for an ice adhesion testing standard by Bleszynski et al.[67].

1.3.2. Ice adhesion mechanics

The mechanics around the exact nature of the failure of ice in an ice adhesion test have not been extensively studied. Typically in a horizontal push test, the ice adhesion strength is represented by the interfacial adhesive strength, which is expressed in terms of the maximum stress reached before failure of the joint [17]. Therefore, average critical shear stress τ_{ave}, is defined as the peak force required to cause removal of the ice interface of area A, such that:

$$\tau_{ave} = \frac{F}{A} \tag{1.7}$$

Ideally, this method of analysis should also take into factors such as the test conditions and the effect of stress concentrations, in order to accurately predict the critical shear stress which leads to failure, τ_c. Other methods of quantifying the ice adhesion strength are by the energy required for removal of the ice under an applied force. The maximum build up of strain energy before the failure of the interface is often described as 'toughness', assuming a linear elastic regime. Both of these methods of would benefit from additional numerical analysis such as FEM. The use of τ_{ave} is effective for small areas when comparing different materials or coatings to one another, however as the testing scales the approach may need to be modified as proposed by Golovin et al. This relationship implies that the force required to remove ice from a substrate scales directly with surface area, whereas in practice the force to remove adhered ice from larger areas is relatively low, and often independent of interfacial

area [68]. This line of thinking introduces two categories of failure modes for ice detachment. The first is a stress-dominated detachment, where the interface S abruptly fails due to the critical stress, τ_c, being reached all along the interface. Therefore, this mode is most prevalent for smaller interface areas, and describes failure all along the interface. The other is a toughness-dominated detachment for larger interfaces, where a crack is initiated over a finite area of the interface δS, which subsequently leads to crack propagation and ultimately failure. This type of failure is dominated by the critical strain energy. The study of Huré et al. developed a fracture toughness approach to explore the difference of Cassie-Baxter and Wenzel states on ice adhesion. For a horizontal push test on ice that is a toughness dominated detachment, it was noted that the crack propagation is likely to be a mixed mode propagation, where it both slides in shear(mode II) as expected, but also opens in mode 1 [69].

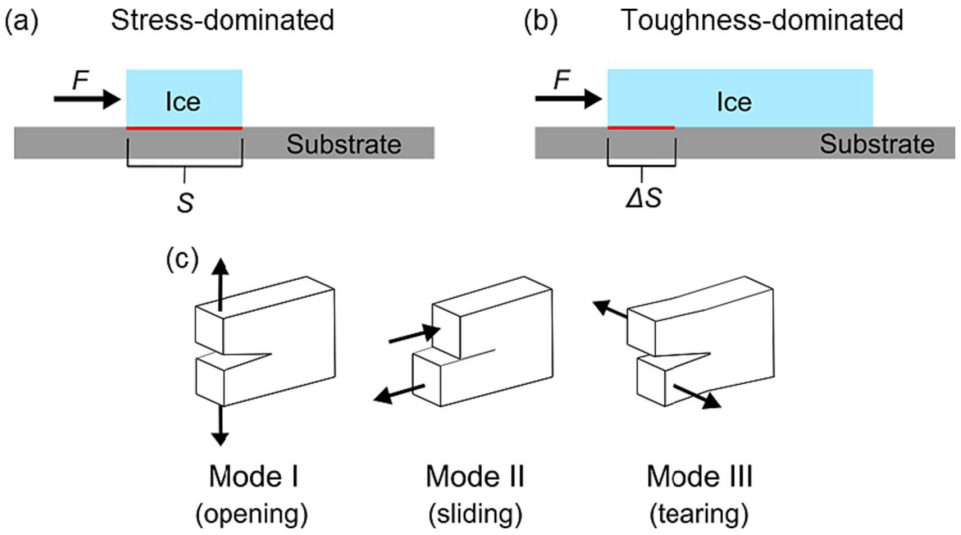

Figure 1.25: (a) Stress dominated detachment, controlled by critical shear stress (b) Toughness dominated detachment and (c) Schematic of the three crack modes present in fracture mechanics, produced from [17].

Stendardo et al. proposed a process for the design of a horizontal push test, taking into account the geometry of the test set-up and the nature of failure [17]. In order to have a predicable result, it was recommended to prioritise a design which promotes a stress-dominated detachment, to avoid the complexities of analysis when dealing with fracture toughness detachments. This recommendation seems especially prevalent considering the large spread of data in literature - an effective design to be validated should first prioritize gaining a foothold in the fundamentals of ice adhesion, before developing further. During the optimisation of the test parameters this study, the effect of the test geometry was found to have a significant effect on the ice adhesion strength. For example, when varying the the pushing height *h* from *h* = 1mm to *h* = 4mm under the same conditions, the average ice adhesion strength on aluminium linearly drops from over 1200 kPa at *h* = 1mm to just under 800 kPa at *h* = 4mm, as seen in subfigure (b) in Figure 1.26. This is likely due to a couple of mechanisms;as the height increases, the bending moment increases, and the loading likely moves further from shear into a mixed mode loading. The author attributes this to more of a build up of strain energy in the bulk of the ice, as opposed to the interface, and the reduced stress concentration as seen in sub-figure (d) Figure 1.26. Similarly, the geometry of the mould and therefore the icing pillar has large effects on the results [17], with the increase in interfacial area dropping the force required for failure by a factor of 4, which is in agreement with the scaling observation made by Golovin et al. [68]. Because of these effects, a geometrical factor known as shear stress intensity factor (SSIF) was introduced in the study, which was obtained by numerically by an FEM analysis of the test bench and is dependent on the pushing height *h*, the ice height *H*, the mould diameter *D*, and the mould thickness and mechanical properties. By obtaining the τ_{ave} and dividing by the SSIF for this particular set-up, the minimum shear stress τ_{min} is obtained. This is deemed to be a more appropriate metric to analyse ice adhesion strength when considering a stress dominated detachment, as the numerically obtained τ_{min} for failure criterion is relatively consistent when considering different pushing heights, implying that τ_{min} is in fact τ_c. It is expected that that experimentally, it should be possible to link the ice adhesion results to some

of the mechanisms discussed if the set-up is designed with some of these considerations in mind.

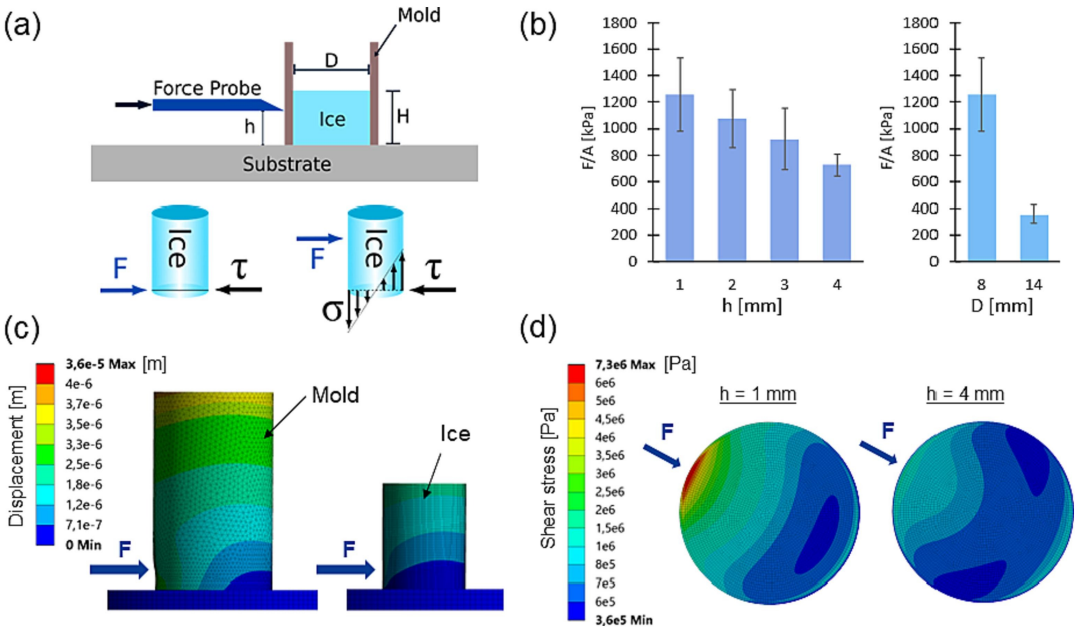

Figure 1.26: (a) Typical push test on bulk ice with schematic of the typical stress components. (b) Effect of changing pushing height *h*, and mould diamter *D*, on ice adehsion strength. (c) Numerical modelling of the mould displacement and (d) Shear stress distribution at the ice-substrate interface for *h* = 1 mm and for *h* = 4 mm, with *D* = 8 mm in both cases. Produced from work by Stendardo et al. [17].

1.4. Discussion & Scope

On examination of the existing techniques that have been attempted to measure ice adhesion strength for different materials, briefly outlined above, it is clear that there is not one perfect solution. The ideal measurement system would likely be very accurate, with precise control over the numerous variables that exist when dealing with ice, along with possibilities to test in multiple orientations, failure modes and icing conditions. However, the lack of standardization in this field has led to numerous approaches to the same problem, with a wide range of results and levels of success that make it difficult to accurately compare data. This is highlighted by the standard deviation of the data obtained for ice adhesion strength - often the standard deviation for the 'better' set-ups is in the range of 10-30% [9, 21], with this being deemed a good result due to the nature of the test. This spread of data is clearly illustrated in Figure 1.27 and Figure 1.27 for push/shear tests on aluiminuim, steel and Teflon, where the standard deviation between 30-80% in many cases. It can be theorized that metals provide the most straightforward substrate to test when it comes to achieving a tighter spread of data, due to their stiffness and isotropic nature. However, many of these studies also just report these materials as aluminium or steel, often without consideration for reporting the alloy type, grain direction or surface treatments. It should also be noted that the majority of the tests which report standard deviations below 10% are studies from the 1980s, where reasonable doubt can assumed of the nature of the tests and degree control of the parameters.

Overall, the question remains whether the significant scatter is caused by poor design choices, oversights or something else, or whether the scatter is actually attributed to what is often quoted as an 'inherent property' of ice and its testing [9, 21]. Ice is of course a chaotic and transient substance, constantly changing and adjusting to various external parameters such as temperature, humidity, loading and the substrate. However, it is worth challenging this idea that understanding the adhesion mechanisms of ice will forever be limited by its inherent nature and testing scatter. Thus, one of the goals of this study is to produce a design that can produce reliable data with a lower standard deviation. By compartmentalisation of the testing parameters in a flexible design, it should be possible to produce this with the ability to investigate singular data points, and thus investigate the root cause of the scatter. A closer look at some the best performing set-ups may gave an idea into the reasons for the reduced

scatter in their data.

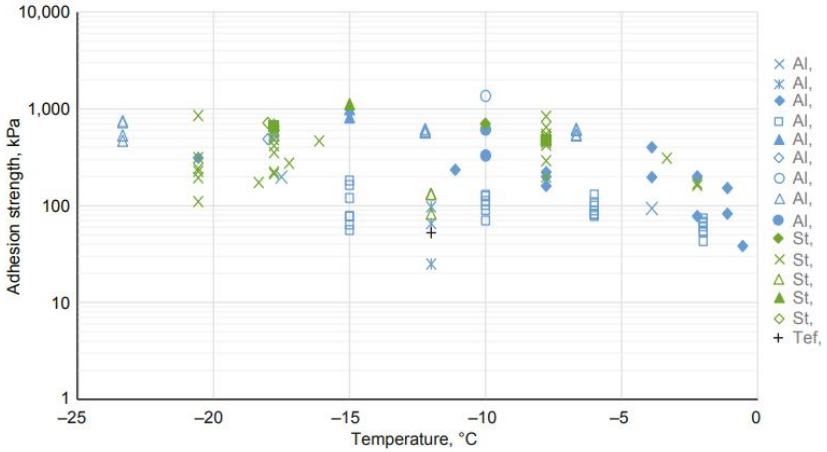

Figure 1.27: Adhesion data from push/pull/shear tests from literature. Al, aluminium; Tef., Teflon; st, steel. Plot reproduced from Work and Lian [9].

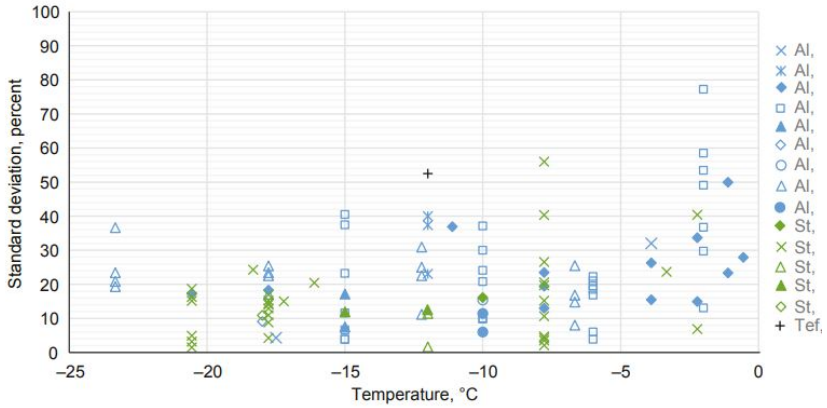

Figure 1.28: Standard deviations of corresponding push/pull/shear tests from literature from Figure 1.27 above. Al, aluminium; Tef., Teflon; st, steel. Plot reproduced from Work and Lian [9].

Only three shear test studies from 2000-2018 reported standard deviations below 10%. On brief analysis of their design set-ups, some issues are apparent, but they also follow many good practices which may point the to smaller spread of data. In the design of Zou et al., a cooled conical tip as seen in Figure 1.29 used to shear a frozen water droplet approximately 1mm in radius from a cooled test specimen, with the standard deviation of ice adhesion strength reported in the range of approximately 6% [70]. In this set-up, all the key parameters are neatly controlled such as the surface temperature and the relative humidity via a nitrogen purge. However, it could be argued that direct contact from the probe with the very small ice droplet is far from ideal, as the ice is no longer 'independent', despite the chilled probe. Additonally, the water contact angle of the droplet on the surface will have a strong impact on the results. The probe speed of 1mm/s likely introduces momentum effects, and is it outside of the quasi-static range with respect to the size of the ice being tested. Additionally, the reported data is purely quantitative, and although consistent it is approximately 330 ± 22 kPa, which is considerably lower than the widely reported range of 700-1000 kPa. The research of Dou et al. provides impressively low ice adhesion results for an anti-icing coating employing a lubricating layer, with bare aluminium substrates dropping from approximately 1000 kPa to less than 50 kPa when they are coated [71]. The impression the article, abstract and images gives is that these tests were performed and all data was recorded in a wind tunnel where wind provides the adhesion force, however the data appears to be

actually gathered from an unspecified home-built push test. The lack of detail about the set-up, sample size and misdirection about the testing methodology brings some doubt into the validity of the results having a stand deviation below 10%, however the values for aluminium and steel do appear to be in the correct range with the many of the reported values, in the range of 700-1000 kPa.

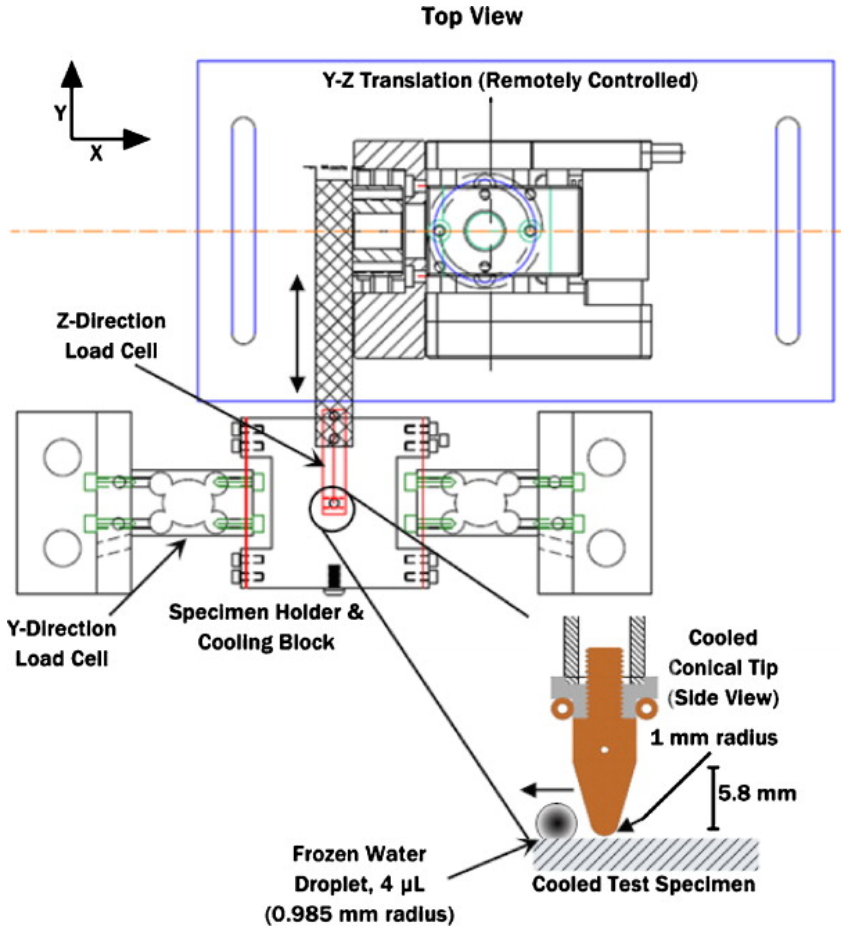

Figure 1.29: Schematic illustration of shear ice adhesion test on frozen droplets employed by Zou et al. to achieve low a standard deviations for ice adhesion strength.[70].

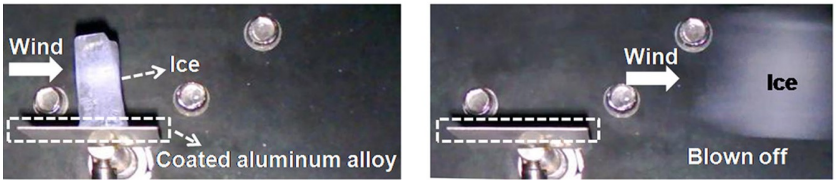

Figure 1.30: Ice adhesion results from unspecified home-built push test, Dou et al, 2014.(a) Ice adhesion strength of an anti-icing coating with lubricating layer over 30 icing/deicing cycles (b) Ice adhesion strength of different substrates before and after being spin-coated with the anti-icing coating.[71].

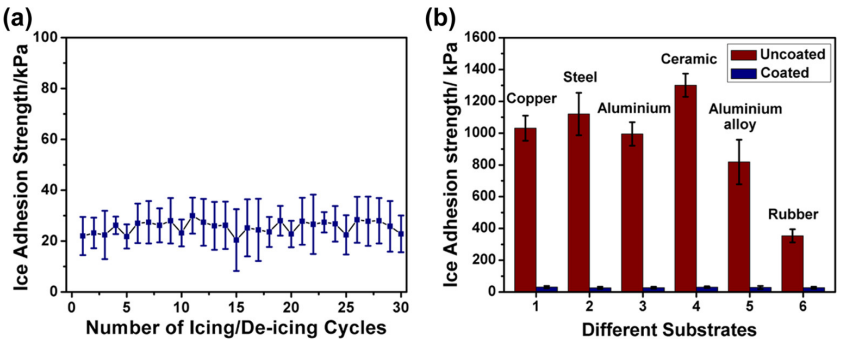

Figure 1.31: Wind-tunnel test on anti-icing coating by Zou et al. The ice on the anti-icing coating could be blown off with a strong breeze of approximately 12 m/s. Arrows denote direction of the wind.[71].

The design which He et al. uses to gather data with a standard deviation of below 10% is in the form a vertical shear test, as seen in Figure 1.32. This is a simple but effective set-up than where the key parameters are controlled, and this allows the researcher to easily correlate ice adhesion strength to variables such as water adhesion force, roughness, elastic modulus and hardness [72]. In this set-up however, there is no consideration for humidity control, which is a critical misstep when taking into consideration the learning from condensation frosting phenomena discussed in section 1.1. Although having low standard deviation, the reported values for aluminium and steel are 486.8 ± 44.3 kPa and 714.0 ± 78.0 kPa respectively, which are quite low with respect to the mean range, and may point to a correlation between high relative humidity and lower ice adhesion strength. With a sample size of just 5 measurements for both aluminum and steel, this also decreases the confidence in the testing procedures. Incidentally, this experimental set-up concept (or iterations of it) is also used for the ice adhesion tests for various researchers and collaborators from affiliated groups, such as Wang et al. on the investigation of ice adhesion on the changing thickness Sylgard-184 and dynamic surfaces [58, 73], and Rønneberg [15, 21] in their works from their impressive PhD thesis on ice adhesion mechanisms. This design feature, or lack of one, does not take anything away from the quality or validity of their work, but it is something to consider when their analysing results or procedures, as they are referenced in this thesis several times.

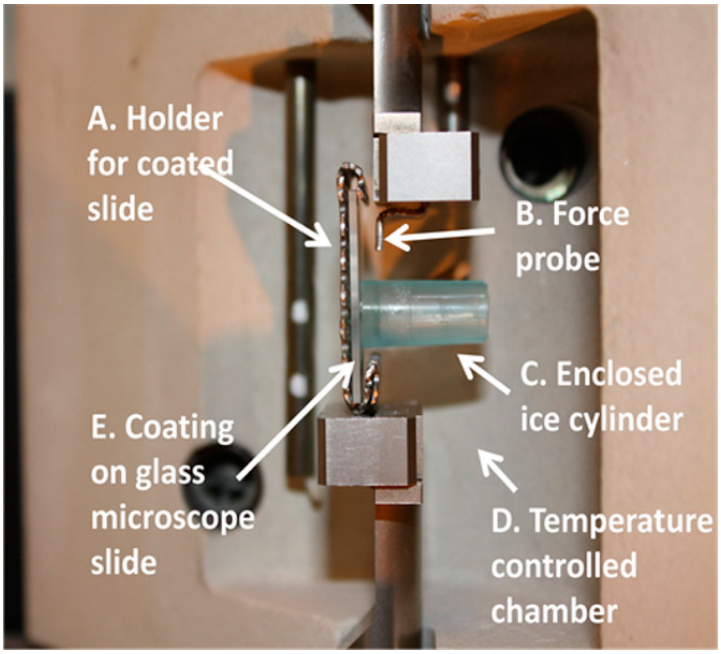

Figure 1.32: Vertical ice-adhesion set-up [18], employed in the various works of Wang[58, 73], He [55, 72] and Ronneberg[15, 21].

To investigate the root cause of the scatter, it is possible take inspiration from what has worked well in the past in achieving a tighter spread of ice adhesion data, as this will also assist in validation. However, it is important to not simply copy these designs, but to first think independently about the unique requirements and objectives for this individual project. When taking concepts from elsewhere, the purpose of each element needs to be thoroughly analysed, before considering any creative improvements or adjustments that may be required to be suitable for this project. The creation of an entirely new conceptual design to measure ice adhesion was considered, but this was deemed to be an unsuitable and flawed approach. This approach is risky, and restricted by the limited resources of a masters thesis. Additionally, implementing a completely new conceptual design may simply add to the saturation of designs which have large standard deviations and scatter with no comparable counterparts. Without validation against other set-ups, the ice adhesion results are difficult to have confidence in, unless the design itself exhibits exceptional results and is easily reproducible by other researchers. This idea once again highlights the need for standardization in this field, and the motivation for taking a slightly narrower outlook when analysing other ice adhesion set-ups.

In summary, many engineering applications which are hindered by icing would benefit from less ice accumulation on the materials surface. However, without the application of external methods such as de-icing fluids, it is generally accepted that ice will eventually form on surfaces in sub-zero temperatures. Patterned materials have the potential to control ice-growth to some degree, in order to either prevent the formation of a thick ice-film, reduce ice-adhesion, or keep parts of the surface dry. The ability to quantify and compare the ice adhesion strength across different materials should therefore be a powerful tool. Many existing techniques which attempt the tackle the issue of icing on surfaces rely on an adjustment in the materials physical or chemical topology, to create some desired change or weakness at the ice-surface interface. Although these surface modification attempts are often flawed due to low durability or the inevitability of ice growth which been outlined already, they may actually unknowingly be decreasing or increasing the adhesion of the ice to the substrate, even if that mechanism for de-icing is designed for something else. The clearest example of this is the exploration of superhydrophobic surfaces for creating 'icephobic' surfaces; after several icing de-icing cycles the ice adhesion increases due to mechanical interlocking at the interface, producing the exact opposite effect. In the case of patterned surfaces which focus on control of frost and ice growth, it is unclear what affect the change in chemical and physical topology will have on the ice adhesion.

Due to the turbulent nature of an aircraft's flight from the perspective of the outer material surface, it can be theorised that a robust low ice adhesion coating will benefit from increased wind resistance and flight maneuvers in general. This also has been demonstrated to some degree by Dou et al. in their wind-tunnel test on lubricating layer coatings [71]. Arguably, ice adhesion therefore becomes the most important parameter to measure and quantify when designing 'icephobic' or 'anti-icing 'materials in this field. However, recreating and measuring ice adhesion scenarios experimentally in a laboratory is a logistical challenge, as ice by its nature is sensitive to various factors, such as temperature, humidity, pressure, wind speed and the substrate on which it grows. Not only is ice difficult to work with, the sensitivity of the testing parameters and geometry with respect to the results for ice adhesion strength must be taken into account results. It is clear that however this is not a straightforward task, judging by the huge scatter in data and differences in results present in literature, which is partly due to the lack of standardization in testing. Before analysing other attempts at this problem in more detail to learn from their attempts, it was important to think through the basics of the problem carefully from the perspective of this project with a well thought out design approach, which will be highlighted in chapter 2. Following the above discussion, the thesis scope becomes clear, and the research questions can be defined to encapsulate the objectives of the thesis:

- What are the key design requirements and equipment required to manufacture, assemble and operate a home-built set-up to test ice adhesion strength?
- What influence do the testing parameters have on the spread and scatter of the data, and how well can this spread be analysed to produce a distribution with a lower standard deviation during validation?
- How do differing materials and topologies influence ice adhesion strength?

2

Background

In this chapter, the problem is scoped out and further defined. A structured design process will be outlined, along with broad initial design requirements and proposals from relevant stakeholders. Although the requirements are designed specifically for this project, particular existing ice adhesion testing designs will be analysed further, to assist with the design process in chapter 3.

2.1. Design Approach

In order to guide the design and construction of the testing apparatus in question, a semi-structured iterative design process was followed. The process was inspired by the study carried out by Atman et al. [74] in their evaluation of the engineering design processes in both students and professional engineers. This particular approach allowed for flexibility in the design and the process, and creativity and compromise where necessary. The design process can be split into three main stages - problem scoping and conceptual design, design activities and project realization. In the first stage, problem scoping, the problem at hand is defined, and the 'need' of the design is identified. This stage allows for the setting of some loose design requirements which may be subject to change, along with certain basic design requirements and constraints that may be non-negotiable. In this stage information required to generate a design is also gathered, such as examination and review of existing solutions, or speaking to stakeholders who may have relevant experience, insight or unforeseen constraints that may apply to the practical side of constructing a measurement apparatus.

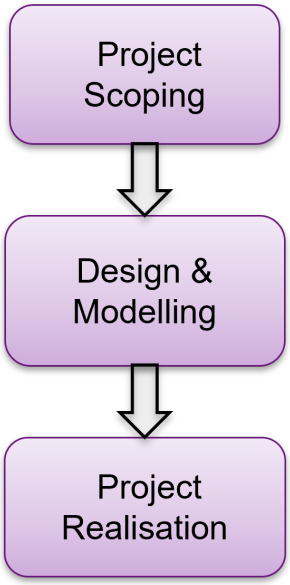

Figure 2.1: Flow diagram of design process [74].

The second stage will incorporate all of the relevant design activities, such as the generation and comparison of different ideas and evaluating trade offs. Requirements modelling is a critical step in this stage - accurately estimating parameters dimensions, loads, and costs will be useful in producing initial design drafts. Feasibility analysis could also be used at this stage of the design process, in order to verify that the design direction still meets the design requirements, and to analyse each component individually to ensure its work-ability and integration in the wider assembly. This also helps with the early identification of potential issues and design bottlenecks. Project realization is the final stage of the design process. In this stage, the design decisions are made, drawings are produced and the parts manufactured, along with the procurement of necessary components and resources. Once all of the components are secured, each of them can be tested individually and calibrated if necessary, and then assembled in the initial configuration and integrated into one system. From here, initial testing can take take place to gather vital information, data and feedback on the effectiveness of the deign, and to the degree to which it meets the design requirements. This feedback can be used to make further design adjustments until the apparatus is improved, and can be validated against other sources to a satisfactory level. Communication is also a vital component in this final stage, especially in an engineering setting. This can come in the form of conversations with stakeholders, the production of drawings and reports, and instructions and insights for future users and/or designers. It should be emphasised that at many stages of this design process an iterative approach was used, especially in the final stage when the first prototype was developed. This approach will hopefully lead to an effective, flexible design which is less prone to errors, as the feedback from the prototyping and testing is the most valuable information when attempting to continuously improve the design.

2.2. Design Requirements

As a starting point in problem scoping, the problem was broadly defined and summarized as follows:

'Novel coatings and surfaces which may have low ice adhesion characteristics which need to be measured and compared, in order to establish their effectiveness. A measurement set-up will be designed to test and analyze these materials in terms of ice adhesion'.

From here, it was necessary define the problem further, and to establish a more specific 'need' of the design. This 'need' essentially encapsulates the purpose, motivation and objectives for carrying out the project. Several questions were useful in getting this process moving:

- Why is the ability to quantify and compare the ice adhesion strength for different materials important or useful?

- What are the primary functions of the ice adhesion measurement set-up that will be designed and built?
- What are the key components required to create an ice adhesion set-up?
- What can we learn from other research projects and set-ups who have attempted to quantify ice adhesion in the past?
- Why does the reported data from these projects have such a large scatter?
- Are there any physical or logistical constraints that need to be considered?
- Who are the key stakeholders in this project and what relevant information can they provide?
- What kind of data is to be collected, and how will this be used to investigate the research question?

Starting from these questions, the shape of the design requirements began to take place. First with a general discussion of the proposals for the set-up itself, and then a closer look at some of the other attempts from literature.

This initial problem scoping and shaping was done alone, before involving key stakeholders of this project which included research supervisors, laboratory supervisors and laboratory technicians. Certain objectives, constraints and 'wants' for the apparatus and project were communicated, along with general input and knowledge from their experience of similar projects. These meetings, which also took place for the design and modelling phase, were incredibly useful in building out design requirements from the ground level and outlining what was expected, which are key factors in any engineering design process. These original design requirements and proposals are as follows:

Design

- **Function:** The proposed primary function of the apparatus is to gain an understanding of how ice adheres to various materials, and to investigate the effect of changing chemical and physical topologies on the ice adhesion strength.
- **Analysis:** The ice adhesion strength can be quantified for each material by the application of a force which will lead to fracture, which can be measured and applied in numerous different ways. The method of loading and mechanism of fracture are naturally linked, so consideration for the analysis of ice and the fracture surfaces during the experiments is deemed to be an important feature.
- **Control:** In an ideal set-up, the differences between one test and the next should be minimal, which points to the need for tightly controlled parameters and environmental conditions in order to achieve consistency and reliability in the results. The ideal type of ice that would be tested is one that is most similar to that found in flight conditions, namely impact ice. However, more importantly the type of ice produced should be somewhat controllable or at least consistent across all tests, as the primary objective relates to the ability to compare materials under identical conditions.
- **Speed:** Feedback from previous users and designers suggests that ice adhesion testing is typically very time consuming. A design which features the ability to test multiple samples in a short space of time would be favored.
- **Modular:** The set-up will require five main components: A housing chamber, a cooling system, a force application method, a data acquisition (DAQ) system, and moulding for the ice. This should be a compact, modular user friendly device that is suitable for a laboratory setting.

Validation and Results

- **Validation:** Once designed and built, the apparatus will need to be validated from data against other similar set-ups from literature. As the scatter in literature is usually quite large, the apparatus design should be closely related to at least one existing design with available data to ensure confidence in validation. This will be reflected in later design decisions.
- **Accuracy:** One of the goals for the set-up design is to bring it to the level of 'accuracy' found in literature with a high degree of confidence, which can be measured by the standard deviation of the ice adhesion data for a particular material such as aluminium. This is approximately in the range of 15-30%, and the objective is to match or improve upon this figure.

- **Data:** To assist in validation and the interpretation of results, the data collected should be both qualitative and quantitative, so that results can be correlated from at least two different sources.

Constraints

- **Time:** The master's thesis naturally has time constraints of approximately 9 months. For this reason among others, a simple but effective design is favoured, with considerations made for the future work and research of other users.
- **Budget:** The project has no set budgetary requirements, but a modest budget should be assumed, with the use of existing components from the faculty where possible. Any larger purchases will need to be justified with solid reasoning and perhaps be multi-functional, so that they can be used for other projects in the laboratory environment in the future.
- **Resources:** Where possible, it is preferable to use or re-purpose components and equipment that is already available in the lab and aircraft hall, in order to fully utilise available resources.
- **Versatility:** Where possible, the design and components should be versatile and multi-functional, so that the components can be used in future projects and for other purposes.

Using these proposals as design guidelines, the design can be produced in such a way that reflects the 'needs' and 'wants' of current and future users. The relevant stakeholders are also taken into consideration, and the expectations of the project are clearer. However, it would be remiss to ignore the input of other attempts at this problem, as plenty of valuable information can be gleaned from others experiences. From here, the design and modelling can begin.

2.3. A case for the horizontal shear design

Taking all of the information learned from the analysis of the existing techniques in chapter 1 into consideration, along with the guidelines from the initial design requirements and constraints, the direction of the design which matches for the objectives of this project becomes clear. A horizontal shear test appears to is the most logical choice in this scenario. It is the most attempted technique, with various examples of both numerical and experimental studies. In a field where numerous parameters and variability decrease the reliability of experiments and data, simplicity is key. Both attempts at the creation of a standard for ice adhesion testing appear to agree with this opinion, as they both employ horizontal shear tests. The horizontal shear test arguably has the least amount of 'moving parts', and is something that is achievable to design, build and validate in the timeline of this project. If designed with the appropriate care for how the set-up will be used and controlled, it should be possible to correlate quantitative and qualitative data to changing parameters, and therefore take the first steps in reducing the standard deviation and investigation of 'inherent' scatter of ice adhesion testing. In addition to this, there are two excellent examples of horizontal shear testing which are both based on similar approaches of Mueler et al. [19]. Biro built an ice adhesion set-up to test charged polymer coatings in his PhD thesis, which had a couple of impressive design features and a standard deviation for bare silicon wafers of approximately 15%. Luca Stendardoalso built a similar set-up to investigate ice adhesion mechanisms, as part of PhD project in the SURFICE consortium to which this project is linked. The ability to contact Luca directly and learn from his experiences presented a huge opportunity in the context of this project, as he has investigated both ice adhesion mechanisms and the effect of changing physical set-up parameters such as ice height and push height on ice adhesion strength, both experimentally and numerically. Additionally, access to raw ice adhesion data for similar materials is invaluable for the validation of the set-up. Therefore, these conversations influenced design decisions, and the intention was to apply the lessons learned form Luca's work. As a result, both Luca's and Biro's work inspired the design of the apparatus. However, an independent process during design was still important, and the potential for improvements in both designs was clear.

Biro's design consists of standard components which also match the needs of this project - a housing chamber, a pneumatic piston to apply force, a cooling system, a load cell with DAQ and a novel method to apply the mould to the surface to grow the ice. This last feature, named a weighted alignment block, allows for the testing of 8 samples in one testing session, with easy repetition and reproducibility between the sessions. The alignment block is also cleverly designed to have holes for injection of the water into the Teflon moulds below, before the ice is allowed to freeze and the alignment block can be

moved from atop the moulds. This technique matched very closely with one the design goals of this project, to increase the speed of the tests, with a very simple solution. Other interesting features of this set-up include humidity reduction with dry air, and slots with clamps to hold the coating samples in place. Cork is used a simple, cheap solution to insulate the chamber. The eight samples is a definite plus in this design, however the orientation of the 4 x 2 it may lead to some operational errors. If the ice adhesion strength is higher, for example when testing aluminium or steel, the ice will detach at a higher force, and this may cause the moulds to propel forward and crash into the pillar of ice on the opposite side which has yet to be tested. This may cause unpredictable errors such as premature crack initiation at the ice-surface interface, that are particularly difficult to detect and record if the housing chamber remains closed for the entirety of all of the tests. Additionally, during operation the box was not opened between tests in order to preserve the environmental control, however this is a significant compromise, as it does not allow for verfication of the ice type or the inspection of fracture surface. This design produced some reliable results and ticked many of the boxes of the design proposals for the design, validation and constraints. Therefore, the overall conceptual design of this project was heavily inspired by Biro, after careful review and discussion with the key stakeholders.

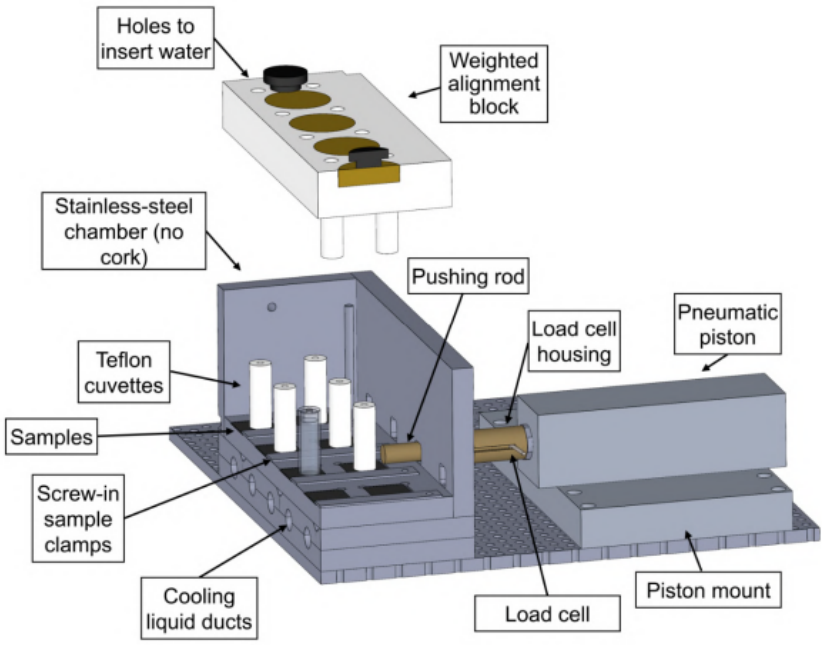

Figure 2.2: Schematic illustration of Biro's ice adhesion testing apparatus[65].

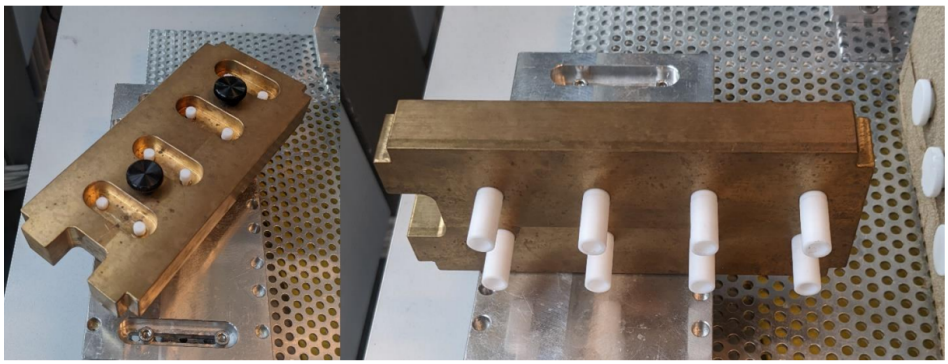

Figure 2.3: Weighted alignment block which increases convenience and reproducibility in the testing procedure. The white cylinders are the Teflon moulds, and the white stoppers on the left hand side allow for injection of the water for freezing. [65].

In Stendardo's set-up, a stainless steel pushing probe is attached to a force gauge, all on top of a linear motion stage. Cooling is applied by a peltier stage, which may be a long term issue as its efficiency decreases over time. A transparent environmental chamber made of perspex is used , which may not the most efficient in terms of cooling and environmental control, however it does allow for the recording of the ice fracture with a high speed camera. The samples are clamped in a similar fashion to Biro, however the major disadvantage of this design when comparing the two is the ability to only test one sample with Stendardo's design at a time versus multiple. The straightforward design and lack of moving parts in the design however implies good repeatability between tests, and multiple geometries and pushing heights can be tested without the constraints of the alignment block from Biro's design.

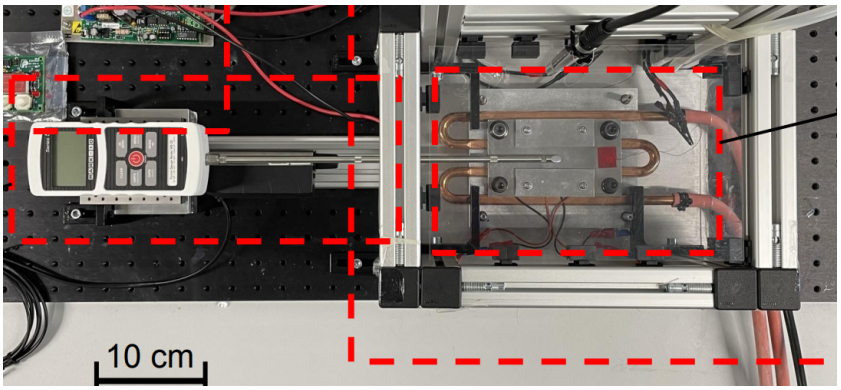

Figure 2.4: Operational set-up of horizontal shear design from Stendardo [17]

.

Also from the published article regarding the set-up, a useful design process flow diagram was outlined to assist in the design of future horizontal shear set-ups, as depicted in Figure 2.5. However, a key part of this design flow and a focus of the study by Stendardo et al. was utilising a numerical model to help understand ice adhesion mechanics further [17], which is outside the scope of this thesis. This may limit the results analysis slightly, as without access to geometrical parameters such as the SSIF as was discussed in chapter 1, the average critical shear stress will be used. In order to mitigate the amount of potential error by remaining in the stress-dominated failure regime and still use Stendardo's analysis to good effect, the key geometrical parameters such as the pushing height h, the ice height H, the mould diameter D, can be chosen according to the optimisation in the study. Using this approach, the raw data obtained from Stendardo for the average critical shear stress will allow for a true and accurate comparison during validation.

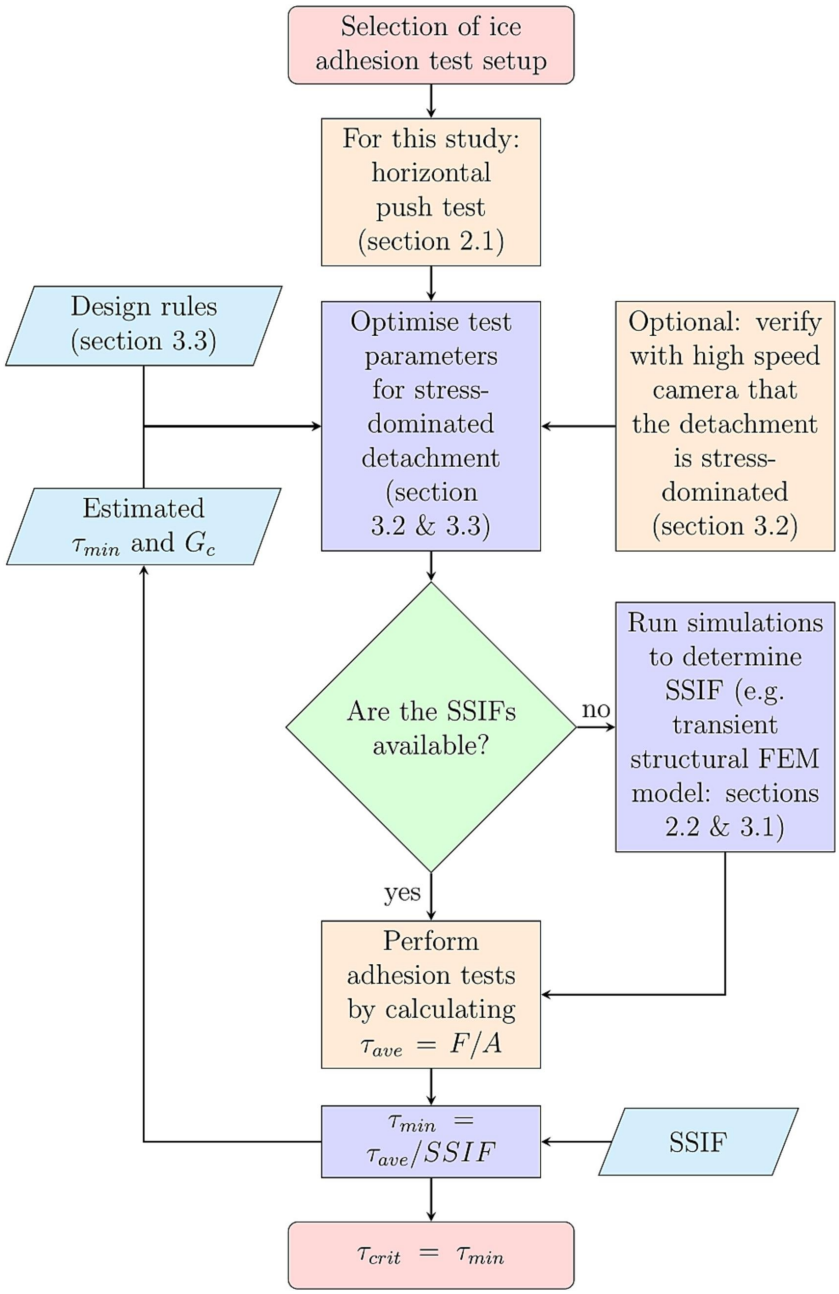

Figure 2.5: Design process flow diagram for horizontal push test from Stendardo et al. [17]

.

Table 2.1: Comparative table of key testing parameters between the designs of Biro and Stendardo

Test parameter	*Biro*	*Stendardo*
Speed of testing	Fast	Slow
Cost	Moderate	Moderate
Complexity	Moderate	Low
Multiple samples?	Yes	No
Impact ice?	No	No
Failure analysis?	No	Yes
Standard deviation	≈ 15%	≈ 25%
Validation	Difficult	Easy
Force curve?	Yes	Yes
FEM model	No	Yes

Comparing both of these designs in Table 2.1, it is clear that they both have strengths and weaknesses. Biro's design is robust, fast and has impressive design features, however lacks critical methods of analysis and abundant data specifically on ice adhesion strength. Stendardo's design is simple, effective and certainly priorities the analysis of results in terms of ice adhesion strength, with the addition of the high speed camera and FEM modelling. However, the tradeoff with the camera is that it restricts the ability to test multiple samples at once, and it could be argued that the cooling and insulation could be optimised, which may be causing the slightly larger data spread. Therefore it seems appropriate to take the lessons learned from this analysis, and attempt to incorporate the best elements of these designs where possible. It is important to not stray too far from what has worked in the past for validation purposes. However, as the design requirements and constraints will always be slightly different for this project, creativity and innovation will be required to incorporate various elements into a set-up that is robust, versatile and accurate.

3

Design and assembly of an ice adhesion set-up

In this chapter, the design procedure and assembly of the ice adhesion set-up will be outlined. Following the general guidelines and information gathered from the previous chapter, a horizontal shear design is chosen. The design begins with general brainstorming and idea generation on the conceptual design, before focusing on how to incorporate key design features into one system. Once this is established, the individual components can be modelled by their requirements and constraints, such as the minimum and maximums for the dimensions, load limits and measurement ranges. Taking these requirements, procurement begins and the suitable components are sourced and compared, to ensure they meet the needs of the design, and also to ensure that they can be suitably integrated and assembled. The process of assembly and operation is then described, noting any significant design changes and compromises necessary to make the set-up work well in practice. Much like any engineering process, this was far from a linear progression, however the design activities from start to finish were an excellent learning process.

3.1. Conceptual Design

The design of choice is a horizontal shear or push test, so naturally many of the basics will not change. The set-up will require a method of force application, cooling, housing and a data acquisition system. With some of the key components established, the first design concepts can be generated. From the initial concepts, it came time to decide on the inclusion or exclusion of certain design features, by analysing their feasibility for this project. There were certain design features that were favoured from the beginning, so naturally they appeared in the conceptual design. The alignment block from the design of Biro [65] was one of these components, due to the overall utility and repeatability it brought to the testing. Not only does it place multiple moulds at once, but it also compresses each of them to reduce the risk of spilling under the moulds, and allows for the injection of water. For this reason, it was a priority to include in the design.

One design element that will be included is a linear rail, which can be operated by hand. This increases the speed of testing as there is no requirement to unbolt, reposition and then rebolt the pushing device between tests. This feature increases consistency and repeatability, making for a more fluid testing experience. A fully functional rail system was already present in the aircraft hall, and was no longer used for the function it was designed for. Therefore, this was opportunity to take advantage of the resources available. The idea to add a Y-directionality to the rail which would be used the X-direction was proposed, so that the pushing device would not be limited by a maximum travel range for example, and the device could be pushed in and out of the chamber manually. However this idea was scrapped after consideration, as an additional Y-rail would need a coupling mechanism with the already fully functioning X-rail, or the entire X-rail would need to be placed on top of the Y-rail. This would add additional height requirements in other aspects of the design, and in a set-up where pushing height is

critical down to the mm range and vibrations or instability could strongly affect the results by inducing unwanted stresses in the ice being tested. In order to avoid adding complexity, stability and simplicity with were prioritised, so the X-rail could be implemented as is.

Figure 3.1: Linear rail which was available for use for this project

The high speed camera would be a useful tool to observe crack propagation as seen in Figure 3.2, however it was found that its inclusion will constrain the design in other ways. An external camera would have to be mounted on a stable system above the housing chamber, directly above the ice being tested. This implies that there is visual access to the ice - as the chamber cannot be open to the surrounding environment, the chamber would have to be glass, perspex or another transparent material that would need to be almost fully transparent for the duration of testing. If there are multiple samples to be tested, that means that the camera would have to be movable, be that on a rail or moving clamp of some sort, which adds increased complexity. Additionally, an alignment block with a similar design to Biro would be out of the question, as the moulds in that case would be closed with a chute for an injection, as opposed to open cylinders. With an external camera considered and excluded for the reasons above, an internal camera inside the housing chamber was pitched. This would likely be less complex, if something like a keyhole camera was used. However, without sufficient lighting in what otherwise would be a closed, dark chamber, the camera would be next to useless. Additionally, an internal camera could only verify perhaps what direction the mould falls upon breaking, which is not near as valuable as viewing the ice itself.

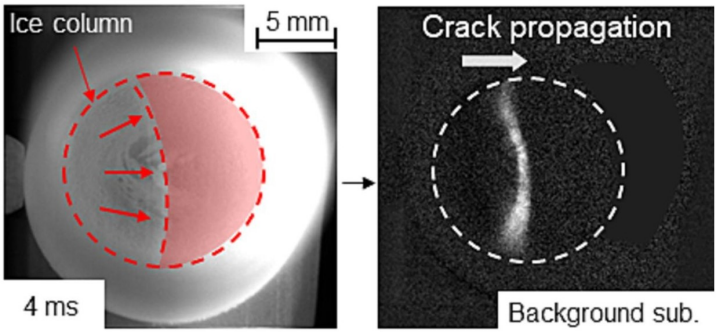

Figure 3.2: Crack propagation in an ice column captured by the high speed camera in Stendardo's set-up [17].

A spray nozzle was considered for the application of impact ice to the samples being tested, in a similar fashion to the centrifugal set-up utilised at AMIL [20]. The ability to test more 'naturally' accreted ice would generally be favoured, in order to replicate the conditions of a flight more closely. A spray nozzle

which produces freezing rain could achieve this, however the drawbacks are also apparent. Logistically, it would difficult to test multiple samples, as the assumption is that moulds are required and driving ice growth in one specific area of a chamber filled with freezing rain would be challenging. Likely the spray nozzle would run into similar issues as the installation of an external camera - mounting, stability, movement etc. One of the requirements of this set-up is to produce a testing device that can accurately compare coatings and materials against one and other. With a spray nozzle, identical conditions between samples would be difficult as the ice which is accreted is unlikely going to be of a similar structure from one test to the next, as there will always be an element of randomness. This is also without considering the other conditions which might influence the result, such as humidity. Bulk ice is much simpler to replicate from test to test. This is likely a very interesting type of test to run to see the influence of spray parameters on the ice accretion and adhesion, but it adds unnecessary complexity and does not fit exactly the goals of this project.

3.2. Requirements Modelling

As a starting point, the initial requirements and constraints for the design from chapter 3 can be referred to. These design requirements are slightly too broad to create a detailed design, so the proposed set-up can be categorised by its individual component and functions in order to begin modelling and shaping the requirements further. In building a set-up that is robust and flexible, a global perspective of all the requirements early in the process is important so as not to get pigeon-holed into a restrictive design. This is represented in Table 3.1 below, where key ideas and considerations from the stakeholder discussions are also included. The initial thoughts for this design were that humidity and temperature control were the priority, along with a precise measurement when recording the forces at fracture. During modelling, further design decisions were made on the best 'type' of component that could assist in achieving the design objectives. Before procurement or manufacturing can take place, it is also important to define the detailed requirements for each component - load limits, ranges, sampling rates, etc. The geometry and dimensions of the procured components will strongly affect the geometry and dimensions of the custom designed components, so this is a critical step to ensure a smooth assembly and system integration.

Table 3.1: Initial considerations and potential functions for the relevant components

Component	*Functions and considerations*
Housing Chamber	Housing, materials, humidity control, temperature control, insulation, sample clamping, sample size, building of tolerances, manufacturing, CAD
Cooling system	Chill samples, peltier, chiller, spray nozzle, create impact ice, create bulk ice, ice control, temperature ramping, cooling rates, heating system
Piston/Actuator/Motion stage	Force application, speed, precision, quasi-static range, minimum incremental distance, versatility, adhesives testing, load limits, constraints, impact, controller
DAQ	Load cell, camera, strain gauge, force gauge, signal amplification, calibration, precision, noise, errors, data collection, data type, sampling rate, automation
Moulding & Accessories	Mould material, alignment block, number of samples, injection, speed, repeatability

Housing Chamber:
For the housing chamber, the critical function is to assist in the control the humidity and temperature to some degree, whilst holding the ice pillars in a stable environment. Stainless steel will be used, for its stiffness, ease of manufacturing and corrosion protection, with additional cork insulation. Additionally, the housing chamber needs to integrate all of the components, so will essentially be the centerpiece for the set-up. The dimensions of the housing chamber are therefore critical, as it becomes a balancing act between dimensional constraints from the piston/actuator, load cell, cooling system, samples, measurement sensors and alignment block. The first design decisions were the amount of samples and size of samples that were to be tested, as this has the largest influence on the dimensions of the chamber and the alignment block. It was decided to build the set-up to be able to test 5 samples in one testing run. This will take place in a 5 x 1 orientation as opposed to the 4 x 2 orientation which was utilised by Biro. The reasoning for this is that when one ice pillar breaks, the mould could be shot forward depending on the forces at play. Therefore, there will be minimal interaction from one test to the next, which could not be guaranteed in Biro's design. This also reduces the complexity and number of components, as the moulds only need to be pushed from one side of the box. 5 samples was deemed to be a suitable amount, to keep the design compact, but still be able to test up to 30 samples per 8 hour day. As the typical samples which were currently being used to create novel materials and coatings in the faculty were 20mm x 20mm x 1-3mm, the slots which would hold the sample were decided to be 22mm x 22mm, with a depth of 1mm into the chamber. For sample thicknesses above 1mm, care will be taken in the other parts of the design to ensure the pushing heights can be adjusted or accounted for in some way. The length of the chamber is now defined, however the width of the box is dependent on the travel range of the actuator or the length of the pushing probe, and the height is dependent on the mould size and alignment block. An excessively large chamber could make life difficult when trying to control the environmental parameters and increase the testing time waiting for states of equilibrium, so a compact design which fits the constraints of the aforementioned components will be prioritised.

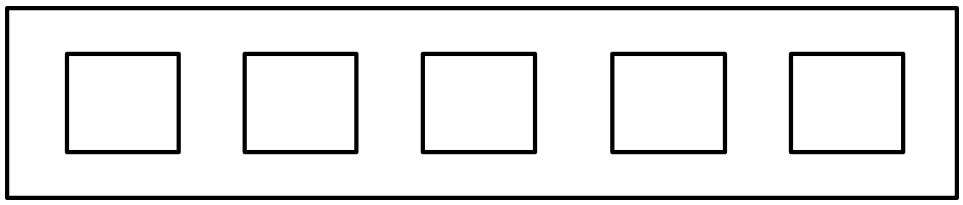

Figure 3.3: Plan view schematic of simplified 5 x 1 sample orientation for the housing chamber.

Cooling & Humidity system:
The primary function of the cooling system is to control the surface temperature of the samples, and to create bulk ice in the moulds. The simplest way to achieve this is apply the cooling to chamber material, which in turn will conduct heat through the material and cool the sample. With a sufficiently cold surface temperature, the low volume of 0.5ml required to create the ice column of height, $H = 10$mm, should freeze upon injection almost instantaneously. This can be achieved using a peltier plate, or an external chiller. The chiller would need an external tubing system to apply the cooling, where as the peltier plate itself mould need be integrated into the dimensions of the set-up, as it would act as the base of the testing chamber. Both were considered for the cooling function, and will be further discussed and compared in the procurement section. As the cooling chamber will frequently be opened to inspect the samples and ice immediately after testing, precise humidity control will be next to impossible. Therefore, it was decided that a low humidity system would be sufficient, as the requirement is predominately a dry testing surface to avoid any external effects from condensation frosting on the ice pillars, and this can be achieved with a weak flow of nitrogen into the chamber.

Table 3.2: Chiller/Humidity requirements

Parameter	*Minimum*	*Maximum*	*Unit*
Operating temperature	-40	50	$^\circ$ C
Relative Humidity	1	10	%

In order to give options and flexibility for future icing research, the minimum operating temperature should be -40° C, while the maximum is of little importance for this application. The relative humidity should always be below 10% during testing.

Actuation & Load cell:
The tool to apply linear displacement and subsequently force with a probe was narrowed down to a pneumatic piston, actuator or a motion stage. A motion stage could be used in combination with a digital force gauge, as shown by Stendardo et al. and Meuler et al. [17, 19]. An alternative would be to combine a piston or actuator with a load cell. The latter option was chosen, due to the increased availability and customization available with a load cell. A linear actuator with a DC motor was chosen over the pneumatic piston for precision reasons, as the DC motor should be much easier to control the speed and minimum incremental motion compared to controlling gas compression, especially if an integrated digital controller is available with the actuator. As mentioned, the capacity and travel range of the actuator will be important for integration with other components. The load cell chosen will also need to be mechanically integrated between both the actuator and probe which will push the mould containing the ice. From a conceptual point of view, the precision of the load cell should be high, due to the nature of the test and the motivation behind its purpose. In an ideal world where extremely low ice adhesion coatings are created, ice will be removed at very low stress values. Therefore, the precision of the measurement system needs match that ambition, whilst also maintain the ability to test materials with expected high adhesion, such as steel or aluminium. Additionally, it was pitched from stakeholders that this device could also potentially be used to test more traditional adhesives in another application. This falls under the versatility requirement, so the load cell and actuator will chosen with this as a second objective, behind the primary objective of testing ice.

Table 3.3: Linear actuator requirements

Actuator Parameter	*Minimum*	*Maximum*	*Unit*
Speed	0.01	2	mm/s
Load	0.5	200	N
Min. incremental motion	0.001	-	mm
Travel range	20	50	mm

Table 3.4: Load cell requirements

Load cell Parameter	*Minimum*	*Maximum*	*Unit*
Load	0.5	200	N
Testing force	Compression	-	-
Operating Temp.	-50	40 -	$^\circ$ C

The linear actuator and load cell are mechanically linked, and therefore need to be considered together. The minimum speed and minimum incremental motion of the actuator are important, as the tests will need to take place at a constant velocity and a quasi-static regime. The travel range is set to between 15mm and 50 mm, a larger travel range gives more flexibility in design and compabikty with the housing chamber, due to the omission of the Y-direction rail/motion stage. The predicted loads of the testing are important, for both the linear actuator and the load cell. For area A of the ice pillar of radius 4mm,

$$A = \pi r^2 = \pi 4^2 = 50.3mm^2 \tag{3.1}$$

For an ice adhesion test, the predicted maximum adhesion for steel for example is in the range of 1500-2000 kPa. This translates to a force approximately 75-100N. Taking the average shear stress

$$\tau_{ave} = \frac{F}{A} = \frac{100}{50.3} = 1988kPa \tag{3.2}$$

Therefore, the load cell and actuator should be able to handle a load of at least 100N. To add a safety factor, the max load is set at 200N. The load cell should also be precise enough to sense low adhesion forces when novel materials are developed further, ideally at loads below 1N. However, the precision is also dependent on the DAQ and the calibration, but it is good to consider moving forward. To add a thought towards future proofing the utility of components, ideally this would be higher to accommodate the testing of adhesives, however this is not a priority, so in procurement these will not constrain the design decisions

DAQ:
With the load cell chosen as a component, the framework of data acquisition system becomes clearer. Depending on the load cell chosen, it is anticipated that this will need to be calibrated with a set DAQ set-up. This will require a signal amplifier, and an oscilloscope to read and capture that signal which corresponds to calibrated force value, all of which reads into a computer. The flow of this system set-up is depicted in Figure 3.4. Much of the equipment for the DAQ system is available in the laboratory, which assists in reducing the waiting time for components during procurement. The sampling rate available should be at least 100 Hz.

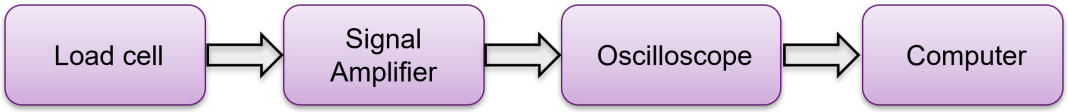

Figure 3.4: Data acquisition system flow diagram

.

Moulding & Accessories:
The dimensions of the mould are defined by the parameters set by Stendardo et al. as discussed in chapter 2, so the dimensions of the mould need to allow for a pushing height *h* = 1-2mm, the ice height *H* = 10mm, the ice pillar diameter *D* = 8mm. The mould also must be suitable for injection and compatible with the alignment block, a mechanism will be required to allow for easy attachment and removal during testing. This should be achievable with a number of materials, but for the purposes of this set-up the material choice Teflon is suitable. Teflon also has a high contact angle making it hydrophobic, so when the water is injected the intention is that the water will preferentially freeze onto the more hydrophilic substrate, and not stick to the sides of the mould or leak out. The samples, with different thicknesses will need to clamped in place during testing, so small adjustable clamps on either side of the samples will be implemented.

With the above considerations and preliminary design decisions, the conceptual design is finalized with the core components integrated with the new design features. The modelling of the requirements was completed with frequent communication to the relevant stakeholders, to ensure that the proposed conceptual design still meets the design requirements, and to reiterate what performance is expected from each component. An example of the outcomes from brainstorming in these meetings is shown Figure 3.5.

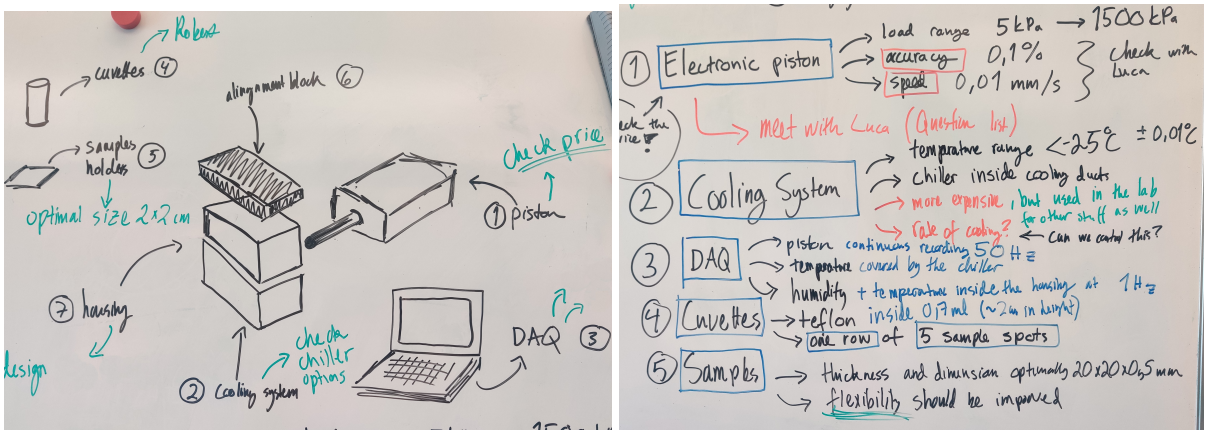

(a) (b)

Figure 3.5: (a) Conceptual design sketch (b) discussions on key requirements

3.3. Procurement and CAD model

Procurement of the necessary components was not straightforward, due to the nature of this being student led project. However, care was taken to stick to the requirement of a moderate budget, with an effort to strike a balance between meeting the requirements and considering the longevity of the set-up, whilst also being resourceful and keeping costs down. The primary components for purchasing were the linear actuator, the chilling component and the load cell. Once these components are decided, the custom components such as the housing chamber, alignment block and accessories can be designed and manufactured. The choice of linear actuator, chiller and load cell are listed below.

Table 3.5: Components selected for ice adhesion set-up

Component	*Product*
Newport	LTA-HL Integrated with CONEX-CC Controller
Chiller	LAUDA-ECO RE1050
Load cell	Home-built

The actuator and the chiller that was purchased fit the requirements of this project perfectly. The chiller had a high temperature range, with the ability to test from -50° C to 200° C, making it a multinational piece of equipment for the laboratory. It also has programmable cooling ramps and a very user friendly interface. Peltier plates were considered, but the decreasing deficiency and non-uniform temperature over the surface were long term concerns. It should be noted that that the cooling liquid chosen and used in the chiller (monoethylene-glycol) only has a more limited range of -32° C , due to viscosity limitations. Similarly, the actuator had very favorable features. A high load, shorter travel range version of the Newport LTA actuators was chosen for this application in favour of a longer range, lower load version. This reduced the travel range to 25mm, but this is with a favorable minimum incremental motion of 0.05 µm and a minimum speed of 0.01mm/s. This allows testing in the desired quasi-static range, and with loading capabilities of up to 120N. This is below the safety factor applied, however was deemed a fair compromise when ice adhesion testing is not expect to surpass 100N. The integrated controller and user-friendly software was also a plus, as it makes the set-up and implementation of the test easier.

It was more difficult to find a load cell which was suitable for this project, but also within a moderate budget. As the precision increases with these instruments, so typically does the price. In terms of mechanical assembly of the load cell and actuator together, it seemed logical to take advantage of the geometry of the actuator which was already purchased, which was equipped with a removable tip and a M6 thread on the inside. Therefore, the search for a load cell was for a double sided M6 thread load cell as seen Figure 3.6, as this would ensure mechanical locking to the actuator and a path to

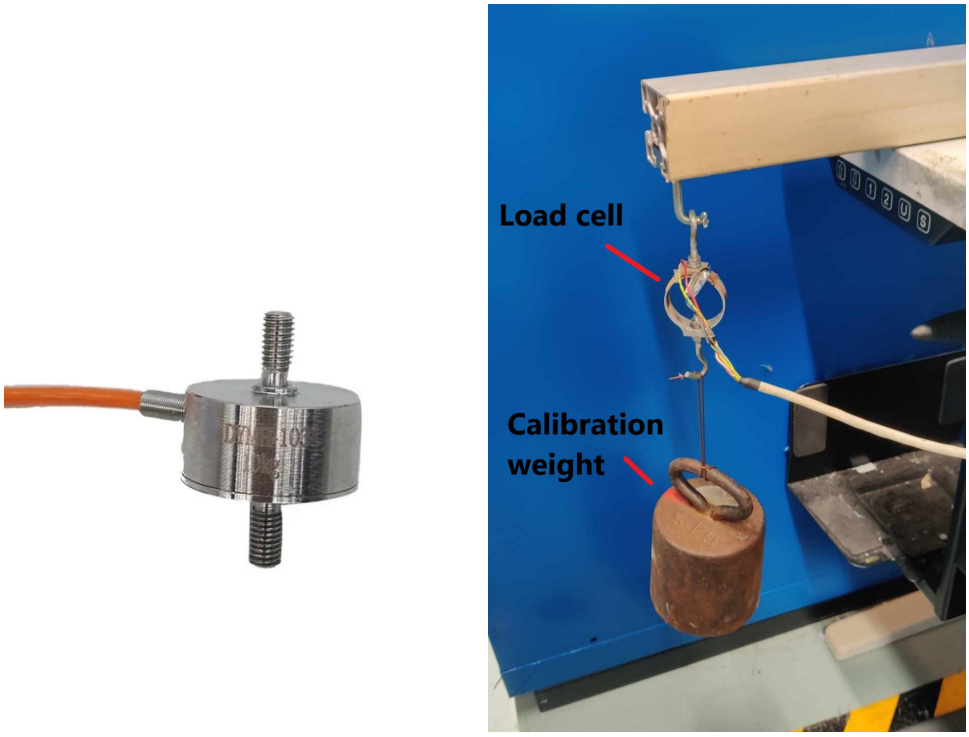

(a) Ideal M6 load cell **(b)** Home built load cell under calibration

Figure 3.6: (a) Ideal M6 load cell (b) Home built load cell under calibration

design a pushing probe with a female M6 thread, so that all three components were integrated into one system. Load cells were readily available in this design for higher load ranges such as 500N, however the sensitivity was poor, and the larger noise signal could potentially interfere with the lower ice adhesion peak stress readings. Other options were not available at trusted suppliers, so instead a different solution was sought. In the end, a homemade load cell designed for an unknown application was located, and adapted to this project. The load cell was not the ideal geometry, however it was in the correct loading range and could be calibrated against known weights so that 1V = 1 $\pm$ 0.002 kg. This was deemed an acceptable level of error for this application. With the majority of components secured and the dimensions set, the custom designed housing and accessories can be modelled in CAD, so that manufacturing can begin. A draft exploded assembly can be seen in Figure 3.7. Using this as a starting point, the conceptual design and project was pitched to the in house manufacturer DEMO, to receive input on what was possible and how the set-up could be efficiently manufactured. There were significant inputs from DEMO on the design of remaining parts where the system integration was slightly more complex, such as the details of cooling chamber under the housing chamber, and changes to the initial alignment block design to make operating the device more practical. After several iterations and adjustments, the majority of the set-up was ready for assembly and construction.

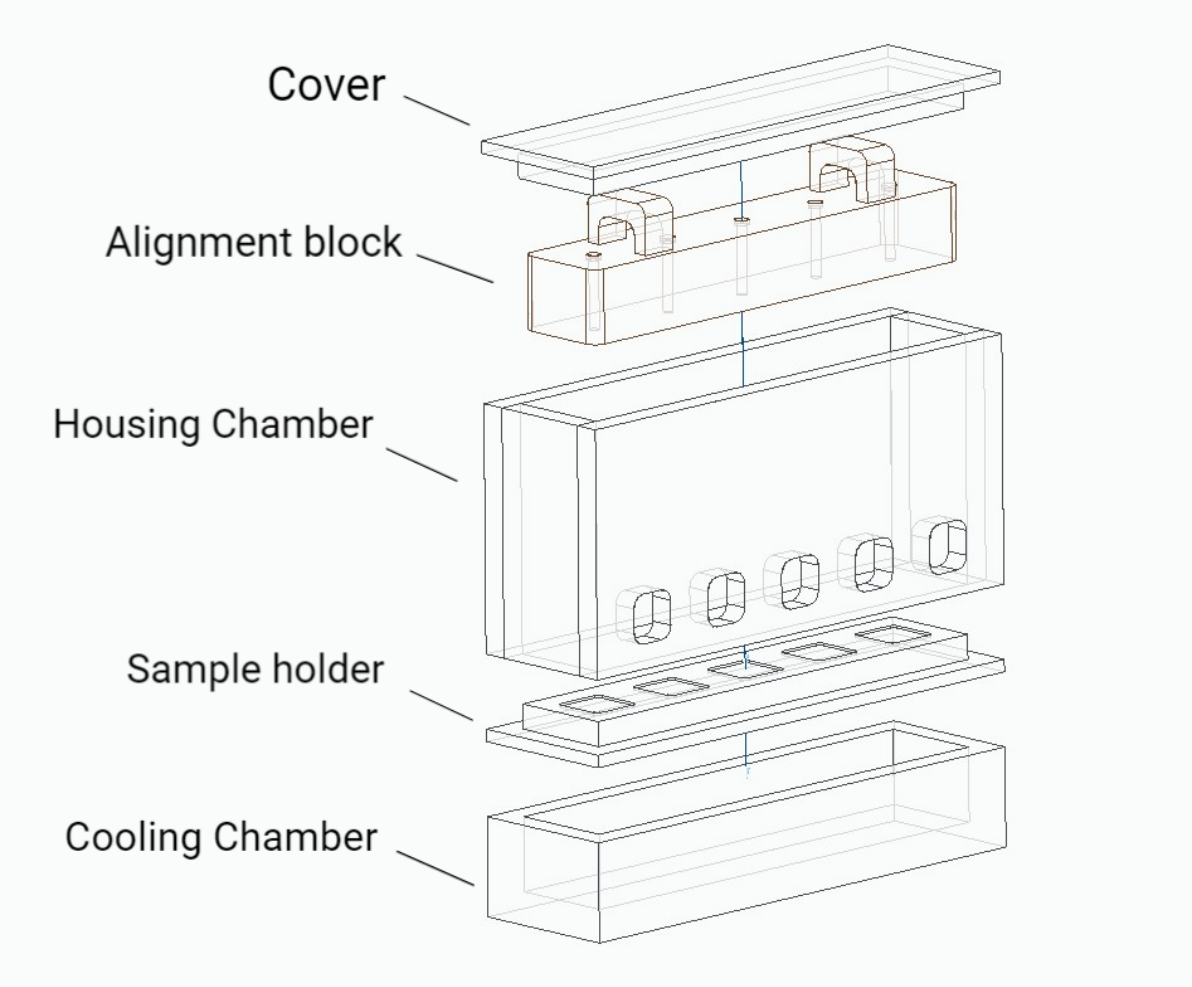

Figure 3.7: Exploded assembly of custom designed housing components and alignment block.

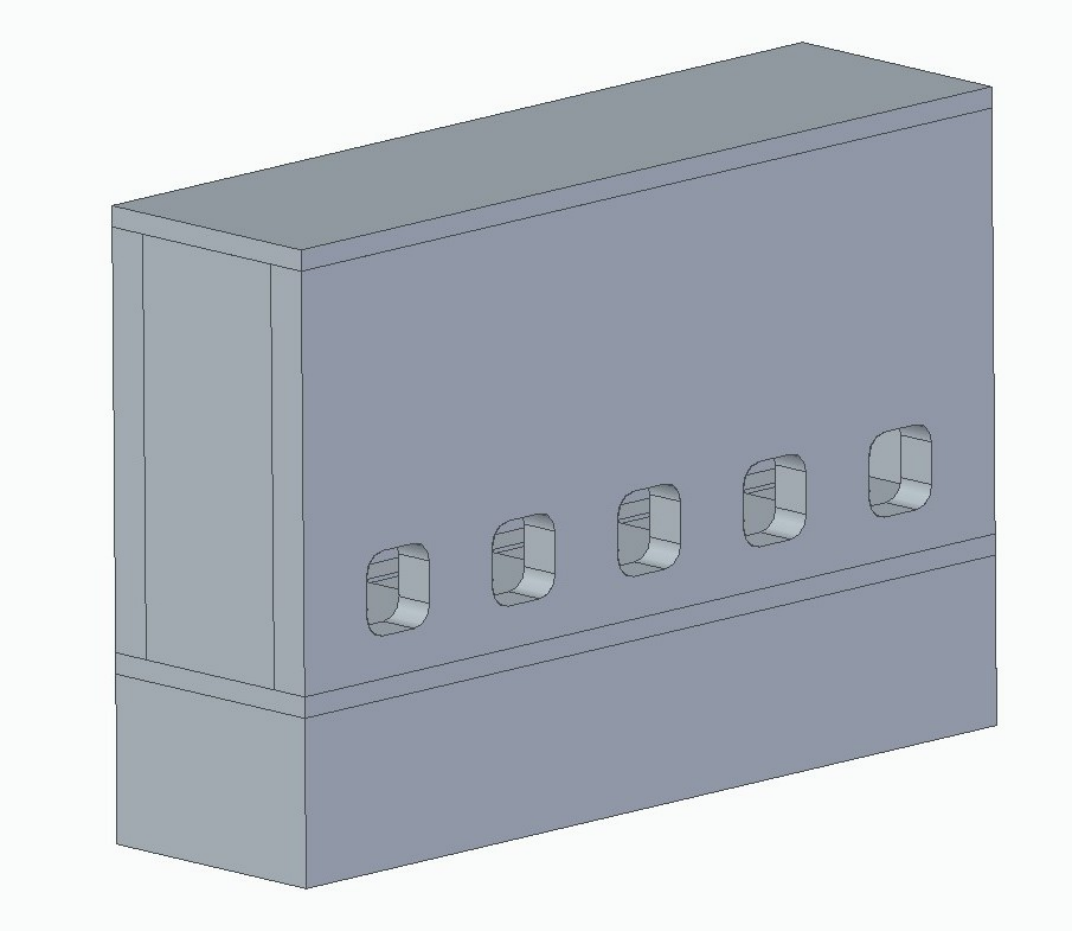

Figure 3.8: Assembly of set-up housing

.

3.4. Assembly & Operation

In the assembly process, each component had to be integrated into one coherent system. As the device is still a prototype at this stage, the functionality of the conceptual design had not been proven. Considering the time constraints of the masters thesis, getting to the proof of concept stage was the priority, in order to begin collecting data as quickly as possible. For example, the set-up is mounted on a series of scrap frames of various heights, which have been tweaked and adjusted to match the heights of the pushing probe with the samples to within approximately 0.5mm. Therefore, many of the fixtures and fittings are temporary, with significant room for improvement in the design. The critical design improvements will be outlined and discussed in chapter 6.

The centerpiece of the design is the housing chamber and other custom components. The majority of the components were precisely machined from stainless steel, and the cooling chamber and sample holder were secured using steel screws at the the four corners of the set-up. The walls of the housing chamber were welded together, with 5 threaded slots machined in the front wall to allow for access for the pushing probe to the moulds. These slots can then be filled with threaded plugs in between tests. Access holes for the temperature sensor and humidity sensor are drilled into the chamber wall, and at a later stage the chamber is semi-insulated with 4mm thick cork. The housing chamber is mechanically bolted to the other housing components to allow it to be removable, but is secure when placed on the sample holder for testing. The alignment block fits smoothly into the housing chamber, and is designed with 5 channels which will allow for the insertion of 5 steel hollow pins, which will hold and align the 5 moulds during injection. The moulds themselves have a hollow chute to allow for injection, and the bottom part of that chute is milled slightly wider and set to create the ice column of height, $H = 10mm$ and diameter $D = 8mm$. The pins are designed to fit snugly into the moulds, and are held in place by a

rubber O-ring. After testing the alignment pins can be used used to push the ice pillar mould for further inspection.

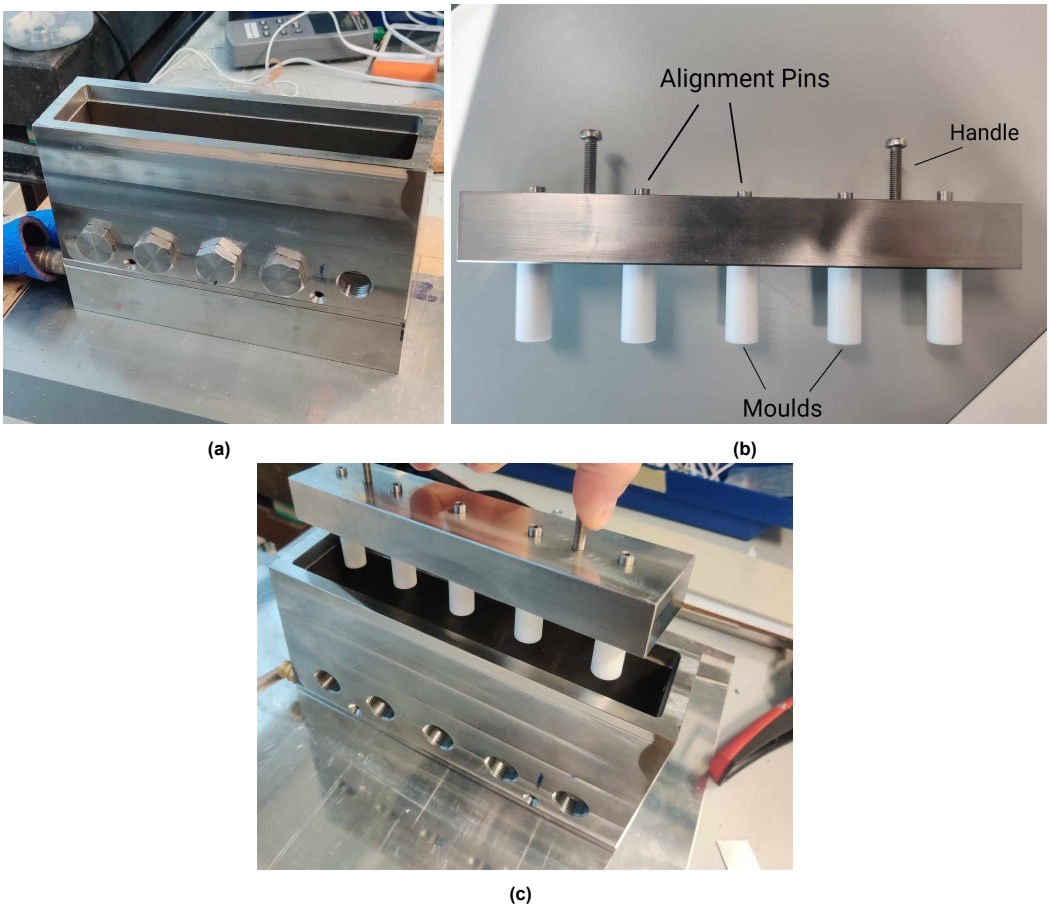

Figure 3.9: (a) Housing chamber with cooling chamber below. (b) Alignment block and (c) Alignment block placement during operation.

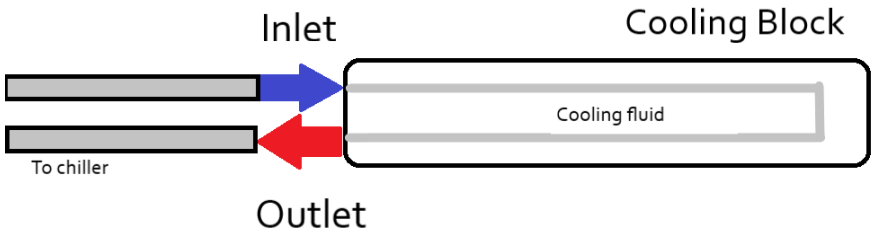

Figure 3.10: Schematic of cooling chamber pipework.

The chiller is attached to the cooling chamber by two insulated silicon pipes, which connect into the pipework of the cooling chamber. The pipework consists of an inlet and outlet which feeds the cooling fluid into a conductive brass block in one run, turning at the fifth slot back to the outlet. This was a simplistic design, but the quickest route to a working system. This in turn will extract heat from the sample holder above and at low chiller set-point temperatures, the samples will be sufficiently cooled to the desired temperature once the system has reached an equilibrium. A simplified schematic of the cooling chamber pipework can be seen in Figure 3.10.

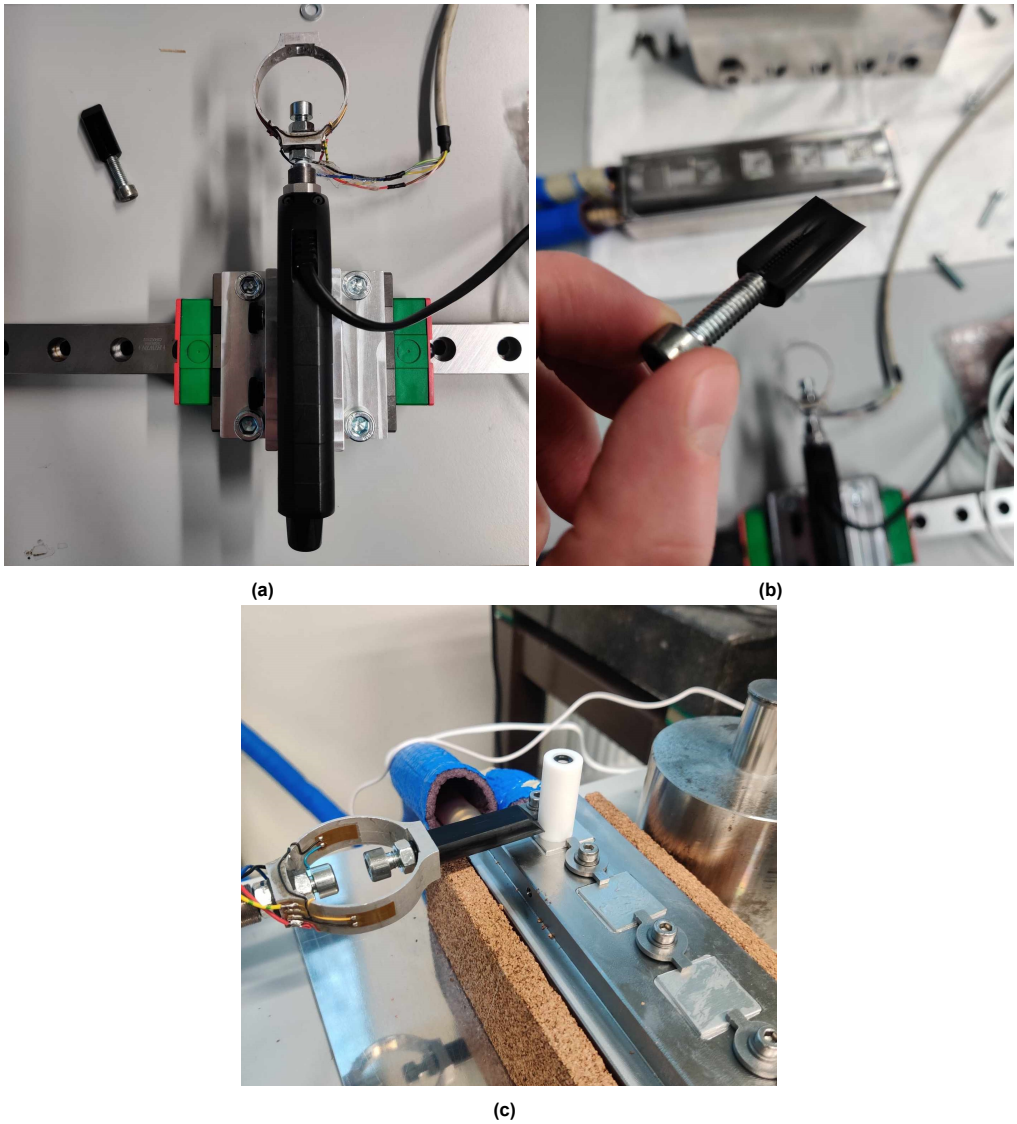

Figure 3.11: (a) Linear actuator and load cell mounted on linear rail (b) Pushing probe connection, (c) Example of pushing during operation, without the chamber walls for visualisation purposes.

As discussed, the home-built load cell needs to be mechanically linked to the actuator. Therefore, a series of nuts, bolts and rubber washers are used to create a M6 link through the load cell. The nuts are tightly fastened, as the compression of the actuator connection against the load cell frame is critical in order to get a consistent and reliable reading. As the load cell frame deforms, the four strain gauges in a full bridge configuration records the deformation in terms of the calibrated load, and this signal is amplified by an amplifier and read by the oscilloscope. The pushing probe is made of polyoxymethylene (POM), which has a high stiffness, good thermal stability and low sliding friction. The probe will push the mould directly during testing. It is designed with a 2mm flat-head tip in a half moon shape, and a M6 female thread in the back of the cylinder to connect to the load cell frame by a simple bolt connection. The linear rail is mounted using countersunk bolts on a stiff plate, which is

Figure 3.12: Set-up without housing chamber for visualisation. (a) Front view and (b) Plan view of moulds on samples,(c) Isometric view with alignment block. By careful removal of the alignment pins, the block can removed from the moulds when the ice pillars are frozen.

simply clamped to the laboratory table, all at 90° angles to the main housing. To integrate the linear actuator and the rail mount, a small additional mount was designed, which also allowed for the linear actuator to be clamped in place by torquing two flat screws against the stainless steel casing. The actuator had to be inverted for this to work, however with the loose and fragile wires from the load cell the orientation worked well. To place the linear actuator within the 25 mm travel range limit required to run a test, the entire actuator can be manually slid into position on the mount so the pushing probe is inside the chamber, before clamping with the flat screws and actuating the pushing probe the at the desired speed and distance. After a test, the plastic wheels can be used to loosen the actuator, and it can be manually slid out of the chamber, and then manually pushed laterally on the rail to the next testing slot. This is not a perfect system as seen in Figure 3.11, but in practice it works sufficiently and is a relatively quick procedure. The final testing layout, which was further improved during the validation, can be seen in Figure 3.13.

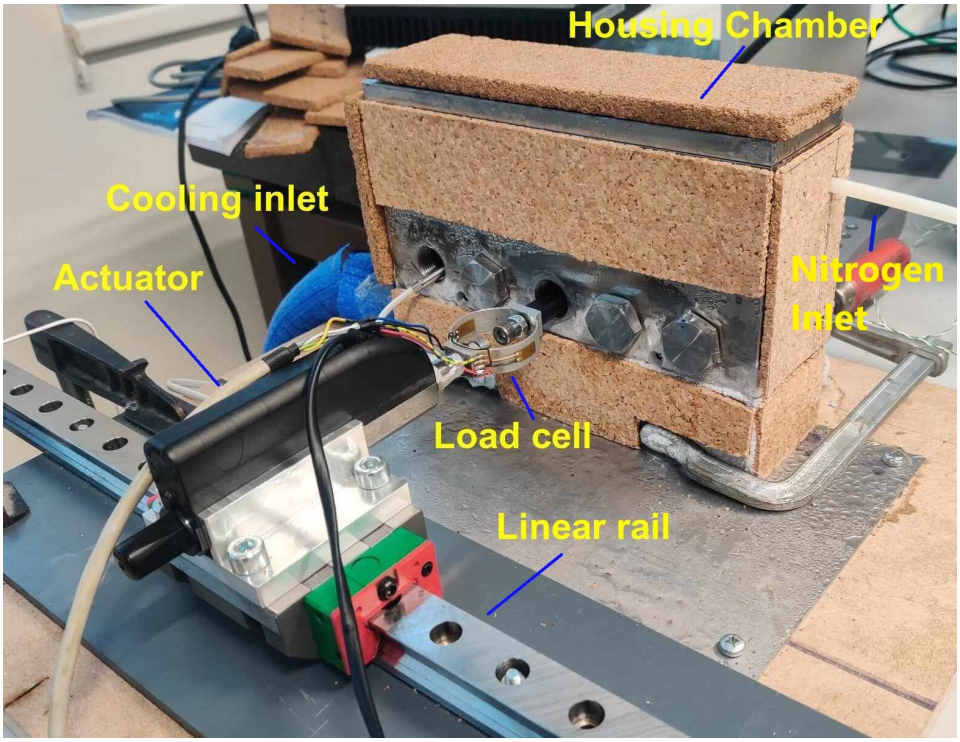

Figure 3.13: Final set-up in operation

The operating procedure is as follows:

- Turn on the chiller and set-up the DAQ for testing. For a testing temperature of -10° C, the chiller typically needs to have a set-point of -16° C to -19° C. Prepare and degrease the samples as needed, and clamp them in place in the appropriate slots. Apply the temperature sensor to edge of one of the samples, place the humidity sensor in the chamber, and turn on a weak flow of nitrogen. Close the chamber and allow the temperature to reach the desired level, and let the relative humidity drop to below 10%.
- Secure the moulds to the alignment block, and place the block on the 5 samples. remove the alignment pins using a pair of pliers, as seen in Figure 3.14, and close the chamber
- Once the system has reached equilibrium, inject the water into the moulds and allow the ice pillars to freeze for the desired time. Once the time has elapsed for all pillars, remove the alignment block and begin testing.
- Unscrew the plug on the slot of interest. Manually position the actuator on the linear rails to be in line and perpendicular to the mould, and then manually slide the actuator inside the pushing chamber until the pushing probe is in line with the edge 20mm x 20 mm. The probe should be approximately 0.5mm to the mould. Replace the cover of the chamber and tighten the actuator using the flat screws on the side of the mount.
- Using the appropriate software, actuate the probe a distance of 3.5mm at full speed of 1mm/s. Change the speed to 0.01mm/s to enter the quasi-static regime.
- Check the oscilloscope is recording and begin the test by actuating the probe to a distance of 10mm. When contact is made, there should be a visual response on the scope due to the changing voltage. Record the data until failure of the ice pillar.
- Return the actuator to its zero position at full speed. Remove the chamber cover and examine the fracture surface and take appropriate pictures. Remove the mould to examine the ice pillar by pushing with the alignment pin, and quickly make an observation on the ice before it melts.
- Save the quantitative voltage data for later processing, and record any notable observations on the testing run, fracture surface, ice type etc. in a spreadsheet for later reference and correlation.

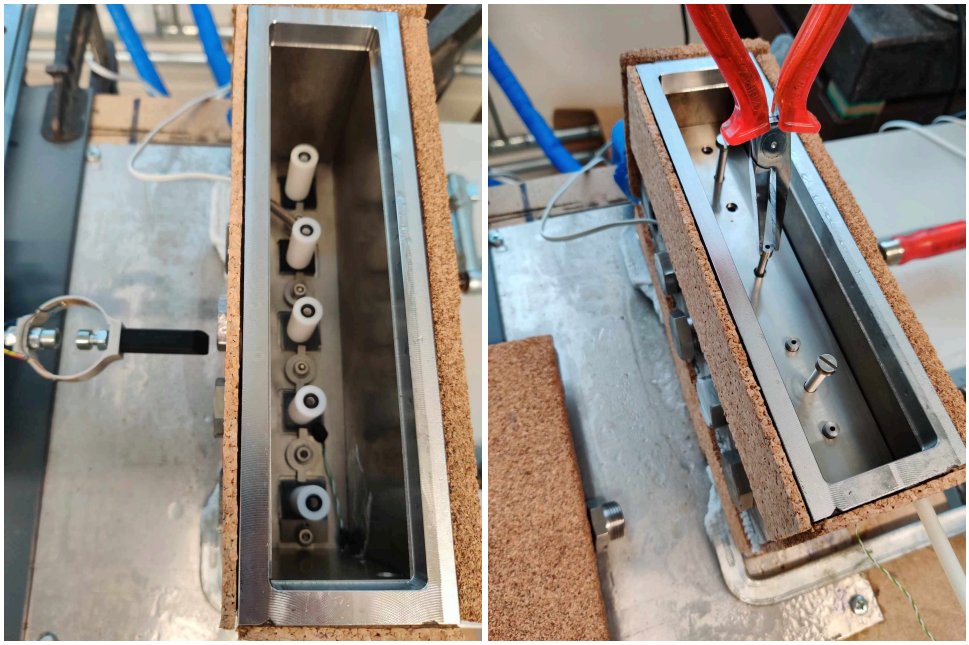

(a) (b)

Figure 3.14: (a) Inside of chamber during during operation. (b) Careful removal of alignment pins during the test set-up. Excessive movement or force may knock the moulds out of position, increasing the probability of an error.

- Return the actuator to an arbitrary position and repeat the pushing procedure for the other slots.

4

Validation of the ice adhesion set-up

Validation of the set-up was a critical component of this project, as it allowed for the interpretation of the results with a known degree of confidence. The approach that was applied was to begin collecting data as early as possible, in order to begin to learn insights about how the set-up was performing. The nature of the data was both quantitative and qualitative - it was possible to correlate individual peak stress data points and force curves to pictures of the ice and fracture surfaces, along with input from laboratory notes and visual observations. From the initial data, the design and operation procedure was adjusted in several iterations until the data began to improve to a level where it became easier to understand and interpret. This iterative approach proved incredibly useful, as the design improvements that were applied were thus data-driven. The purposefully flexible design also allowed for investigations of the influence and effect of individual design parameters on the ice adhesion results. Once the set-up was improved to a level where the errors were reduced results could be consistently interpreted, the data could then be compared to sources from literature. In this chapter, this entire validation process will be outlined and discussed thoroughly.

4.1. Validation Round 1

With the design finalised and the prototype set-up assembled, data collection could begin. This was done with the knowledge that the set-up was not perfect, and as expected there were some teething issues. The initial data collected was for the ice adhesion strength for samples 20mm x 20mm x 1mm, aluminum alloy AA-6082. It should be noted that many uncontrolled parameters were present, but this first round of data was collected with the goal of learning about the design, proving the concept and establishing a reliable procedure and order of operations. The only parameters that did not change throughout the entire validation process are were the probe speed and mould diameter. As the validation procedure progressed, this list grew as more parameters were fixed for increased control.

Table 4.1: Conditions and testing parameters during first round of testing

Parameter	*Notation*	*Target Value*	*Real Value*	*Units*	*Comments*
Probe speed	*s*	0.01	0.01	mm/s	Fixed
Mould diameter	*D*	8	8	mm	Fixed
Push height	*h*	2	3	mm	$\pm$ 0.2
Ice Height	*H*	10	6-12	mm	Injection volume issue
Surface Temperature	T_s	-10	-10 to -18	$^\circ$ C	$\pm$ 0.5
Air Temperature	T_a	-10	-8	$^\circ$ C	$\pm$ 0.5
Relative humidity	*rh*	?	?	%	Relative to T_{amb}, 20° C
Freeze time	t_f	30	30 to 90	mins	Variable

There were many parameters at this early stage which were either not considered critical, or were

poorly measured, which actually proved to be quite important. The target value and real value columns in Table 4.1 reflects this oversight, as some parameters were not controlled as tightly was originally thought. It is clear that this is far from an ideal testing scenario, and this is reflected in the data below in Figure 4.1. The constant tweaking of parameters was necessary at this stage for learning purposes, however it made it very difficult to draw any meaningful conclusions on which individual parameters were having the strongest effect on the results.

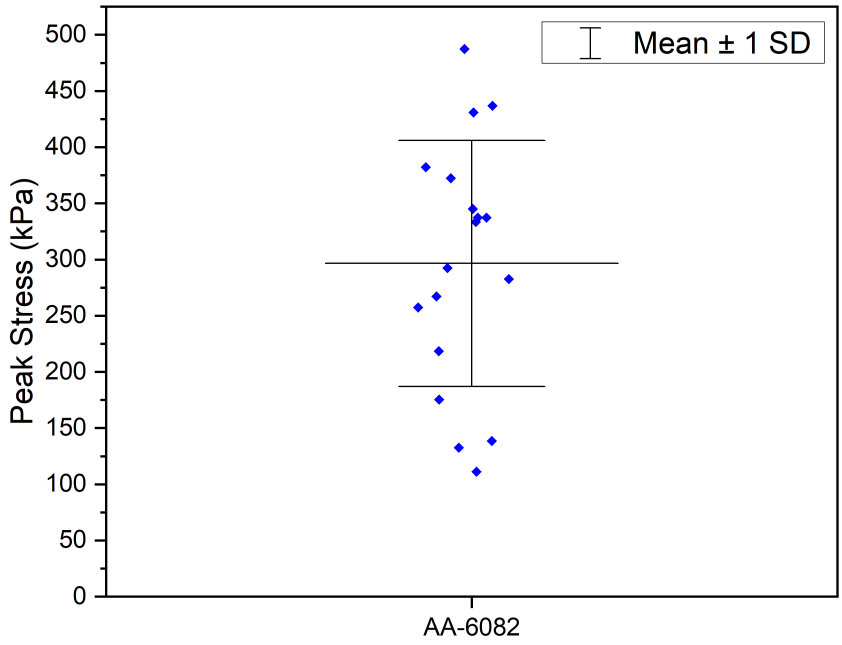

Figure 4.1: First data with peak stress recorded for Aluminium 6082 with uncontrolled variables.

The first observation from Figure 4.1 is that the spread of the data is quite high. In this plot, the individual blue dots represent one test for aluminum. The slight spread in the horizontal direction has no physical meaning, this is purely to separate the data points for visualization purposes. For a sample size of N = 18, the mean value was 297 kPa, and the standard deviation with respect to the mean value was 37%. This is by no means an impressive result, but the spread was perhaps smaller than anticipated when considering the uncontrolled testing parameters. Additionally, many of the tests produced the expected force curves, where the force linearly increases until a clean, adhesive fracture. An example of a typical force curve is shown in Figure 4.2. However, the peak stress values are not in the range of values that are expected when considering an ice adhesion on an aluminum alloy, which is typically between 700 kPa and 1000 kPa in similar ice adhesion set-ups. The typical force curve for The first logical step to interpret these results is to take a closer look at the parameters, qualitative data and testing procedure to begin isolating sources of deviation that may be causing this spread.

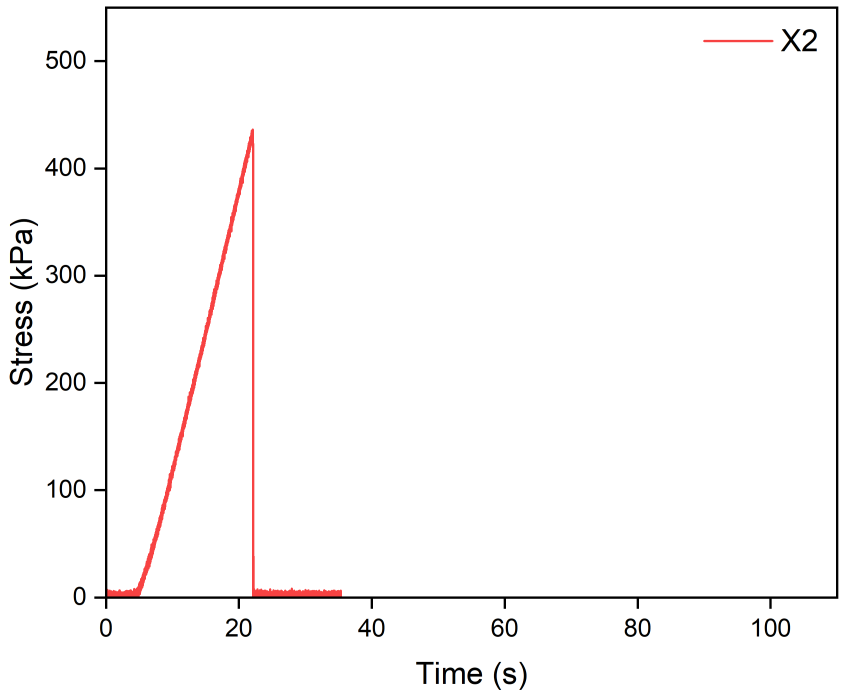

Figure 4.2: Typical force curve for an ice adhesion test with an adhesive failure. X2 corresponds to the second slot location in the set-up.

4.2. Sources of deviation

Upon reflection of the initial data and the testing procedure, the potential sources and explanations for the deviation in the data from the first round of testing became apparent. The investigation began by looking at the influence of the testing location on the set-up. In Figure 4.3, the individual data points from Figure 4.1 are allocated to the slots they correspond to along the set-up, namely X1 to X5 as seen in Figure 4.4.

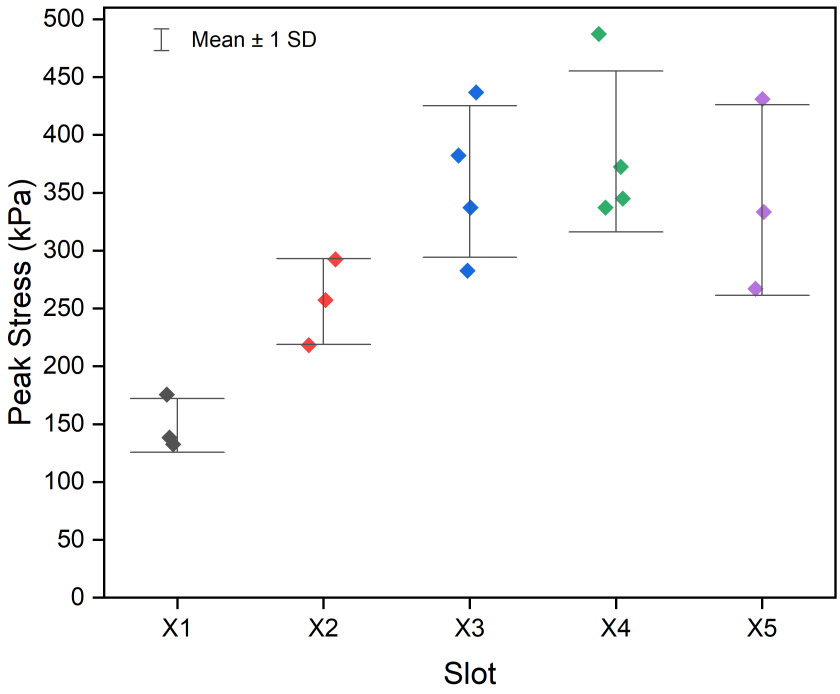

Figure 4.3: Data for first round of testing with uncontrolled parameters plotted against slot location.

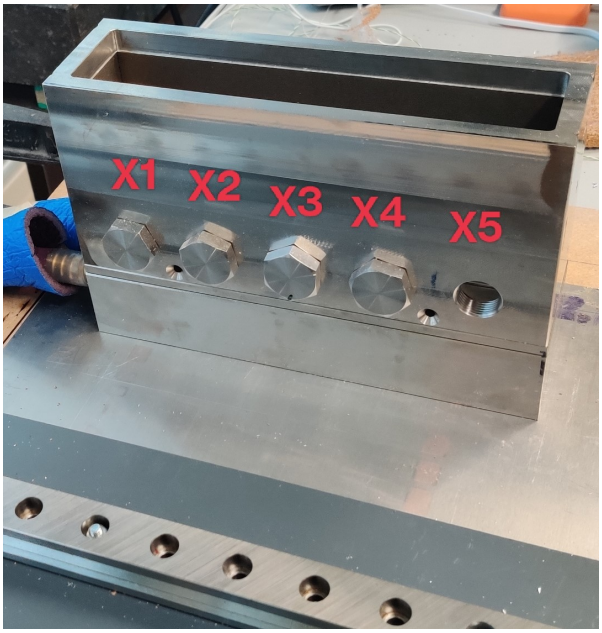

Figure 4.4: Slot locations in the testing set-up.

Immediately, a clear trend is apparent. From left to right when looking at the set-up from the pushing direction, the mean ice adhesion strength increases linearly until the 4th testing slot, X4, before dropping back slightly for X5. Slots X3 and X5 have a similar spread of data, and similar mean ice adhesion strength. The error bars in the data are still quite large, which implies that there are at likely

two or more different uncontrolled parameters causing the overall scatter. Something is causing a spread in the data between the slot locations, whilst other uncontrolled parameters may be sources of deviation between data points at one singular testing location. As this is a freezing experiment, the logical starting point was to investigate the influence of the surface temperature at each slot location, for a constant chiller setpoint, on the results. The surface temperature was recorded across all testing locations with a thermocouple, which was taped onto the corner of the samples using tacky tape. This experiment was also conducted at different chiller setpoint temperatures which would simulate a typical test, and with both aluminium and polypropylene to examine if the trends remained consistent for both metals and polymers.

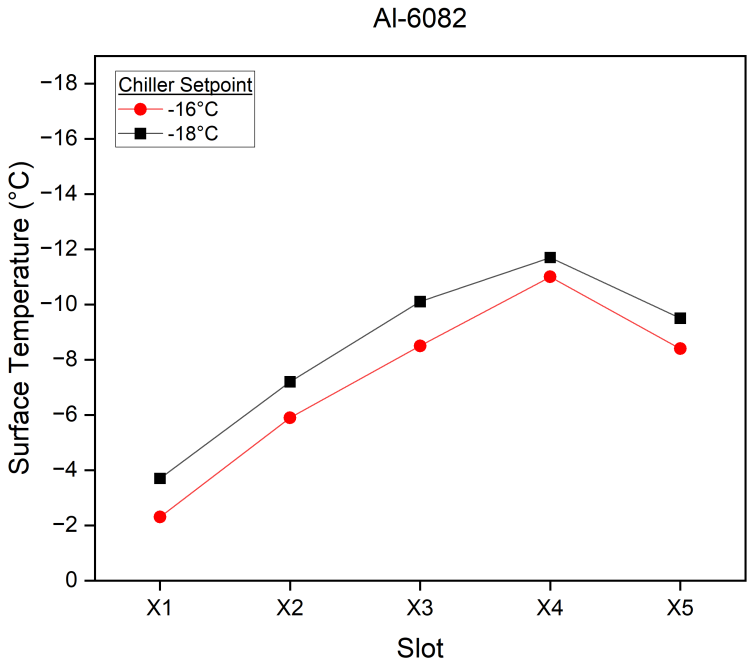

Figure 4.5: Surface temperature gradient across set-up for AA-6082 samples, from slots X1 to X5, recorded at different chiller setpoint temperatures.

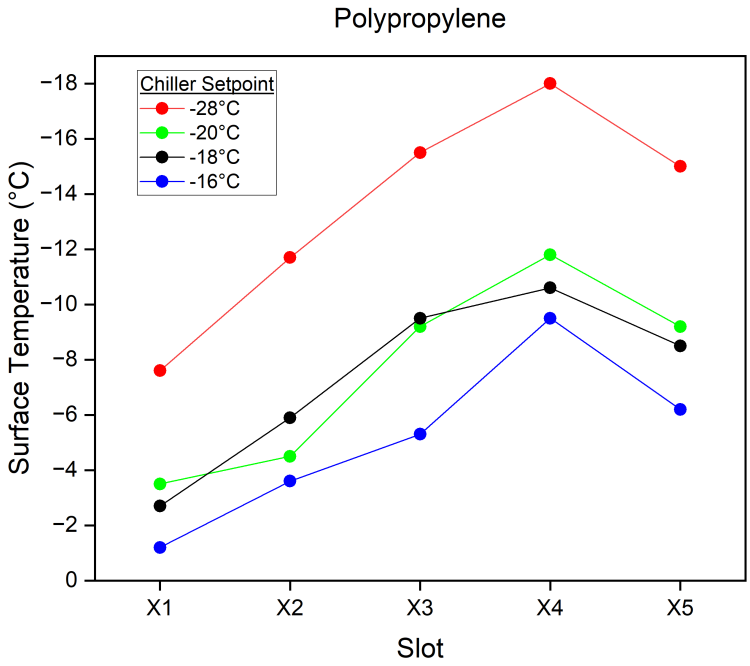

Figure 4.6: Surface temperature gradient across set-up for polypropylene samples, from slots X1 to X5, recorded at different chiller setpoint temperatures.

From Figure 4.5 and Figure 4.6, it is immediately obvious that there is a significant temperature gradient in the set-up. This trend is consistent across various chiller setpoints, and affects both the polypropylene and aluminum samples in a similar fashion. This discovery was a significant one, as the temperature trend correlates significantly with the trend of the ice adhesion strength across the set-up. It has been shown in multiple studies that ice adhesion strength has a strong temperature dependence [58], where lower temperatures corresponds to lower ice adhesion strength values.

The root cause of this issue is likely a flaw in the design of the set-up, and if possible this flaw will be mitigated when examining the set-up improvements. However, it does provide an opportunity to test the samples at different temperatures, and to examine further the effect this has on the results. Being fully aware of this source of error is important, as this allowed for more confidence in the explanation of outliers and interpretation of the results moving forward. The temperature data for X3, X4 and X5 implies that the adhesion data collected was all in an acceptable range when testing at a surface temperature of -10° C, as the deviation was at maximum $\pm$ 2° C either side of -10° C. In almost all tests, the chiller setpoint was usually between -16° C and -20° C depending on the needs of the test. Additionally, X3 and X5 appear to at be almost identical temperature in all of the tests, so this at least provides a 'true' comparison if needed.

This explanation goes a long way to explaining the scatter across the slots, but the causes of the spread of data at each individual slot is still unknown. Due to the likelihood of a combinational effect from various parameters and the difficulty in isolating one parameter at this stage, all of the potential sources of deviation with respect to the testing procedure will now be listed and discussed.

Table 4.2: Potential sources of deviation in the data from the first round of testing

Source of deviation	*Explanation*
Sample Treatment	The aluminum samples in this round of testing were not degreased prior to testing, and the samples were left clamped in the testing chamber between tests for convenience. This was an error, as the surface characteristics between tests were not consistent due to potential dust, condensation and frozen shards of ice left behind from previous fractures.
Pushing height, *h*	The first round of tests took place at a perceived pushing height, h, of 2.3mm. This figure was based on calculations from the dimensions of the prototype set-up and handheld measurements. On re-calculation at a later stage, this actually proved to be closer to 3 mm $\pm$ 0.2 mm. Stendardo et al. already proved the strong effect that the pushing height can have on the peak removal stress, as the loading mechanism moves further from pure shear as a larger bending moment is introduced [17], reducing the ice adhesion strength. As the peak stress values are in a lower range than expected, this may be one of the explanations for the data.
Ice Height, *H*	The water was injected with a syringe, with 0.5ml required to create an ice cylinder of H = 10 mm. However, consistency proved difficult, and often the ice pillar afterwards was actually anywhere between 6-12mm, despite not changing the procedure. This was also completed in two separate instances in an attempt to prevent spills, but an inconsistent clear 2-phase ice structure occurred as seen in Figure 4.7.
Humidity control	The relative humidity was uncontrolled for this dataset. The effect of the uncontrolled humidity may not be completely clear in the ice adhesion strength data. However, Figure 4.8 and Figure 4.9 highlight the presence of condensation and subsequent frost growth on the aluminium samples and testing chamber, which is certain to be affecting the ice pillars in some way. This is a clear example of the phenomena of condensation frosting, which was outlined in chapter 1.
Freeze time	The freeze time was inconsistent due to the order and speed of operations. All moulds were injected at the same time, and it took 10 minutes between tests to save data and adjust the actuator and DAQ system. Therefore X1 would be frozen after 30 minutes, X2 would be frozen for 40 minutes, X3 for 50 minutes, X4 for 60 minutes and X5 for 70 minutes, which is a huge inconsistency across tests. It has been shown in the past the relationship between increased freezing time and increased ice adhesion strength. REFRENCE.
Failed tests/spills	Spills were a common occurrence in the testing procedure, and no adhesion data was included for those tests. In these cases, the water either spilled and froze directly outside of the perimeter of the mould, or the pillar did not freeze at all. This occurred particularly in the first two testing slots (X1 and X2) nearest the inlet and outlet of the cooling chamber, likely due to the reduced temperature.
Clamping	For some tests, the actuator was not clamped properly, resulting in an equilibrium where the actuator slowly slid backwards in the mount. On clamping the actuator correctly, the force curve responded appropriately - a sharp decline, before typically increasing until a clean fracture. In other cases, the force-time graph exhibited strange behaviour, and the ice pillar would not break. This resulted in long plateaus on the force curve, strange oscillations or extensive declines to zero force. The clamping for the actuator was double-checked in this case, along with the mounting and rail system. It was unclear at this stage whether this was a mechanical fault, or a mechanism of the ice adhesion.

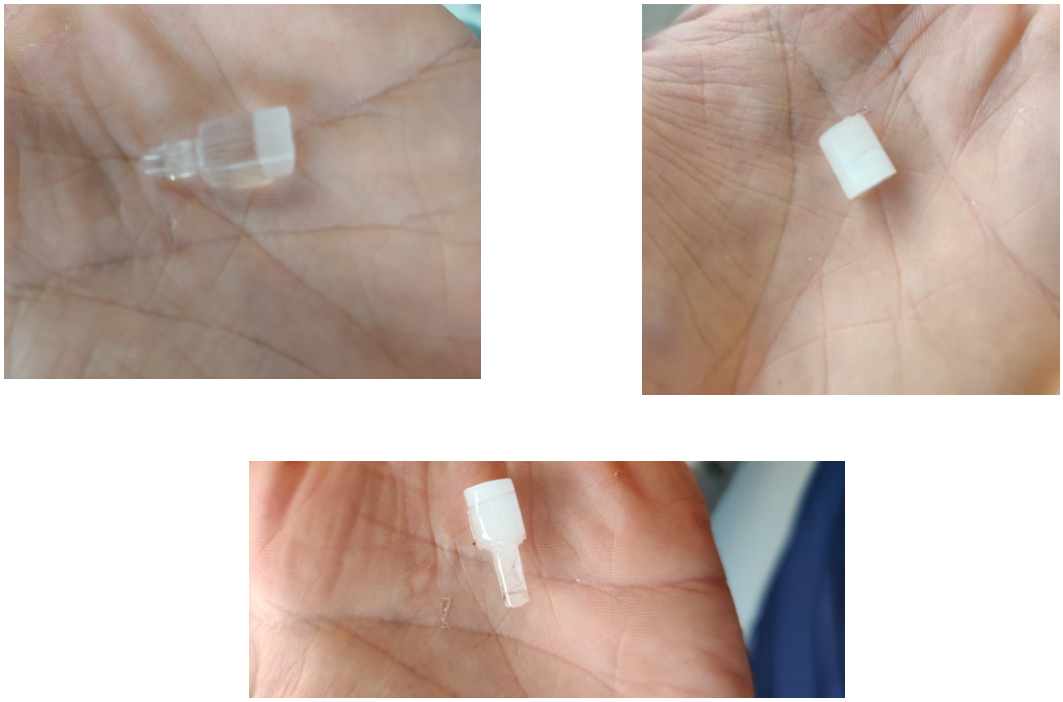

Figure 4.7: Examples of errors and inconsistencies with the ice pillars post testing, namely the two-phase ice, overfilling the mould and milky ice.

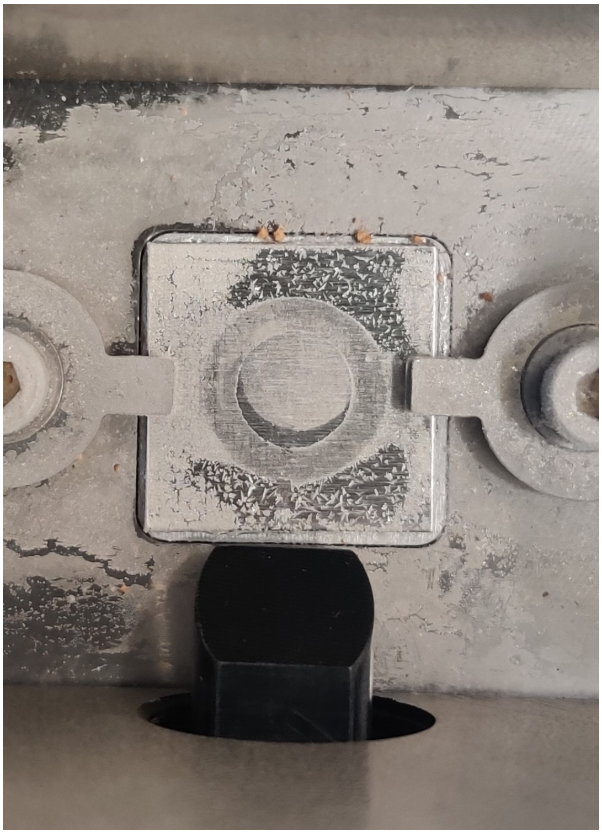

Figure 4.8: Example 1 of frost growth inside chamber and sample surfaces due to a lack of humidity control

Figure 4.9: Example 2 of frost growth inside chamber and sample surfaces due to a lack of humidity control

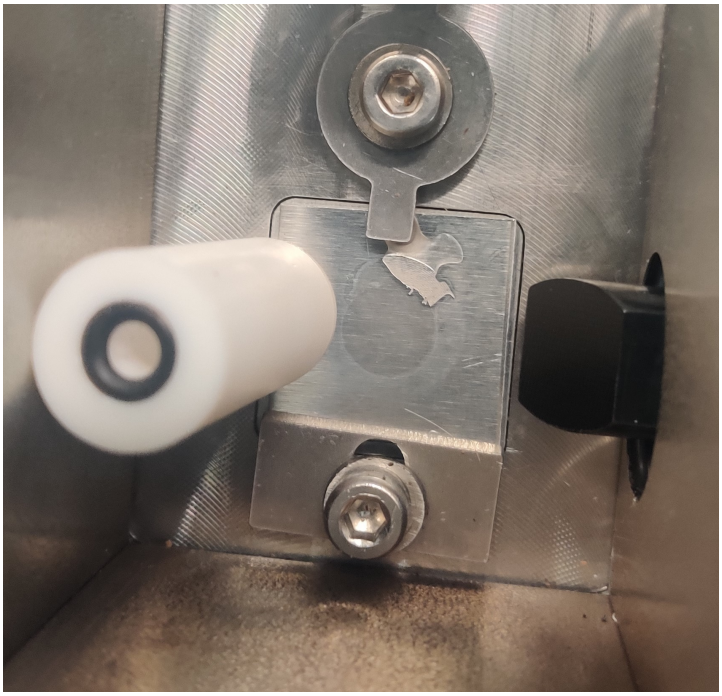

Figure 4.10: Evidence of a spill at slot X1, on an aluminium sample

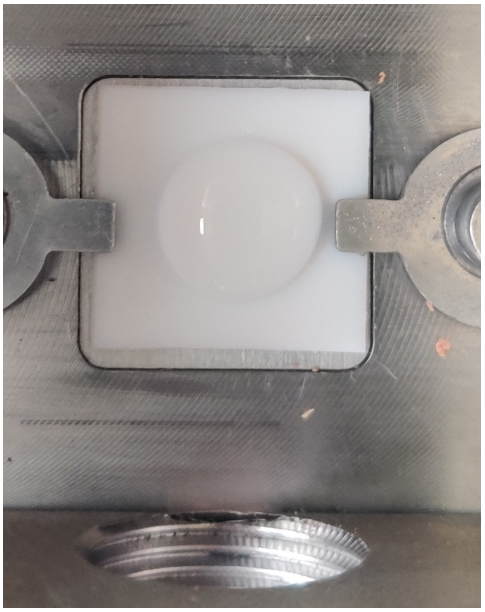

Figure 4.11: Water not freezing on a Teflon at slot X2.

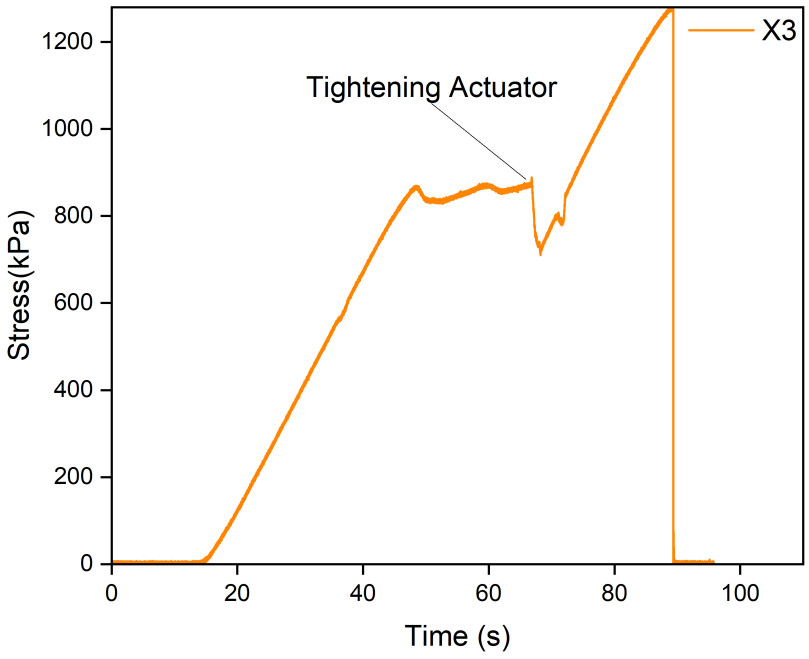

Figure 4.12: Example of a test where the actuator was not clamped sufficiently. Upon tightening the actuator to a sufficient level, the force increases linearly until failure.

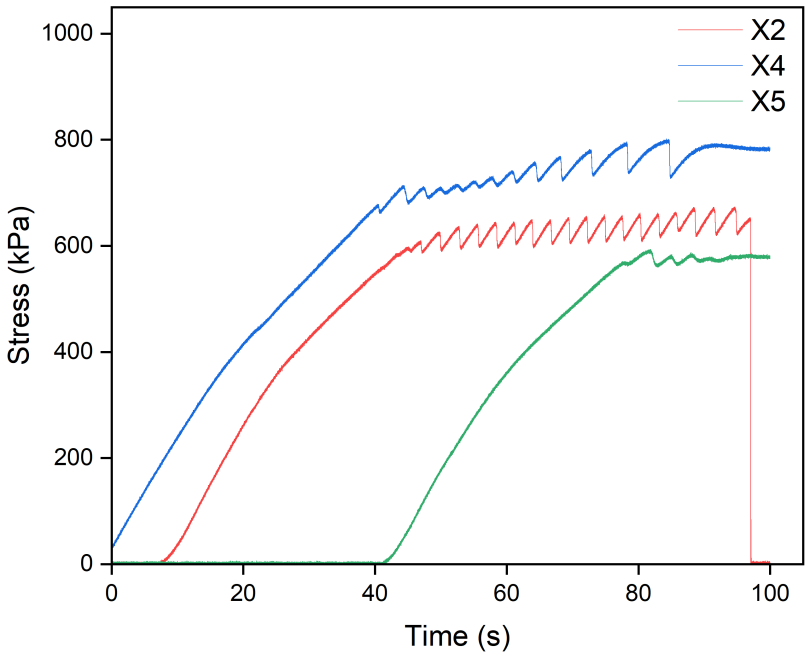

Figure 4.13: Example of three tests from the same testing run which produced oscillations. After 100 seconds, the ice pillar in X4 and X5 did not break and the force graph plateaued. The ice pillar in X2 did break, after a number of consistent oscillations.

4.3. Improvements and Failures Investigation

It is clear from the discussion in Table 4.2 and the evidence from the qualitative and quantitative data that the errors in the set-up need to be addressed. It was deemed to be more efficient to make these necessary fixes in a global fashion, rather than investigating the parameters one by one. By improving the set-up overall and then doing another round of testing, there should be a significant change in the data spread. This was done by fixing parameters to set values and making design and operational changes where applicable. The set-up however remained flexible enough to investigate the individual effects of some of these parameters individually if required.The applied improvements are listed below in Table 4.3.

Table 4.3: Improvements made to the testing procedure and conditions

Source of deviation	*Improvement*
Sample Treatment	The samples were dried and then degreased with acetone between each test. This ensured a consistent testing surface.
Clamping, Pushing height	The base structure of the set-up was reconstructed. This allowed for recalculation of key parameters such as the pushing height, and the entire system was fixed more securely with an improved clamping system, in order to reduce any potential errors from poor clamping.
Ice Height, *H*	The syringe was swapped out for a micro-pipette, with a maximum volume of 0.2ml. This proved to be much more accurate, and allowed for two injections of 0.2ml. Therefore, the ice height was now fixed to H = 8mm. The most consistent results in terms of the ice pillars for both occurred with an injection procedure of 0.2ml, before injecting the second volume of 0.2ml after 30-60 seconds. The improvements in the ice pillars can be seen in Figure 4.15.
Humidity control	The control of relative humidity was addressed by administering a weak flow of nitrogen into the testing chamber, and all tests now took place when the relative humidity was at lower than < 10%.
Freeze time	The freeze time was set to 30 minutes, and staggered injections were introduced to combat the issue of the inconsistent freeze time. As the speed of data collection increased, the time between tests reduced to around 5 minutes on average. Therefore, the injections are staggered every 5 minutes, so that by the time the first text in slot X1 is ready to be pushed, the ice pillar on X5 has already had at least 10 minutes to freeze. This proved to be long enough to not be affected by the removal of the alignment block.
Failed tests/spills	The surface moulds were further pre-treated to make them more hydrophobic. The injection procedure was analysed to examine effect on number of failures. The alignment pins were lubricated to reduce friction on removal and reduce risk of misalignment of the moulds during injection.
Data Collection	The sampling rate was reduced from 1000 Hz to 100 Hz. For each test, an increased amount relevant metrics were tracked including: temperature and exact time at both injection and pushing, pictures of fracture surfaces and ice pillars, and any additional notes and observations on the testing run, operational errors, fracture and outliers. This made data analysis and correlation much easier, and provided a data trail from multiple sources to any individual test.

Improving the control over the parameters, and therefore regulating the testing conditions, had an immediate effect on the results. The volume of tests were increased for this round of testing, with N = 50 for AA-6082. The spread of the data for ice adhesion strength reduced, and the mean value moved into the expected range with respect to literature, between 700 and 1000 kPa. There were also clear visual differences - the ice pillars were much more consistent, and the testing surface inside the chamber remained clean and dry as seen in Figure 4.14, with the frost growth prevented by the nitrogen flow keeping the relative humidity in the chamber below 10%.

Figure 4.14: Clean and dry testing conditions after controlling and improving testing parameters

There were certain sources of error that persisted in the testing set-up however, despite the attempts to reduce them. In particular, there was a high volume of spills and therefore failed tests, which hampered the momentum and progress of the testing. It was suspected at this stage that the temperature gradient across the set-up was responsible for many of the failed tests, but there were other issues that may have been significant. As outlined in Table 4.3, three main changes were made to investigate the issues.

The logical place to first investigate was the moulds. As the bottom of the cylindrical mould and the sample surface will never be atomically flat, there will always be a minuscule air gap between the surface being tested and the mould. Care was taken in the sample clamping procedure to not unevenly clamp or over-tighten on one side, as this may be causing a tilt on the surface and therefore causing a spill. The weighted alignment block, along with the choice to make the moulds from the hydrophobic Teflon, is designed to help mitigate these potential problems. However, it was proposed that this may not be enough to prevent the water from spilling underneath, and perhaps the effects of surface tension were causing increased wetting across the surface. Therefore, the surface moulds were further pre-treated to make them more hydrophobic. Although this initially appeared to make a difference and likely was a net positive in the context of the project, it is unclear the direct effect this had on the results.

Next, the injection procedure was analysed. In the beginning, the injection took place in two stages - 0.1ml of water was injected into each mould, before waiting 15 minutes to inject the remaining 0.4ml to achieve a 10mm ice height. Although this method had other issues as seen in Figure 4.7, it was chosen in the beginning to mitigate spills, with the idea being that the small amount of water would freeze very quickly on the surface which was at -10° C from the reduced pressure from having only one fifth of water column. However, the spills persisted, even when the injection with the syringe was changed to the much more precise micro-pipette, where 0.2 ml was added in each instance. Several iterations of the injection procedure were attempted, such as adding smaller volumes in 3 injections, but nothing appeared to have a significant effect on the results, and the test failure rate was still in the range of 30-40%.

As discussed in chapter 3, the alignment pins which were a key part in the injection procedure caused some issues in regards to lack of friction between the moulds and the pins, causing the moulds to slip out under the force of gravity. This was solved using a rubber O-ring, but the compromise to this was that this solution arguably provided too much friction - the pins sometimes stuck too well in the moulds, making them difficult to remove without causing the alignment block to shift and subsequently

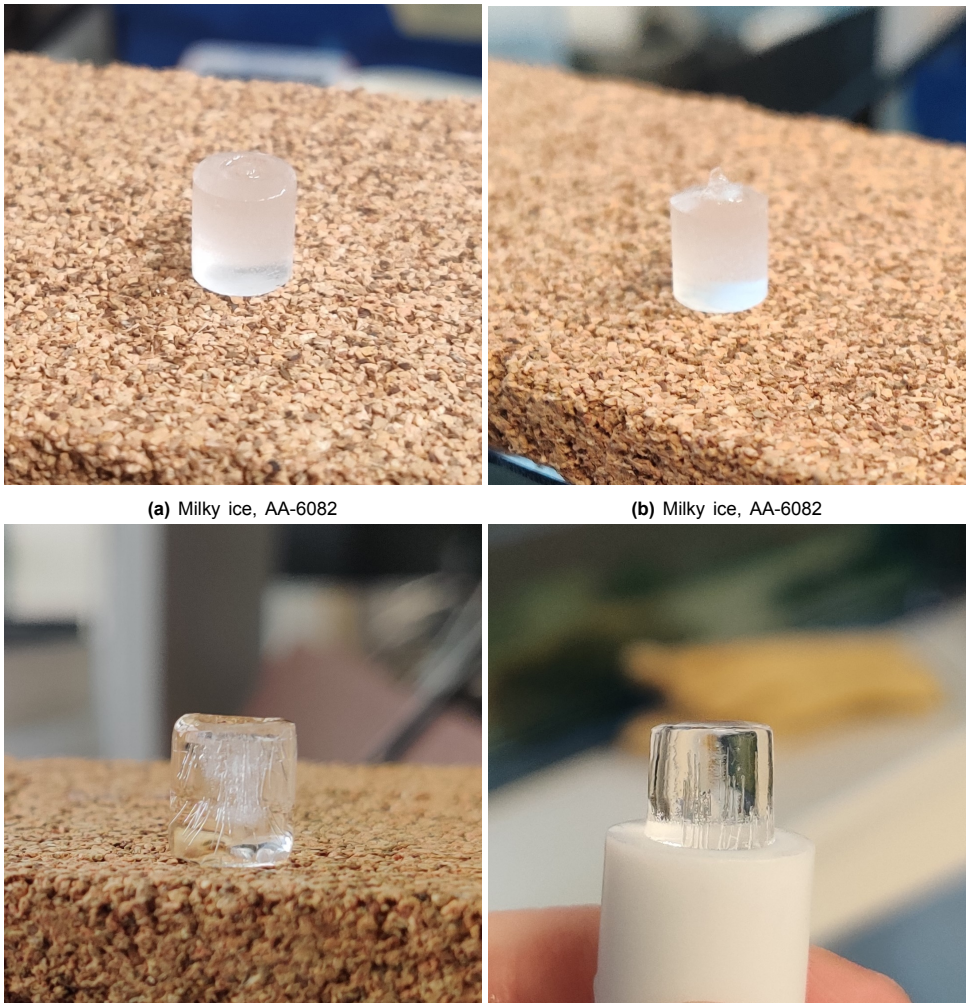

(a) Milky ice, AA-6082 **(b)** Milky ice, AA-6082

(c) Clear ice, Polypropylene **(d)** Clear ice, Polypropylene

Figure 4.15: Examples of consistent ice pillars after improving test conditions. (a) and (b) show milky ice pillars found when testing aluminum, and (c) and (d) shows clear ice pillars with minimal bubbles found when testing polypropylene

the moulds underneath to move or shift slightly. This potentially could be causing some of the moulds to slide out of position. If the pipette and mould are no longer fully aligned, the risk of injecting some water on top of the mould increases, which may explain certain cases were the spilled water appears to be frozen on the side and perimeter of the mould. Therefore, the pins were greased with a lubricant, and extra care was taken during removal with the pliers.

All three of these adjustments are certainly improvements to the repeatability of testing procedure, however neither revealed any large reductions to the number of failures and spills. To investigate how strongly the temperature gradient is influencing the number of failures, the number of failures are plotted against the corresponing slot location.

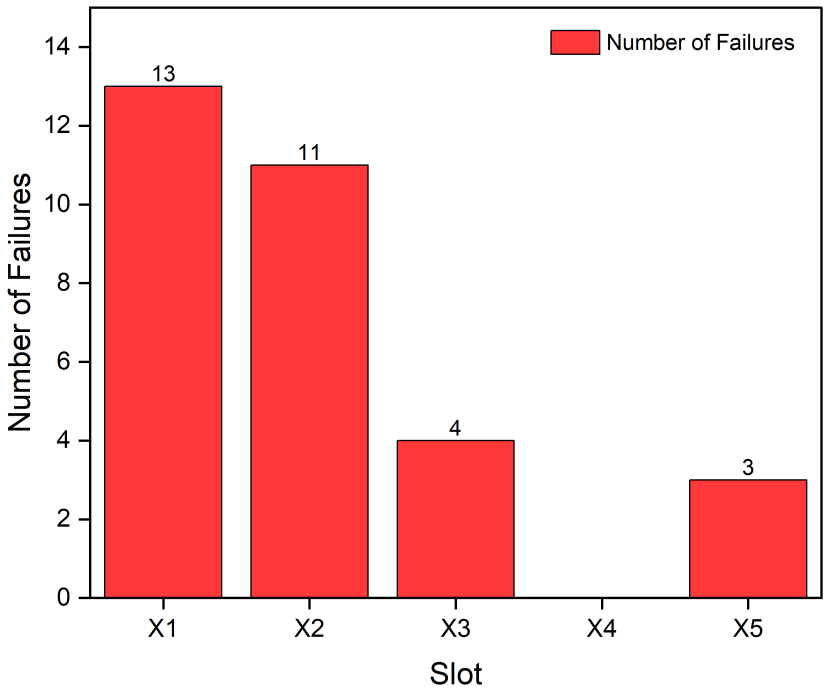

Figure 4.16: Number of failures and their corresponding location in the set-up for 113 tests, over 23 testing runs.

From the beginning of the validation process to the end, for a total of 113 individual tests over 23 testing runs, 31 were failed tests due to a spill. This is a failure rate of approximately 27%. Of those 31 failed tests, 13 were failures attributed to slot X1, 11 were attributed to slot X2, 4 were attributed slot X3, 0 were attributed to slot X4, and 3 were attributed to slot X5, as visualized in Figure 4.16. This shows that across all of the testing runs for the validation, both the first two slots led to failed tests approximately 50% of the time. This shows a clear correlation with the temperature plots in Figure 4.5 and Figure 4.6; the lower temperatures have a higher volume of failures. In these slots, the temperature wasn't low enough to sufficiently freeze the column of water after injection. This was especially prevalent when testing polymers such as Teflon, PVC and HDPE (which are all less conductive than aluminium), for the first time.

It was known from the beginning that the surface temperature control on the set-up was not perfect. The temperature that the sensor of the external cooling source (the chiller) reads will never be the exact same reading as the surface temperature reading, unless the insulation is perfect and there are no external losses. This was never going to be the case in the current set-up, as the cooling chamber was not insulated from beneath the set-up, and there external insulation certainly had room for improvement. This issue was mitigated by manually setting the chiller to a temperature below what was required - for a goal surface temperature of -10° C, the chiller was set to a value of approximately -18° C. The chiller could be adjusted to a slightly higher or lower temperature as needed, such as when the box had been opened between tests to change the samples, and the outcome was reflected by the surface temperature reading. As the set-up improves over time and the chamber is fully insulated, the chiller will be under less pressure and require less energy when asked to produce temperature of -10° C on the sample surface. In an ideal scenario, this process would be automated, using a feedback loop to link the internal thermocouple and the external temperature sensor in the chiller. The goal surface temperature of -10° C was never maintained perfectly, however it was relatively easy to adjust the chiller accordingly, and the maximum fluctuation was between -9.5° C and -11.0° C. It should be noted that the chiller was never adjusted after the water was injected for freezing and ready for push testing, but only between tests, so as not to introduce inconsistencies that may occur with a new target

temperature on the chiller. It was concluded that the approximate degree of precision of -10° C ± 2° C was a fair representation of the imperfections in relation controlling the temperature. The root cause of this issue is likely due to a design flaw in the cooling chamber, the poor insulation or a combination of the two. For the context of this project, it was an accepted error, and from this point forward, only data from slots X3, X4 and X5 is deemed to be valid for testing and reporting values at the standard target temperature of -10° C. It was concluded that the approximate degree of precision of -10° C ± 2° C was a fair representation of the imperfections in relation controlling the temperature. Recommendations of how to reduce this error and improve the set-up further will be outlined in chapter 6

4.4. Data analysis

With the testing conditions improved and the potential sources of error well established, the data from round 2 of validation can be analysed. The parameters relevant to this dataset are listed below in Table 4.4, along with the number of tests per material that took place in Table 4.5. In this table, N_t refers to number of total tests on all testing locations, and N_v refers to total number of valid tests, meaning tests only that produced valid data points before further analysis. (N_t) encapsulates all testing attempts, so this includes failed tests and spills.

Table 4.4: Validation Round 2: Improved conditions and testing parameters

Parameter	*Notation*	*Target Value*	*Real Value*	*Units*	*Comments*
Probe speed	*s*	0.01	0.01	mm/s	Fixed
Mould diameter	*D*	8	8	mm	Fixed
Push height	*h*	2	2	mm	± 0.2
Ice Height	*H*	8	8	mm	Fixed
Surface Temperature	T_s	-10	-10 ± 2	° C	-
Relative humidity	*rh*	< 10%	< 10%	-	Relative to T_{amb}, 20° C
Freeze time	t_f	30	30 to 35	mins	-

As the majority of the testing took place on aluminium thus far, it is the logical starting point. N_t = 50 for this dataset, however the amount of available data points for this test is actually only N_v = 30, due to the high number of spills and failures returning reduced valid data, and this is plotted in Figure 4.17. For this dataset and plot, the statistics are as follows, with the mean and standard deviation with respect to the mean reported:

Table 4.5: Statistics of validation round 2: Number of valid tests (N_v) on all testing locations, units kPa

Slots	*Material*	N_v	$\overline{x}$	σ	% σ
X1 - X5	AA-6082	30	860	254	30%

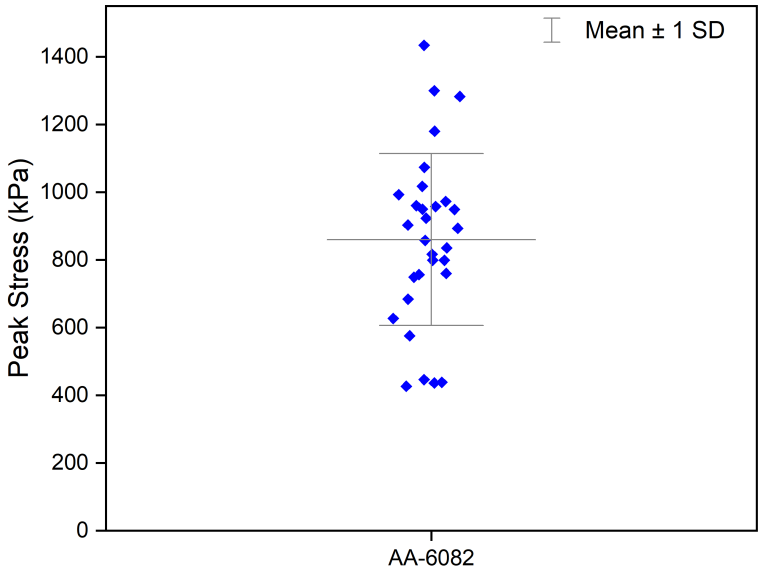

Figure 4.17: Peak stress values for AA-6082, all data points in the second round of validation. $\overline{x}$ = 860, % σ = 30.

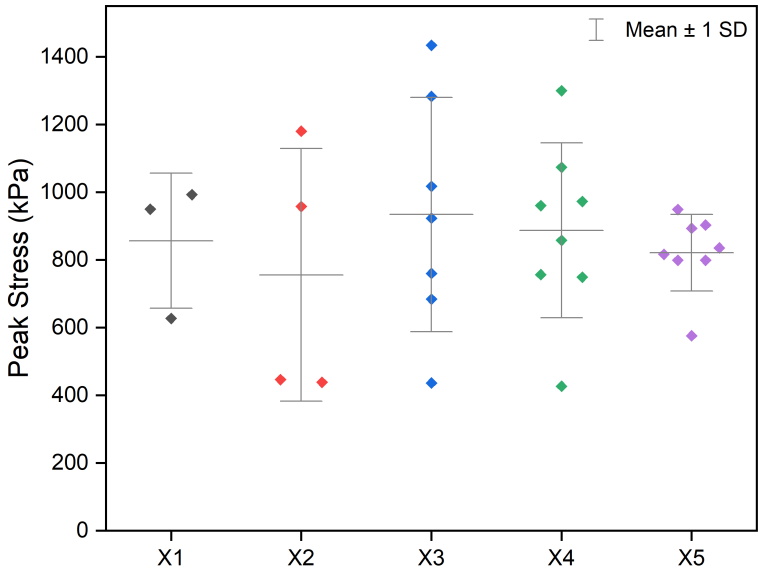

Figure 4.18: Peak stress values for AA-6082 plotted by slot location, including all data points in the second round of validation.

Before further analysis, this scatter is filtered down further and plotting by slot location in Figure 4.18. The lack of data points in X1 and X2 reflects the number of failures present in these locations, as highlighted by Figure 4.16. However, in comparison to the earlier plot Figure 4.3 which had poor

uncontrolled parameters, it is interesting to note that 3 of the data points from X1 and X2 in this dataset have peak stress values close to the overall mean, which is just over 800 kPa. This may imply that if the surface temperature in these slots is sufficient to freeze the pillars and the test doesn't spill (so likely at least below -5°), the samples can still have similar ice adhesion strength values as the the rest of the data points. However, there is too much uncertainty in that analysis, so the data points from X1 and X2 are no longer of interest when reporting the testing temperature of -10° C, and are omitted. Therefore, the number of valid data points is reduced further to N_v = 23.

Table 4.6: Statistics excluding X1 and X2, units kPa

Slots	*Material*	N_v	$\overline{x}$	σ	% σ
X3, X4, X5	AA-6082	23	878	245	28%

Excluding X1 and X2 for valid tests does little to reduce the overall spread, and this agrees with the above analysis - it could be argued that valid tests on X1 and X2 should be included in the overall analysis, however there is still too much uncertainty. The rest of the data in X3, X4 and X5 still has considerable spread and clear outliers, with a standard deviation of 28% with respect to the mean. By correlating the qualitative and quantitative data together that has been collected it may be possible to explain these outliers and decide whether they are still valid.

First examining slot X3, there are 3 clear outliers in the data. The data point at approximately 1300 kPa is the easiest to explain, as there is clear evidence of an operational error. In this case, this was a test where the actuator was not clamped correctly, which is reflected in the force curve in Figure 4.20. The data point which is lower than the rest produced a different type of ice pillar as seen in Figure 4.21 that the majority of the other data points in X3, X4 and X5 did not have. The underlying reasoning as to why different ice types causes a lower ice adhesion strength is still unknown, however it can be omitted as it is not comparable to the milky ice that was observe in the other tests. The major outlier with very ice adhesion over 1400 kPa has a small portion of ice left on the aluminium surface, and the force curve did show strange behaviour in the last 10 seconds of the test, which may imply crack propagation and a mixed mode adhesive/cohesive break. The force curve and surface in question can be observed in Figure 4.22. It may be the case that this is simply a natural outlier in the dataset, as the reasons remain unknown for the high adhesion. It may be the case that for a mixed mode adhesive/cohesive break, the thickness of the ice 'left behind' combined with its position with respect to the pushing implement may have a influence of the results. Cases such as these will be analysed further in chapter 5.

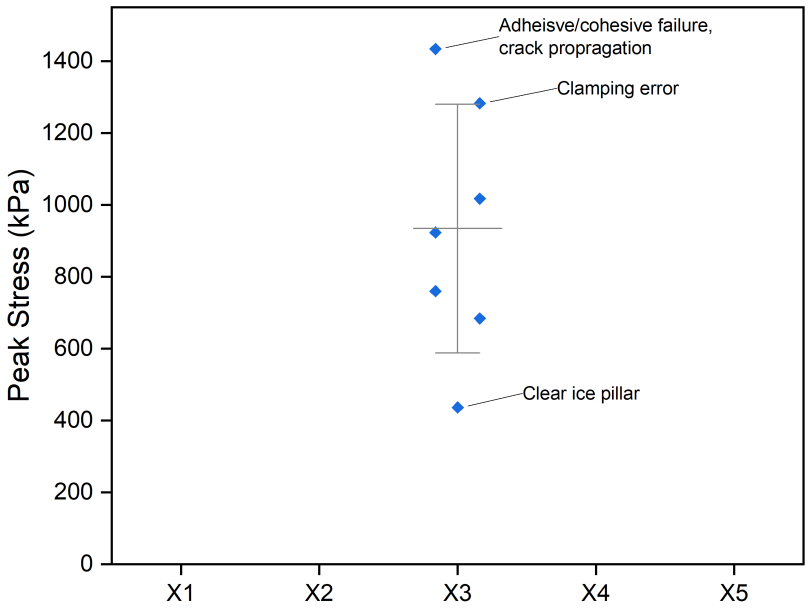

Figure 4.19: Outliers at slot X3 for AA-6082

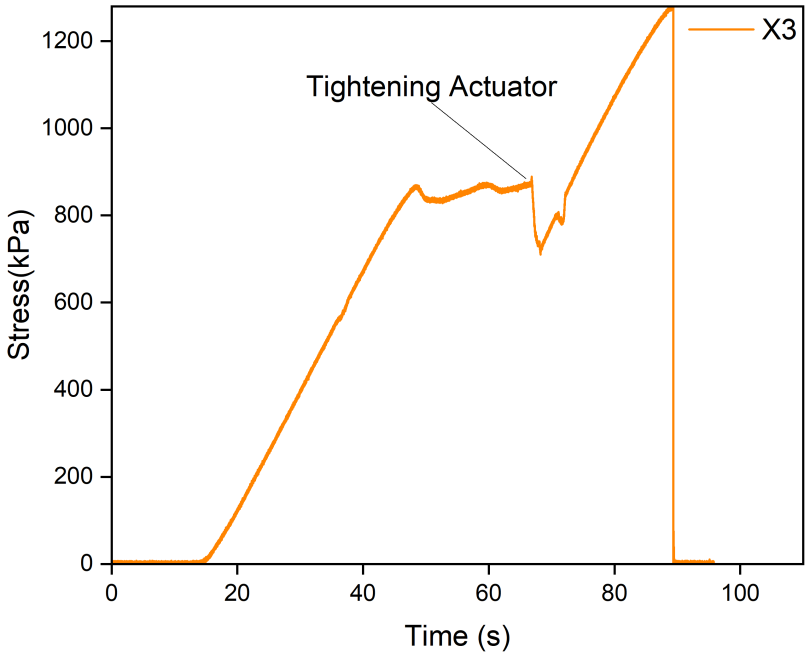

Figure 4.20: Actuator clamping error which caused outlier in data

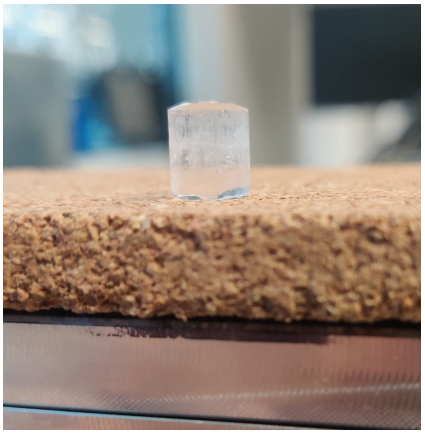

Figure 4.21: Clear ice on AA-6082 is uncommon and caused a significantly lower ice adhesion strength

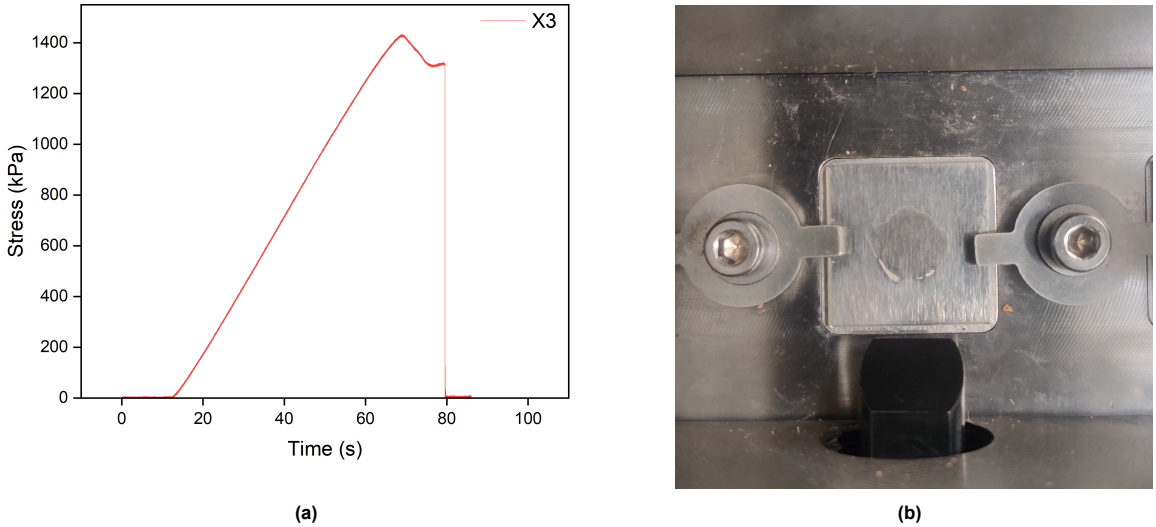

Figure 4.22: (a) Force curve for sample exhibiting very high adhesion strength and (b) corresponding fracture surface.

A similar identification of outliers can be performed for both X4 and X5. Both of these slots also contain data points with similar sources of error. In slot X4, there are only two outliers which is not unexpected, as this was the location with the coldest temperature and the only location with no failed tests as seen in Figure 4.16. The first point which was investigated is the test which outside the range of 1 standard deviation, with a high peak stress of 1300 kPa. Upon investigation, it turns out from the laboratory notes that this was actually a data point that should not have been included in the first place - which implies there was an error in the data collection. By cross-referencing this with the icing fracture surface and the force data, the source of the error becomes clear. In this test, the ice pillar did not break within the 200 seconds of the test, instead reaching a slowly oscillating plateau shown in Figure 4.23 and therefore is classed as failed test. The fracture surface provides a logical explanation for this, as there was a spill outside of the perimeter of the mould. For further examination, the mould was removed by hand to examine the surface. The thin layer of ice covering the sample suggests the formation of a crack; when the mould was pulled out by hand, the detachment interface was approximately 2mm above the surface, indicating that this was the weakest point and the interface with the ice and sample beneath. Although no longer a valid data point, this test can still provide valuable information about the nature of the test and helps to improve the testing procedure. It also serves as further validation to the robustness and utility of this methodology - without the ability to cross reference this data point from different sources, this data point would remain in the spread unexplained, without the information

that it was due to an operational error.

The other outlier on X4, which fractured with a lower relative peak stress of 427 kPa is an anomaly, and be attributed to random error. It was a predominately adhesive fracture, with the force curve remaining linear up until the instantaneous fracture. However, in this particular testing run there were no failures, and the peak stress across all of the slots was 993 kPa, 958 kPa, 923 kPa, 427 kPa and 800 kPa, from X1 to X5 respectively. This completely defies the trend that has been observed at all other tests - the testing surface with the temperature gradient was sufficiently cold to gather 5 legitimate data points which all had instantaneous fractures, and yet the coldest slot location fractured at half the peak stress of the other locations. As the temperature sensor is on the sample at this slot, perhaps there was human error and interference with the sample surface in setting up the test. This data point highlights that when testing ice, there is an element of random error that is sometimes difficult to explain, perhaps similar to the 'inherent' property of ice adhesion testing that is sometimes refereed to in literature. However, with a robust testing process, the probability of random error can be mitigated.

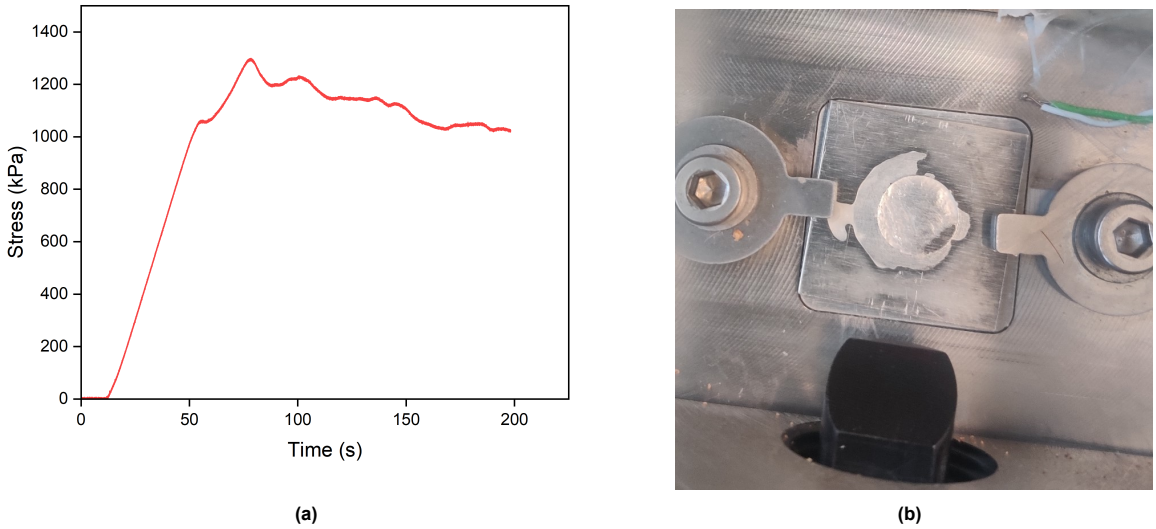

Figure 4.23: Outlier test for AA-6082 where the ice did not break after 200 seconds (b) shows the sample surface after the pillar was broken by hand, and (a) shows the corresponding force curve.

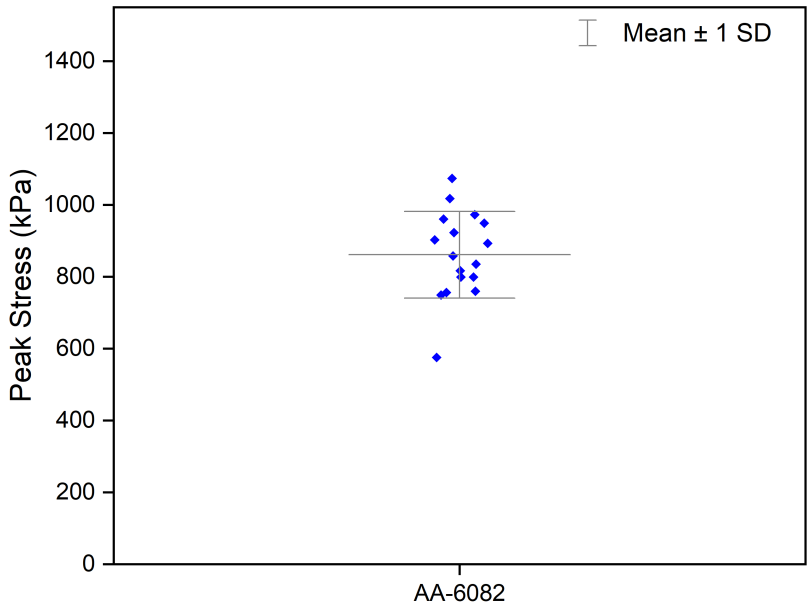

Figure 4.24: Improved dataset with outliers removed, with all valid tests from X3, X4 and X5.

Table 4.7: Statistics of improved dataset, excluding outliers

Slots	*Material*	N_v	$\overline{x}$	σ	% σ
X3, X4, X5	AA-6082	17	861	120	14%

Removing the clear outliers for the reasons stated above, we see a logical improvement in the data scatter. Without the outliers, N_v = 17, and for this sample size standard deviation %σ = 14 %. Removal of one sensitive data point at just under 600 kPa would reduce the standard deviation to 11%; however this may not be a fair representation of the data for this specific analysis, as there is no conclusive evidence from the fracture surface, force curve, observations or ice type as to why this data point is an outlier. This is deemed to be a satisfactory result and comparable to the range of the better results reported ice adhesion testing designs in literature. As a final litmus test, the results are directly compared to those of Stendardo, with access to the raw data and testing conditions a huge advantage. The testing conditions of these tests were almost identical - the only unknowns are perhaps the mould material, as the moulds from Stendardo's test are made of nylon, whilst in this experiment they are made from Teflon. Additionally, the aluminium alloy is different, AA-6060 as opposed to AA-6082. In the first plot Figure 4.25, the data without outliers is compared to Stendardo's with outliers - this is not a fair comparison without more information on the result itself, so the unknown outliers from both plots are removed, at the expense of a reduced sample size for comparison which is now N = 6. Making this comparison, the mean value matches up very nicely, with the mean values both around 870 kPa, whilst Stendardo's standard deviation is %σ = 27% in comparison to % σ = 11% for this project. It should also be noted the visual difference between Figure 4.25 and Figure 4.26 - with the outliers removed, the standard deviation reduces, and now the remaining data points are all either grouped around the the upper or lower bounds of this new deviation. The two groupings in Stendardo's dats at 600 kPa and 1100 kPa may be indicative of something such as a difference in fracture mode, however without further information it is difficult to draw a conclusion. Considering how closely the testing conditions match up and the similarities between the tests, this is ultimately the best dataset

for validation without a standard, and brings validity to the results. This result is certainly a success for the set-up, considering the knowledge of the temperature gradient, and the potential effect that this significant source of deviation may have had on the results.

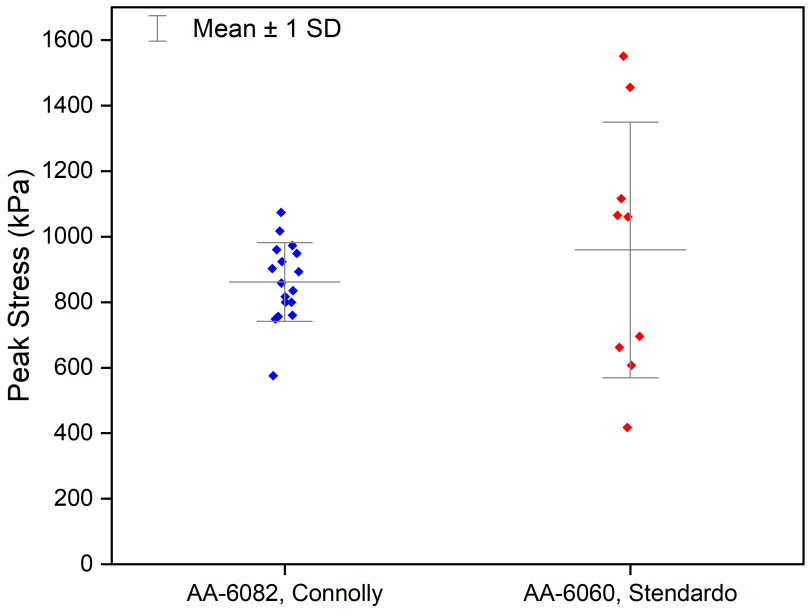

Figure 4.25: Comparison of analysed peak stress data versus available data from Stendardo's ice adhesion test.

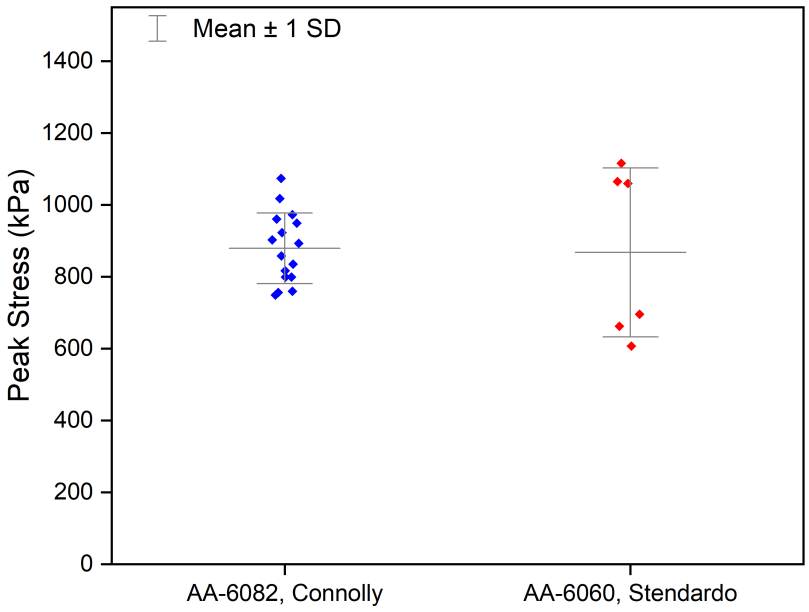

Figure 4.26: Comparison of analysed peak stress data versus data from Stendardo's ice adhesion test, excluding significant outliers

Table 4.8: Statistics of both datasets for comparison, excluding significant outliers, units kPa

Author	*Material*	N_v	$\overline{x}$	σ	% σ
Connolly	AA-6082	16	879	98	11%
Stendardo	AA-6060	6	867	235	27%

In this chapter, the entire validation process was outlined and discussed. Starting from the initial data from the first round of validation, valuable lessons were learned about the nature of the set-up. From this data, improvements to the set-up and testing procedure could be applied, and the effects of individual parameters on the spread of data could be investigated. Once a reliable testing procedure was established and the data was collected, the data could be processed and analysed thoroughly. With confidence, each of the data points in these plots can be explained and correlated from various sources of qualitative and qualitative data, and the quality of the results could be compared to other sources to a satisfactory level. Not only do these results successfully validate the set-up, they also validates the utility and value of a well-thought out and thoroughly researched design methodology and experimental approach for reliable ice adhesion testing.

5

Influence of material and topology on ice adhesion

In this chapter, the influence of different materials and surface characteristics on ice adhesion will be analysed. As the aluminium alloy AA-6082 has been used for the purposes of validation, it has the largest dataset, and therefore is the material which will be utilsied most to show some common results in terms of ice adhesion. Polymers are explored to a lesser extent, but also provide some interesting insights.

5.1. Aluminium

The first step is to establish the groundwork for this analysis. The results can be categorised according to their failure type, in a similar fashion to traditional bonded joints - either adhesive failure, cohesive failure or a mixed mode, adhesive/cohesive failure. The methodology for categorising these results was predominately based on the fracture surface, and whether or not there was ice still adhered to the surface after fracture. Additionally, the force curves could be analysed to assist in the analysis. In cases where no ice where the ice pillar was attached, and a clean fracture surface, implies that a test was an adhesive failure. A fracture surface with some remaining ice can be defined as a mixed mode failure. Often times a mixed mode failure can have very little ice or a lot of ice on the surface, and the thicknesses can also vary, so it may be necessary to state whether a failure is predominately adhesive or cohesive - surfaces with a % area coverage of over approximately 70% will be considered cohesive. If an ice layer remains and fully covers the surface area taken up by the circular ice pillar area, this will be categorised as a fully cohesive failure. Due to the nature of the testing, there are two additional subcategories in which the results will be analysed in terms of mixed mode failure. A spill implies that water has spilled out from the external perimeter of the mould, and this therefore will be categorised as an invalid test. A partial spill however, implies that the water has leaked slightly out of the inner circumference where the pillar is frozen, but has remained within the perimeter of the mould, and has frozen between the mould and the substrate. It could be argued that a partial spill is not valid for analysis, as the surface area by which the average critical shear stress is calculated, $\tau_{ave} = F/A$, is no longer known. However, depending on the case, the partial spill can be minimal, and the surface area can be considered close to the original calculated 50.3 mm^2. Threfore, for partial spills the inclusion in the data will be on a case by case basis. Additionally, as discussed in chapter 1, a stress dominated fracture is defined in literature as an instantaneous fracture at all points of the interface, whereas a toughness dominated fracture indicates the propagation of a crack either at the usually larger interface or in the bulk of the ice [68]. By correlation of both the qualitative and quantitative data, it should be possible to describe and interpret the results in these terms.

Table 5.1: Failure analysis by surface description

Failure Category	*Description of surface, inner circumference*
Adhesive	Clean surface
Cohesive	Full ice coverage
Mixed Mode	Partial ice coverage
Spill	Ice frozen outside of mould perimeter
Partial spill	Ice frozen under mould

5.1.1. Failure Analysis

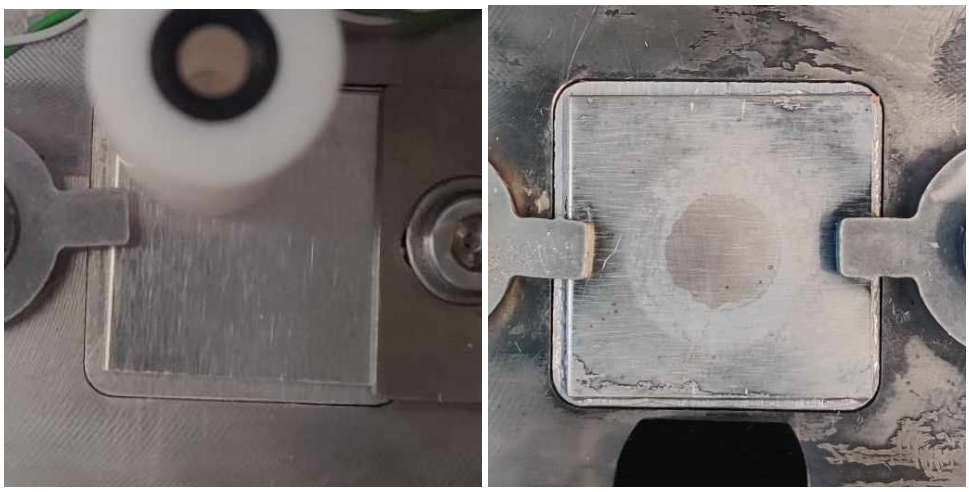

(a) X5, 31-01, clean adhesive failure

(b) X4, 26-01, clean adhesive failure

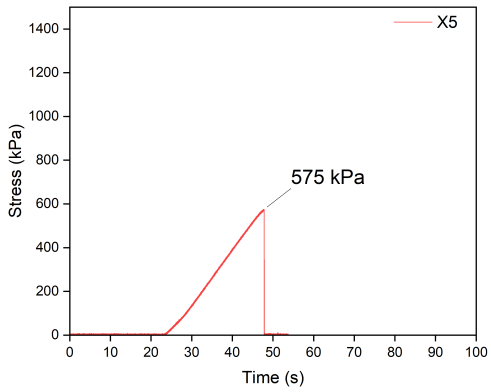

(c) Force curve for surface X5, 31-01

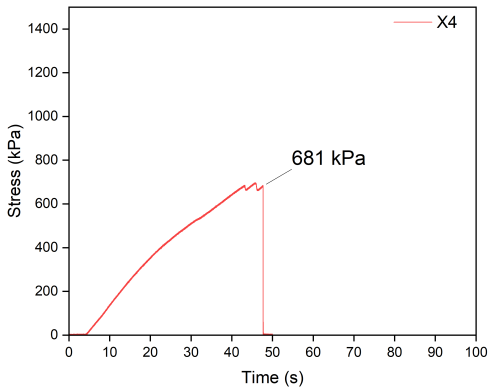

(d) Force curve for surface X4, 26-01

Figure 5.1: Examples of adhesive failures on AA-6082.

Figure 5.1 is an example of typical adhesive failures. The surface is completely clean, and in combination with the force curves, they can be characterized as a stress dominated fracture due to the linear curve and instantaneous interface failure. If the fracture is mixed mode, but predominately adhesive (estimating by the relatively clean surface area at the inner circumference), then the failure will behave similar to an adhesive failure. The shape of the mixed mode failure curves in Figure 5.2 and Figure 5.1 are both linear and similar. In the case of these mixed mode failures with a estimated low % ice area coverage, it is not clear whether there is any significant crack propagation in the ice bulk from the failure of the interface, as the force curves still suggests a stress dominated failure. However, while the clean adhesive surfaces correspond to peak stresses of 575 kPa and 681 kPa respectively, the mixed mode failure surfaces correspond to slightly higher peak stress values of 810 kPa and 916 kPa respectively.

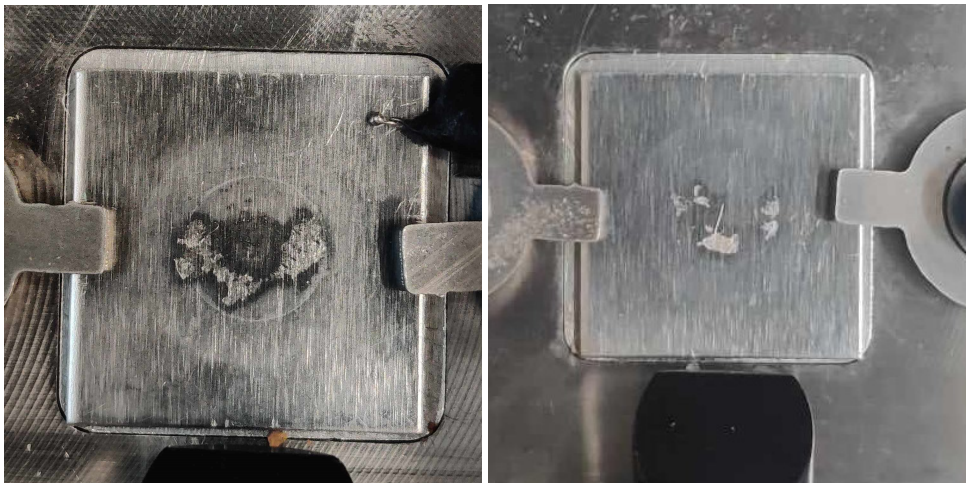

(a) X4, 29-02, mixed mode failure

(b) X3, 31-01, mixed mode failure

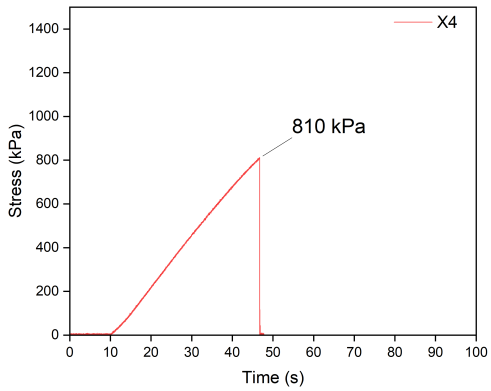

(c) Force curve for surface X4, 29-02

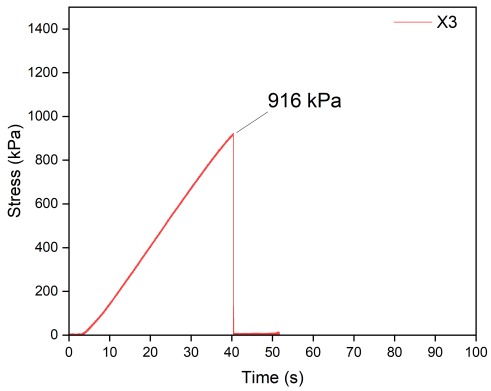

(d) Force curve for surface X3, 31-01

Figure 5.2: Examples of mixed mode failures on AA-6082

Intuitively this makes sense; the ice which is left on the surface is evidence of a mechanical adherence or anchoring to the substrate, and more evidence of ice suggests increased adhesion, which implies that higher forces are therefore required to remove the ice pillar from the substrate. This analysis deals with degreased but unpolished AA-6082 - it may be the case that the topology type and defects increase the anchoring to the substrate. It is interesting to note that the peak stress of mixed-mode failures appear to be closer to the mean value of approximately 870 kPa than adhesive or cohesive failures, this agrees with anecdotal experience and observations. This is likely due to the nature of the results, as purely adhesive and purely cohesive fracture surfaces were quite rare, and therefore mixed mode fracture surface was the most common result. The wide range of surface area coverage for mixed mode failures is also a factor, and it is expected that there would be a linear relationship between % ice area coverage and ice adhesion strength if further analysed.

Following the above line of analysis, the cohesive failure surfaces in Figure 5.3 can be considered. In these examples, the % ice area coverage is quite high, so these can be categorised as cohesive, as fully cohesive failures are rare in this testing. The trend discussed continues in these cases, as both of these examples have higher peak stress values as the % ice area coverage increases. Interestingly, Figure 5.3 subfigure (b) has a very high adhesion, which is likely due to the partial spill in this case; some water has spilled and frozen under the mould. The violent nature of the fracture is evident by the appearance of loose ice shards in the photo, and indicates this is still a stress dominated and instantaneous fracture, also judging by the linear force curve.

This observation is further validation of the set-up at least in the case of aluminium, as it shows for

(a) X3, 31-01, cohesive failure

(b) X3, 29-02, cohesive failure

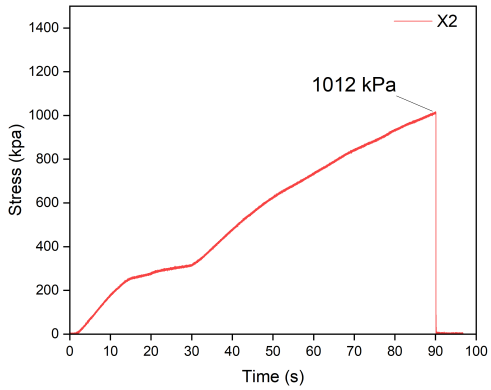

(c) Force curve for surface X3, 31-01

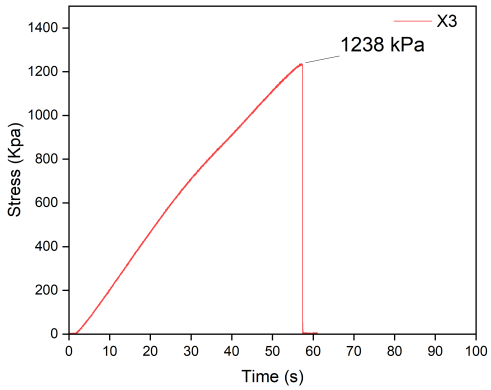

(d) Force curve for surface X3, 29-02

Figure 5.3: Examples of cohesive failures on AA-6082

multiple failure modes that the set-up is shear stress dominated due to the small interface, given by the widely cited definition of Golovin et al. when discussing the effect of a critical interface length on ice adhesion [68]. However, their analysis implies that in a shear stress dominated fracture, that crack growth is not present and therefore not contributing to the instantaneous delamination of the interface. Challenging this idea, subfigures (a) and (c) in Figure 5.3 are referenced. This is a cohesive failure with nearly full area coverage of the inner circumference where the ice pillar stood, and the peak force is 1012 kPa, which is higher than the mean but lower than the very high adhesion of 1238 kPa in subfigure (d). Notably, the time until failure is 90 seconds which is longer than the average test, and there is a small force plateau for 20 seconds near the beginning of the test. This plateau appears to be evidence of crack initiation, just above the interface in the ice, which creates a weak spot in the ice. This crack propagates rapidly through the interface and bulk ice at the critical peak stress, resulting in the cohesive failure as evidenced by the significant ice left on the surface. The surface itself suggests that the crack propagated in a mixed mode as similarly suggested by Huré et al.[69], mainly sliding in shear but also opening slightly, as evidenced by the varying thicknesses of ice left on the surface. Comparing the surfaces and force curves in Figure 5.3, it suggests that the early crack initiation in test (c) reduced the ice adhesion strength, compared to the test (d) with no evidence of crack initiation. This implies that ignoring the crack initiation on small interface lengths that will be 'stress dominated' is reductive when analyzing ice adhesion, as these failures do not exactly fall under the 'toughness dominated' criterion. The mould dimensions and pushing height in this set-up were mainly chosen based on the FEM analysis by Stendardo et al.[17], in order to promote a stress dominated fracture the majority of the time. However, it is clear over small interfaces slow fracture and cracking mechanisms are also

at play in some of the results, and it appears an oversight to not thoroughly analyse and report these phenomena. Admittedly, this differing analysis may be a result of the differing goals of the respective studies, as Golovin et al. were more interested in interfacial toughness over larger areas. However a critical attitude to widely cited publications is important, especially in the standard-less field of ice adhesion testing.

5.1.2. Roughness & grain direction effects

The effects of roughness and grain direction were analysed in two separate testing sessions. The AA-6082 which has been tested up to this point was as tested manufactured, apart from the acetone degreasing before each test. The roughness for this aluminum was evaluated as S_a, which is defined as the difference in height of each point compared to the arithmetical mean of the surface. To investigate the effect of changing roughness, some AA-6082 samples were ground, polished and tested. The corresponding roughness values and distributions can be seen in Figure 5.4 below.

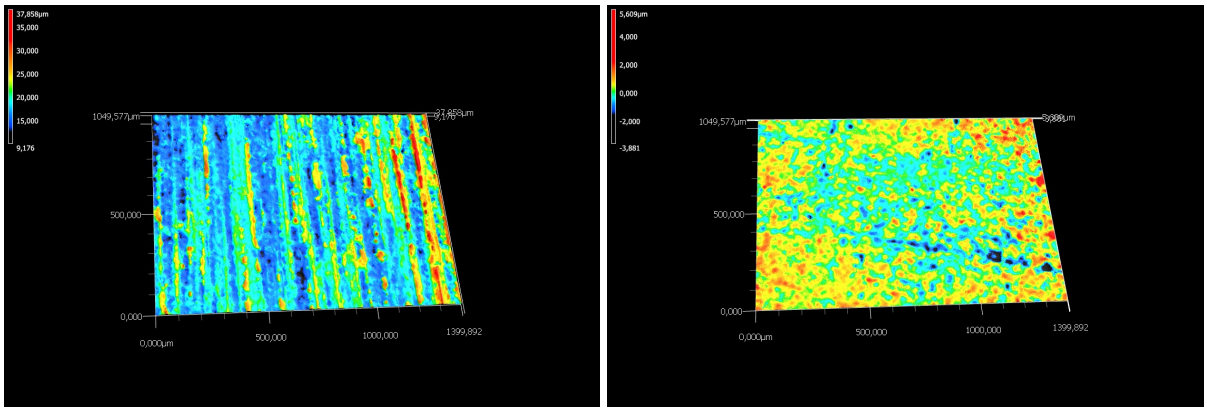

(a) **(b)**

Figure 5.4: Roughness profile of (a) As manufactured AA-6082, S_a = 2.59 $\pm$ 0.06μm and (b) Polished AA-6082, S_a = 0.42 $\pm$ 0.11μm

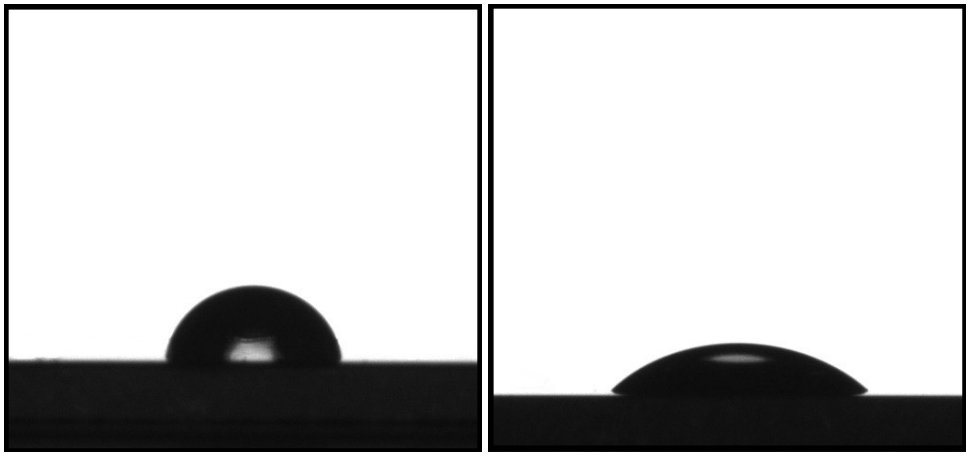

(a) Unpolished AA-6082, WCA = 86.5$\pm$ 0.4 $^\circ$ **(b)** Polished AA-6082, WCA = 43.6$\pm$ 0.2 $^\circ$

Figure 5.5: Water contact angles of AA-6082 with differing roughness.

Table 5.2: Roughness of aluminium samples

Material	S_a (μm)
AA-6082	2.59 $\pm$ 0.06
AA-6082, polished	0.420 $\pm$ 0.11

Polishing and grinding the surface naturally decreases the roughness, and this in turn reduces the WCA from 86.5 $\pm$ 0.4 $^\circ$ on the unpolished AA-6082 to 43.6 $\pm$ 0.2°, making the surface significantly more hydrophilic as clearly seen in Figure 5.5. It is expected that this would have a strong effect on the results. However as seen in Figure 5.6 below, the distribution remains similar to the distributions for the AA-6082 discussed during validation. The spread is initially quite large without further analysis, and the mean is just below 800 kPa. Adhesive failures and a range of mixed mode failure types are present across the dataset where N = 9, along with three points that have a partial spill, where some water was frozen under the mould. The three partial spills were all in similar positions on the respective surfaces and from the same testing run, and this suggests a operational error, or perhaps increased wetting promoting a partial spill due to reduced water contact angle.

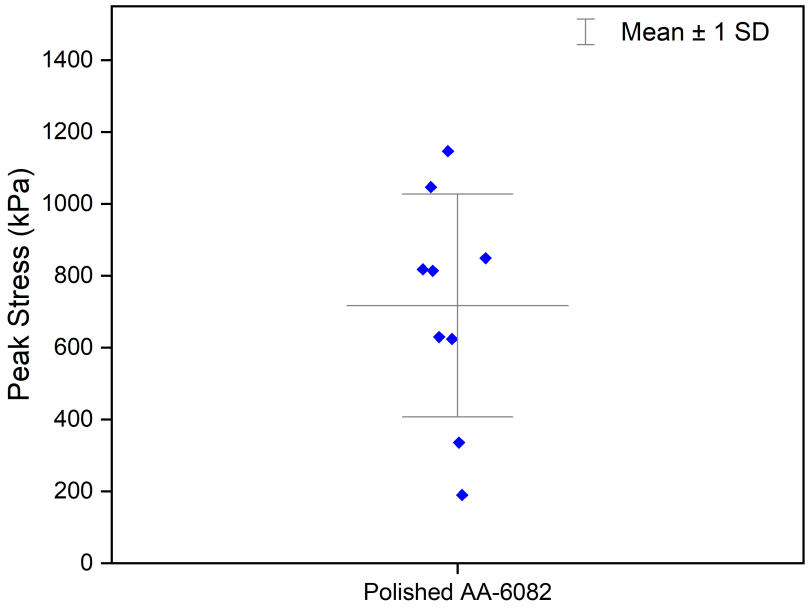

Figure 5.6: Distribution of peak stresses on polished AA-6082

Comparison of predominately adhesive failures from both unpolished and polished samples is likely the fairest comparison when analysing roughness effects, as the influence of the remaining ice in a mixed mode failure is more difficult to quantify. Taking the examples of purely adhesive failures from Figure 5.1, both of these failed at a peak stress 575 kPa and 681 kPa respectively. The only test which failed as purely adhesive in the polished dataset failed at 624 kPa as seen in Figure 5.7, which is in a similar range. The analysis of a mixed mode failure for the unpolished sample versus the polished sample returns a similar result. The unpolished samples from Figure 5.2 have peak stresses of 810kPa and 916 kPa respectively, in the range of the mean value of 879 kPa. An example of a similar fracture surface on the polished samples is seen in Figure 5.8, which has failed in mixed mode with a peak stress value of 848 kPa, which is very close to the unpolished mean. In short, it appears that the decrease in roughness did not have any significant effect on the ice adhesion strength, albeit for a relatively smaller sample size, N = 9.

Comparison of the effect of longitudinal versus transverse grain direction on the unpolished AA-6082 yielded similar results. From the tests focused on comparing the grain direction, the distribution was similar to the typical aluminium distribution, with all types of failure modes, errors and some clear outliers. In a singular testing run two fracture surfaces and force curves are directly compared, with the test on slot X4 showing adhesive failure for longitudinal grain, while the test on slot X5 shows

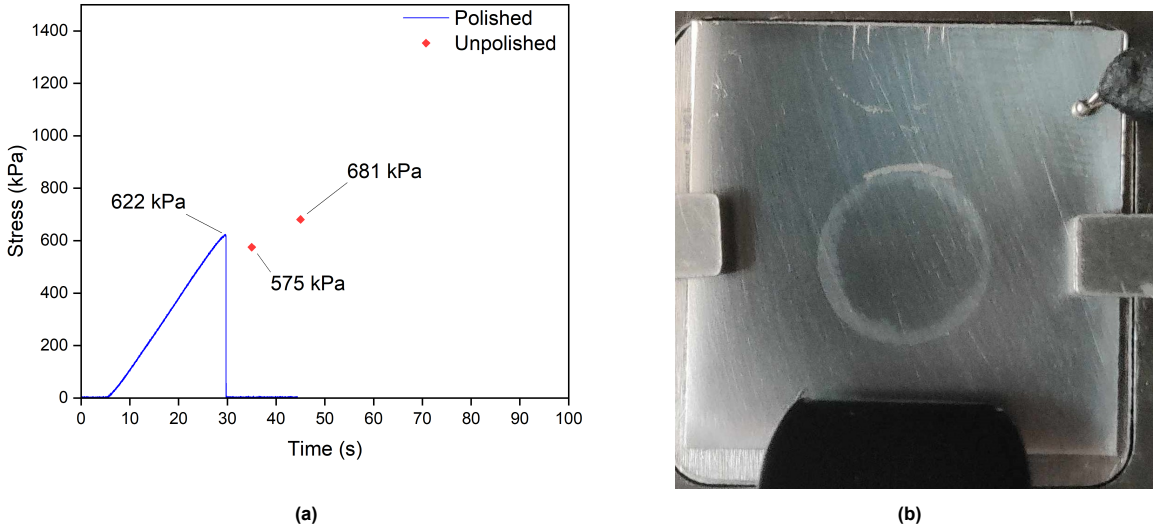

Figure 5.7: (a) Force curve for adhesive failure on polished AA-6082, with unpolished peak stresses for comparison, with (b) corresponding polished fracture surface. There is no significant change in ice adhesion strength comparing polished and unpolished samples in adhesive failure.

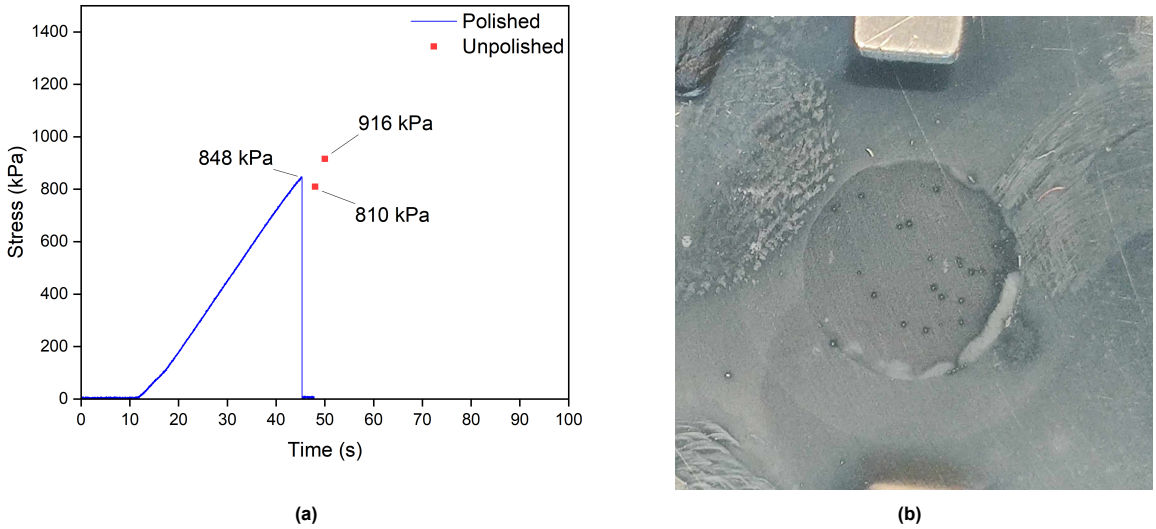

Figure 5.8: (a) Force curve for mixed mode failure on polished AA-6082, with unpolished peak stresses for comparison, with (b) corresponding polished fracture surface. There is no significant change in ice adhesion strength comparing polished and unpolished samples in mixed mode failure.

similar adhesive failure for a transverse grain shown in Figure 5.9. It should be noted that the tests starting at different times in this plot is purely an operational effect, the slopes of the graph are almost identical, indicating a very similar test. The longitudinal grain at slot location X4 failed at 716 kPa, whilst the transverse grain at slot location X5 failed at a slightly lower 654 kPa. These values are quite comparable given typically overall spread for this set-up is % σ = 10-15%, and therefore there is no conclusive evidence to suggest that grain direction has a strong effect on ice adhesion. In this particular case with almost identical failures, the small difference in peak stresses is most likely due to the small temperature difference between X4 and X5. During testing X4 is on average approximately 1-2° C lower than X5, which may explain the higher ice adhesion strength. The analysis to this point seems to suggest that for this ice adhesion set-up, the ice adhesion strength is much more sensitive

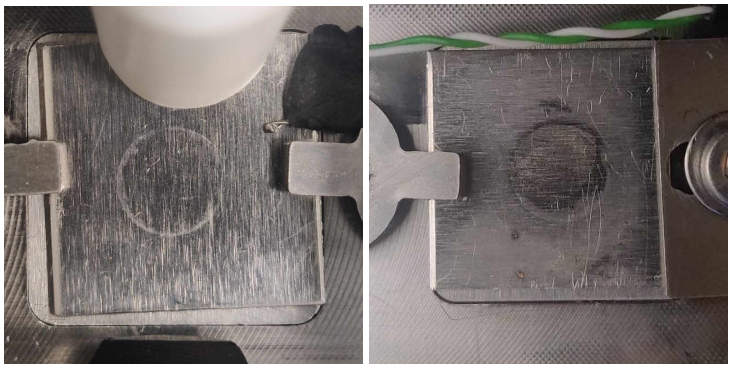

(a) Longitudinal grain, X4 **(b)** Transverse grain, X5

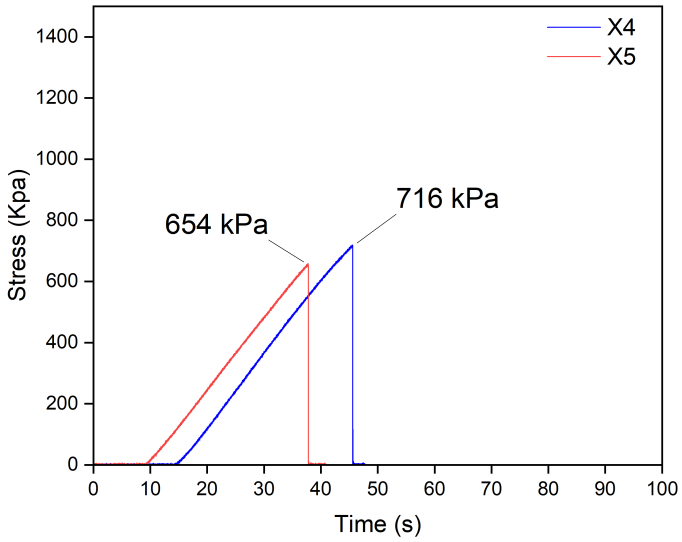

(c) Force curves for surfaces (a) and (b)

Figure 5.9: Ice adhesion test on sample with (a) longitudinal grain direction and (b) transverse grain direction (c) corresponding force curves. The red curve is for the longitudinal grain, while the blue curve is for the transverse grain direction.

to the type of failure and any variability in the testing conditions, rather than the surface characteristics such as the surface roughness and grain direction. Of course, it is likely that the surface characteristics are in turn influencing the types of failure, however without further analysis and a larger sample size it is difficult to conclude what exactly that influence is.

5.1.3. Analysis of outliers

In the breadth of testing aluminium substrates, very few results had identical counterparts for direct comparison, with the exception of course being adhesive failures. Most of the results could be categorised as shown above, however some tests exhibited unique behavior which are very interesting to analyse. This may be in the past what was referred as the 'inherent property' of ice adhesion testing [9, 21], and likely in another testing set-up these results would be omitted from the dataset without explanation. However, with this set-up the outliers and unique results can be thoroughly analysed, which is a powerful capability.

Some outliers were already discussed in chapter 4, however the polished AA-6082 distribution has two clear outliers that are of interest. The first data point to examine has a peak stress at 332 kPa, which implies failure at this value. However, closer examination of the fracture surface and force curve shows a unique mixed mode failure, as it appears this was a sliding break. In the force curve shown in

Figure 5.10, it is suggests that this is a toughness dominated fracture, as the dip and plateau indicate crack initiation. How that crack propagates and whether it does completely is difficult to infer, as the ice pillar is clearly sliding along the surface, but still requiring a force of approximately 215 kPa to overcome friction. In the test, the force value slowly crept towards zero, so the rest of the data was not included. This failure mechanism was unique in the testing of AA-6082. Some other unique fracture surfaces can be found in the appendix.

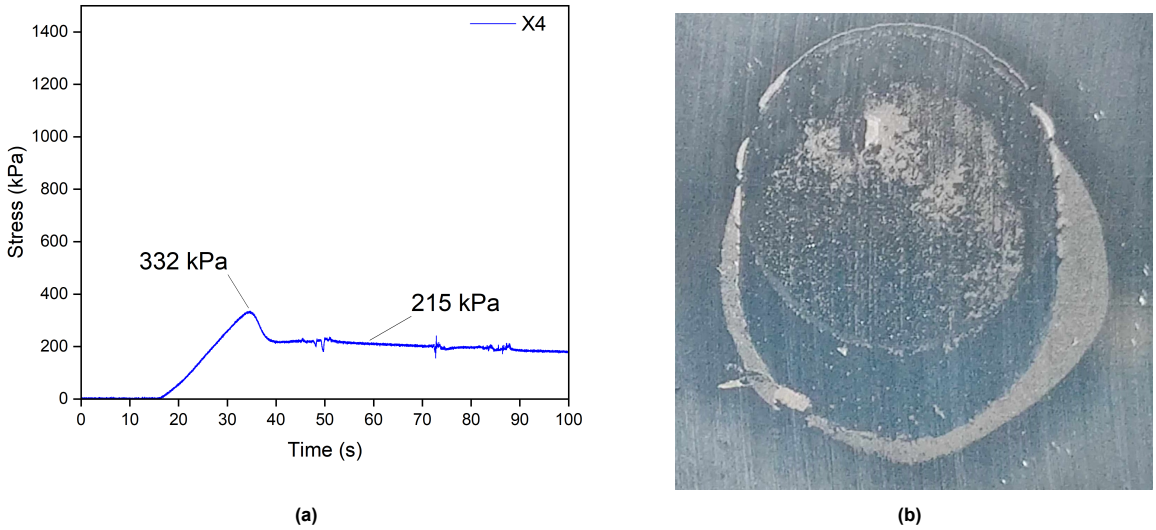

Figure 5.10: (a) Force curve for sliding failure on polished AA-6082 and (b) corresponding fracture surface

The other data point worth noting is the outlier which failed adhesively at 190 kPa in the polished AA-6082 distribution. This result was actually by design, as the testing conditions were changed for this one particular test. In the testing run, X3 and X4 were tested as normal, however when injecting the water into the X5 mould the nitrogen flow was switched off for 20 minutes until pushing, which means it was no longer under low humidity testing conditions. As X3 and X4 were already frozen at this point, it was expected that the change in humidity would have little effect on those data points, whilst X5 would be strongly effected as the humidity affects the freezing process. As expected, the relative humidity does indeed strongly affect ice adhesion, as the tests in which the relative humidity was kept below 10% failed in mixed mode at peak stresses close to the mean, whereas the test with no humidity control fails at 190 kPa. This test validates concerns discussed in chapter 1 about existing set-ups and proposals for standards which are not designed for low humidity - it is perhaps the most important parameter to consider in ice adhesion testing.

In the design of low ice adhesion coatings, it may be beneficial to analyse the outliers of ice adhesion tests, in order to gain an early understanding of the goal result. Coatings could then be designed to consistently promote failure modes at low peak stresses, such as in the sliding behavior seen in Figure 5.10. Other strategies could perhaps take advantage of the humidity ice adhesion relationship with a coating in some way. This reverse engineering approach could save time and effort by pursing coating strategies that promote specific failure mode, which can then easily be tested on the validated set-up.

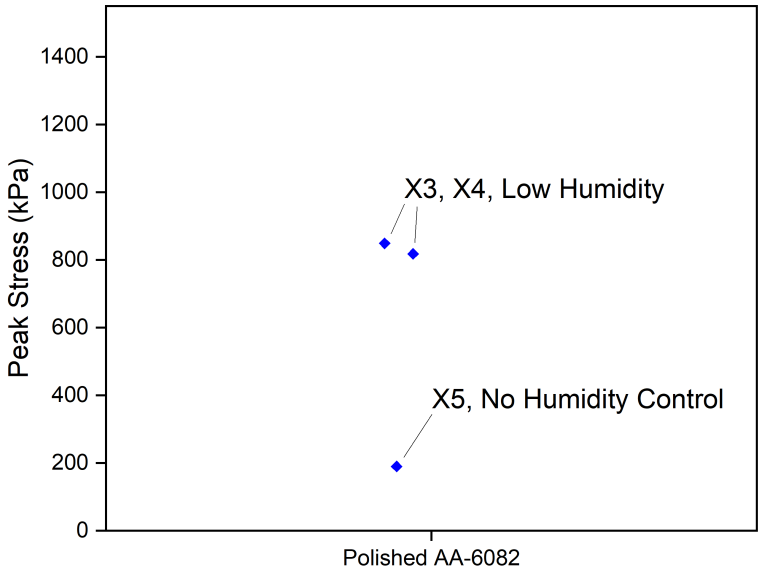

Figure 5.11: Effect of changing humidity on the ice adhesion strength

5.2. Polymers

The volume of testing on various bare polymer substrates was much less in this project, therefore the depth of analysis of the results is limited. However, it became clear that stiff polymer substrates did behave significantly differently than aluminium. It should be noted that all testing the polymers took place and h = 1, and the substrate thickness was 3 mm in all cases comparison to the 1 mm aluminium samples. In this analysis, polypropylene (PP) will be used as the example polymer, due to the increased data points which are available for this material. The only issue with this material is the colour, as the cream colour provides poor contrast when observing ice on the surface.

5.2.1. Failure Analysis

The distribution of peak stresses for polypropylene can be observed in Figure 5.12. The first observation of this plot is that the range of peak stress values is significantly different when compared to aluminium, with the mean value almost exactly half at 444 kPa. The initial spread appears lower when considering all the data points, as the outliers have yet to be investigated for errors. However, it is apparent that this distribution is slightly misleading, as the mode of fracture for the majority of the polypropylene samples is different when compared to the aluminum, which predominately had linear force time curves and instantaneous fractures. Although the PP did also show similar behavior at times, many of the failures actually failed with a more rounded force curve. Therefore, this distribution does not accurately tell us about the failure, so instead all of the force curves can be plotted together and analysed in Figure 5.13.

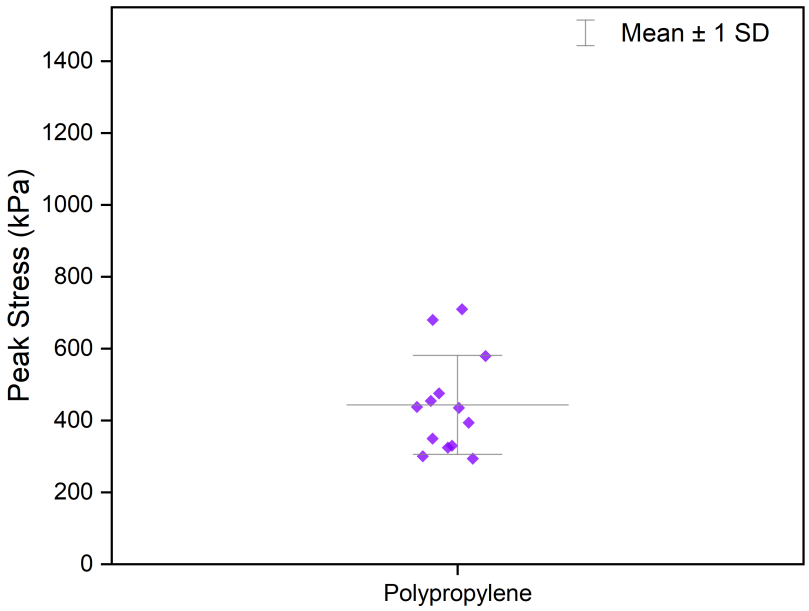

Figure 5.12: Distribution of peak stresses for polypropylene.

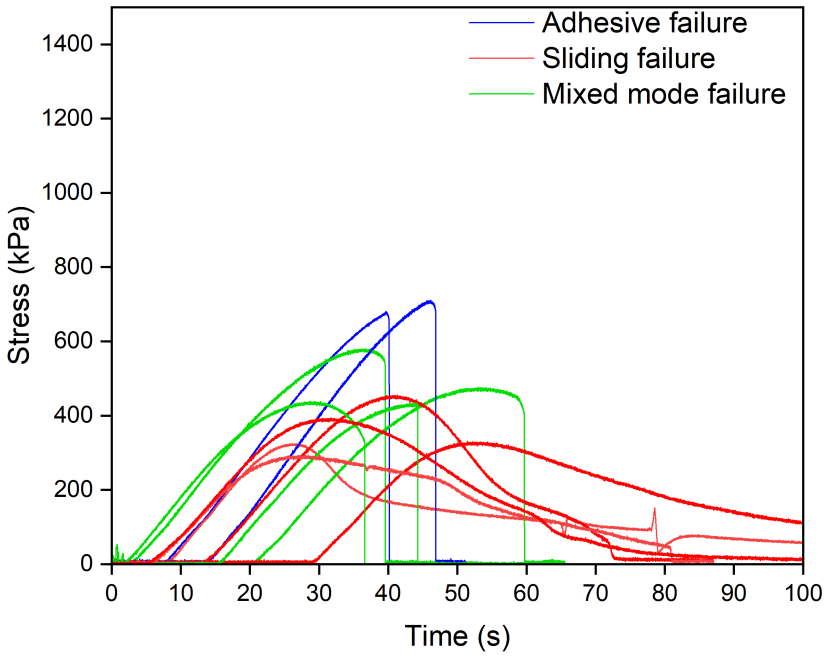

Figure 5.13: Force curves for bare PP surfaces. The force curves be categorised by their failure type - adhesive, mixed mode or sliding.

Immediately, it is notable that there are three distinct failure modes - adhesive failure, mixed mode failure and sliding failure, as distinguished by the blue, red and green curves. There were no data points when testing polypropylene that could be classed as cohesive failures, apart from spilled tests which were omitted from the dataset. It is clear that due to the curvature of many of the failures before final fracture, analysing just the peak stresses is an oversight. To create a clearer picture, two force curves from each failure type are analysed in Figure 5.14. The first observation is that conversely to the analysis on aluminum substrates, the purely adhesive failures have the highest peak stresses, and require more force to remove that mixed mode failures. The adhesive failures in this case fail fully across the interface, and it is assumed they remain fully in the stress-dominated regime. The mixed mode failures exhibit a significant rounding the curve before failure, indicating a crack initiation before relatively quick propagation at the interface and failure. Examples of the fracture surfaces are included below in Figure 5.15.

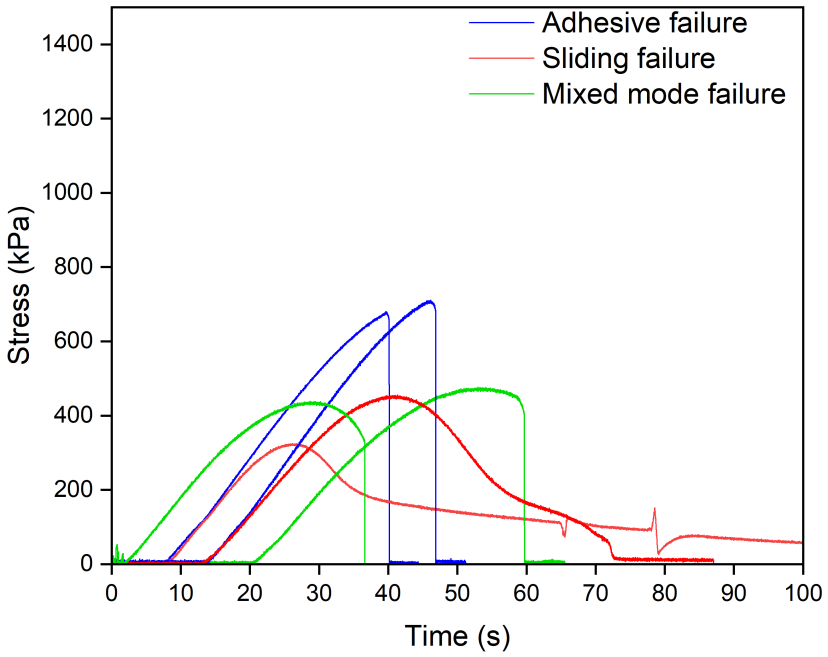

Figure 5.14: Six force curves for bare PP surfaces. The force curves be categorised by their failure type - adhesive, mixed mode or sliding.

The sliding behavior present in the outliers section of the analysis of aluminium, is actually quite a common result when considering polymer substrates. Technically this is also a mixed mode failure, and the force curves often tend to zero rather over a long period. This can be classed as toughness dominated, where a crack initiates over a finite area somewhere along the interface. Once initiated it slowly grows, and then semi-plateaus as it decreases minimally over time. It is hypothesized that this plateau is the critical point where enough ice which has been removed from the substrate, due to the interfacial crack, which assists in reducing the friction of the interaction. The ice pillar is still attached to the substrate at various points, as there is still resistance to the applied force, and there may be a stick/slip phenomena at play. There is likely some interaction at the molecular level which is not yet fully understood - ice is a crystalline structure, however before detachment and under force there may be a phase change to a more amorphous state, or perhaps a freezing and refreezing process. It also may the case that lower ice adhesion substrates promote an apparent sliding failure - a violent cohesive fracture will send the mould crashing, whereas at lower ice adhesion values sliding may just be more common. However, as the forces are still well above zero during sliding failures, it is clear there is still some resistance and attachment to the surface. Further analysis and modelling of these states with consideration for other influences such as wetting state and surface chemistry would be needed before a complete conclusion. However the results are a very interesting experimental insight into these phenomena, which could later be utilised to promote low sliding ice adhesion with coatings.

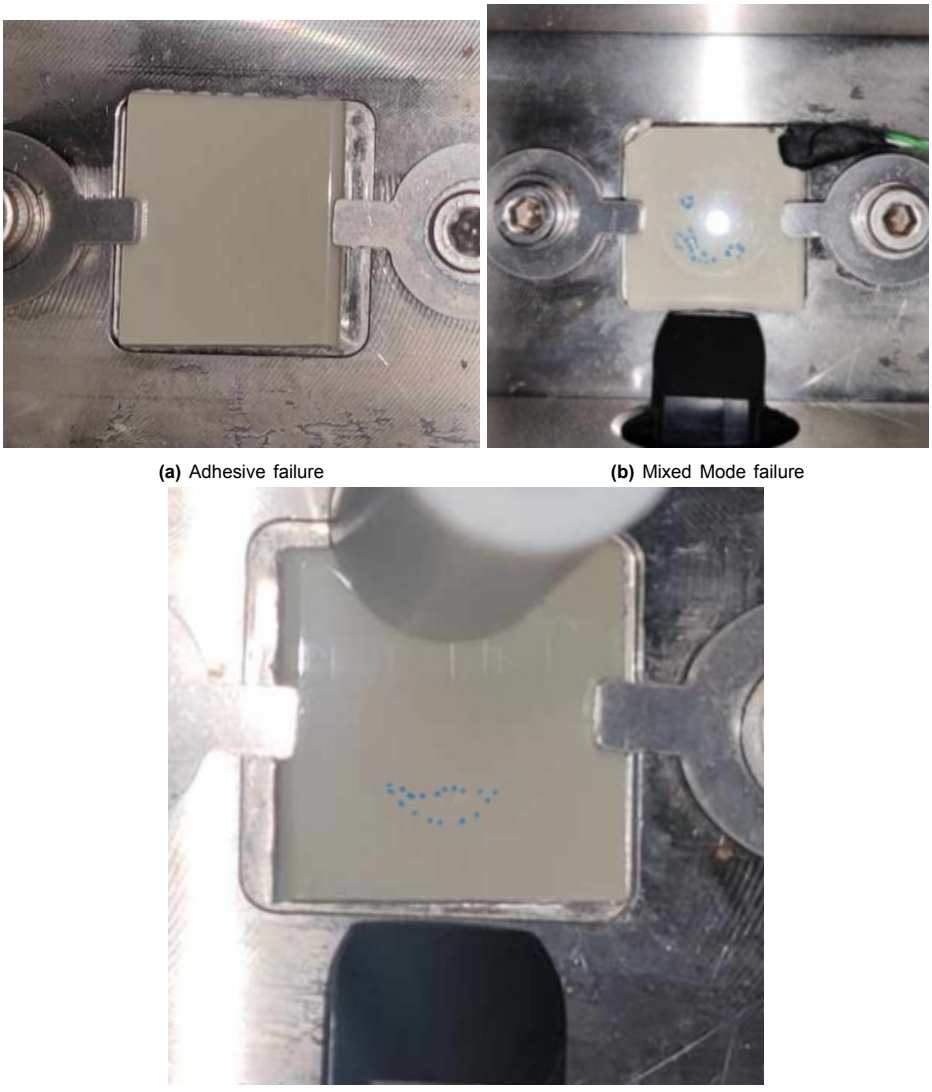

(a) Adhesive failure **(b)** Mixed Mode failure

(c) Sliding failure

Figure 5.15: Fracture surfaces on polypropylene. The blue markings are to indicate where the remaining barely visible ice is approximately left on the surface

5.2.2. Additional Observations

Data on other polymer substrates for comparison is limited, but some observations can be made. The roughness of the polymers are compared, in order to see what effect this has on the ice adhesion strength. The expectation is that ice adhesion strength increases with surface roughness, due to the increased surface area and anchoring points available for the ice to adhere to the substrate.

Table 5.3: Roughness of polymer samples

Material	S_a (μm)
Polypropylene	0.156 ± 0.02
PVC	0.803 ± 0.18
Teflon	1.31 ± 0.39

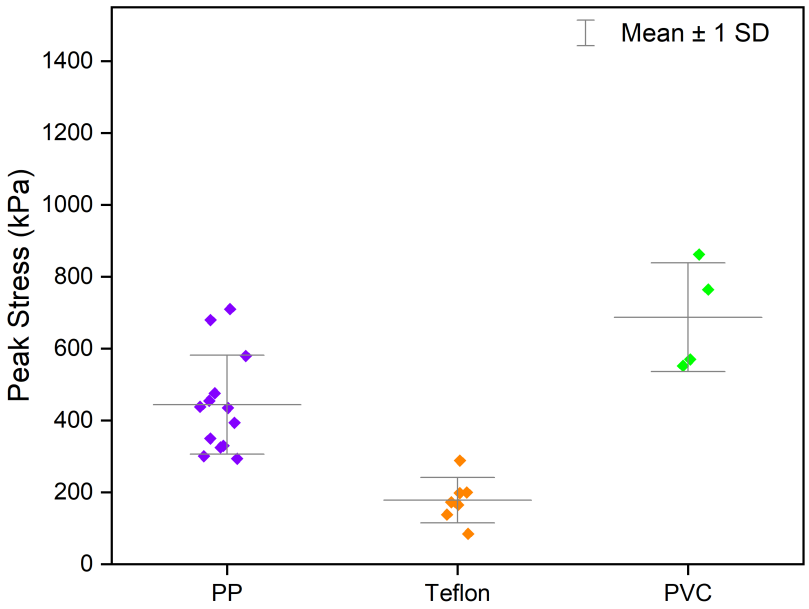

Figure 5.16: Peak stresses of polymers from ice adhesion tests.

Comparing PP and PVC, it is clear that PVC had higher roughness values and higher peak stresses, which agrees with the above analysis that smoother surfaces will reduce ice adhesion strength. The values for Teflon and PVC agree with the typical ranges found in literature [9, 19]. It is worth nothing the issues with comparison using the distribution in Figure 5.16, as it has already been discussed above the effect that crack propagation and rounded force curves has on the interpretation of the data when testing polymers. Additionally, PVC and PP are similar but fundamentally different chemistries, so the effect of that difference in unknown with this simplified analysis. The results for Teflon help to support this idea, as even with the highest roughness, Teflon has the lowest ice adhesion strength. This is largely due to its aggressive surface chemistry, which have a combined effect with the roughness to reduce the surface energy. Aluminum also showed little difference in ice adhesion strength with unpolished surface compared to a polished surface. This shows that while roughness certainly plays a significant role, the surface chemistry is also of the most important substrate characteristics to consider when testing ice adhesion.

With this in mind, a brief note is made on attempts at testing chemically modified surfaces. A bifunctional polymer was spin-coated onto the PVC or PP, and that surface was then exposed to UV which links the bifunctional polymer to the surface. The bifunctional polymer is used as an initiator for a polymerization of a hydrophilic monomer. If the entire surface is exposed to UV, the entire surface becomes a functionalized hydrophilic surface. If a striped mask is used during UV exposure, then only the exposed stripes will grow the hydrophilic polymer, and therefore creating a required pattern. This method allows for the creation of a fully hydrophilic surface or a striped hydrophilic surface on a hydrophobic substrate, which can create a preferential condensation effect as discussed in chapter 1.

Figure 5.17: WCA of 40° on hydrophilic poly-HEMA coating.

In short, almost all of the tests on chemically pattered surfaces failed in some way or another, mainly because of leakages under the mould perimeter. This gives another insight into the operation of the set-up, as it appears from these results that hydrophilic substrates produced more invalid and failed tests due to spills. This is likely because the when the water is injected into the mould, if it does not freeze on impact it will wet the surface as quickly as possible. The more hydrophilic the surface is, the increased wetting, which is likely increasing the probability of the water leaking under the moulds before freezing. The WCA of 40° for the hydrophilic poly-HEMA is shown in the Figure 5.17. The moulds were modified to be more hydrophobic to help mitigate this issue; however it may be the cases that this is actually promoting wetting underneath the mould as the water will preferentially choose the hydrophilic substrate. A simple fix may be to just increase the weight of the alignment block, or test the polymer samples at a lower temperatures so the water column freeze quicker and has less time to spread. Additional testing would be needed to investigate these effects further.

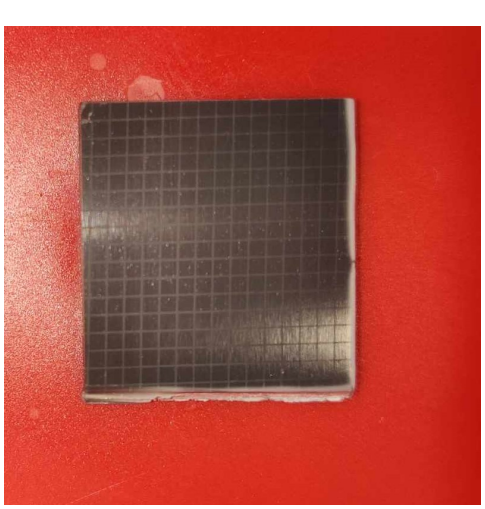

(a) Criss Cross pattern on PVC

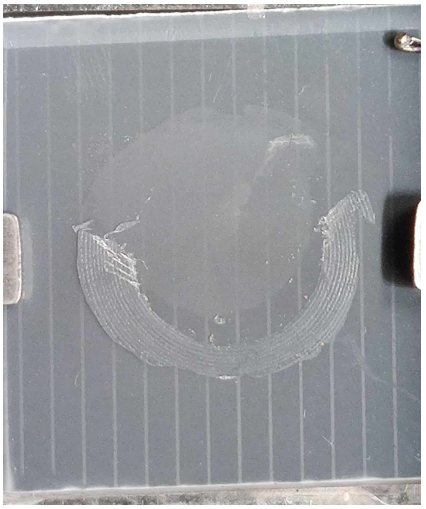

(b) Lined pattern on PVC with failed ice adhesion test

(c) Single striped pattern from ice adhesion tests with frost halo

Figure 5.18: Chemical patterns. The result in (b) is an invalid test and (c) may be an indication of condensation frosting phenomena - frost halo.

6

Conclusion and Recommendations

6.1. Recommendations for future work

The first recommendations for future work will revolve around research which utilises the set-up which was designed and built in this project. The design of the set-up as currently built has definite room for improvement. The natural place to start would be to address the temperature gradient in the set-up. It is hypothesized that this temperature gradient is a function of the design of the cooling block, but also the poor insulation around the chamber. The set-up is semi-insulated with 4mm cork around the housing chamber, however there are significant losses underneath the set-up and on the side of the inlet and outlet. Therefore, better insulation is necessary. The design of the cooling block could be improved, as the linear system with one turn is likely causing some issues. Although the temperature gradient was measured longitudinally, it is anticipated that their is also an effect in the transverse direction. The proposed solution is shown in Figure 6.1, with the recommendation to switch to an S-shaped cooling system to create a more even heat distribution across the testing surfaces.

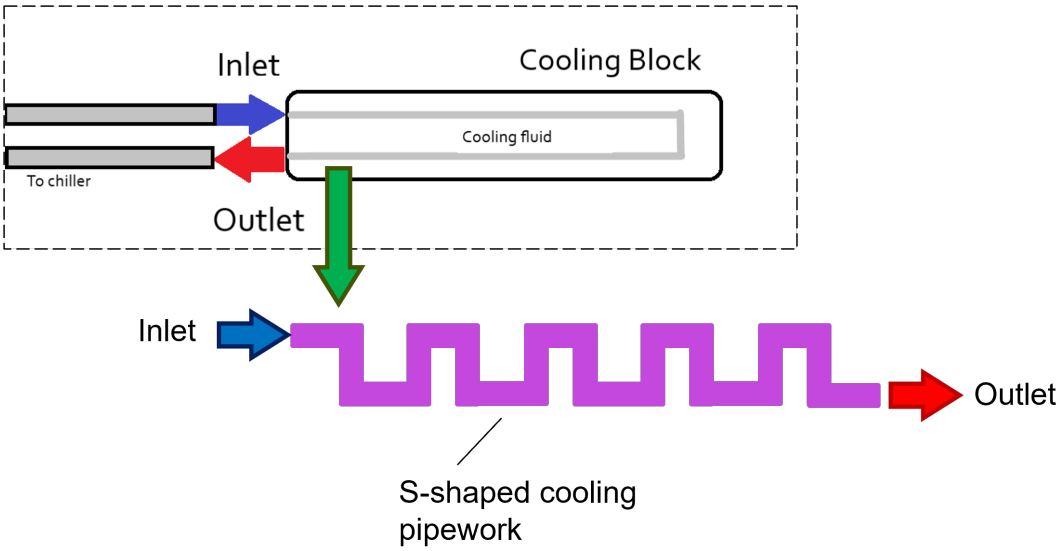

Figure 6.1: Current cooling block design versus recommendation. Proposed cooling solution is to switch to S-shaped cooling block to reduce the temperature variance both longitudinally and transversely

The clamping and framing of the entire set-up could be improved. Simple clamps are holding the scrap frames and set-up in place to prevent the sliding of the set-up as seen in Figure 6.2, which is not ideal. A frame which raises and holds the entire set-up on one platform could work, and this would also allow for insulation underneath the cooling chamber. If well designed, it should be possible to

create a compact, aesthetically pleasing set-up that be used in various locations with a 'plug and play' configuration. The load cell could be replaced with a threaded M6 load cell for a cleaner mechanical connection between the probe and actuator. It may be interesting to run a FEM model on the set-up, to improve the depth of analysis in terms of stress concentrations and the interaction at the mould and pushing probe, and to optimise the set-up parameters further. Additional tests should take place practically on how to optimise the injection procedure, as from anecdotal experience it appears that this may have a strong influence on how the water wets the surface. It may be the case the the speed of injection is also causing spills from time to time.

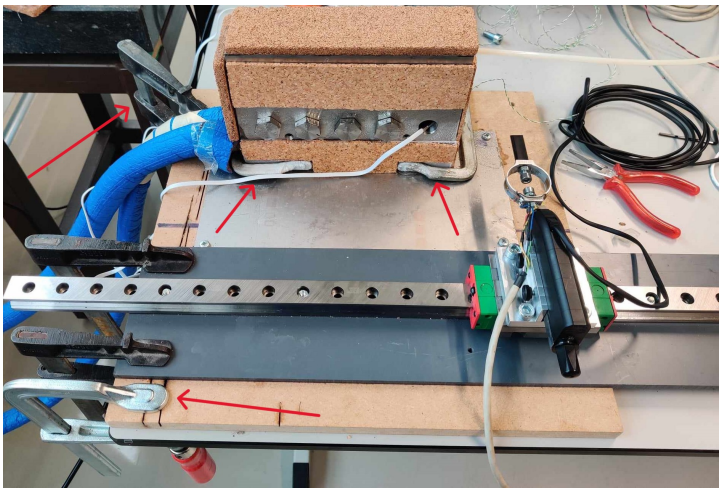

Figure 6.2: Current clamping and framing of set-up. The red arrows indicate the horizontal and vertical clamping solutions

With this set-up, the avenues to explore ice adhesion are plentiful. With the basis of the analysis presented, one could develop a more refined framework to consistently characterize ice adhesion. Once the design of the set-up is further improved, each individual parameter could potentially be explored for its sensitivity to the results influence of ice type and density on ice adhesion mechanics is one avenue to explore, along with perhaps introducing defects or ions into the water itself. Similarly, known defects such as scratches and dust could be introduced onto the testing surface to observe the effects on ice adhesion. The effects of patterned coatings are still on ice adhesion would be interesting to explore, along with the durability of coatings over many icing/deicing cycles. Further modelling on crack initiation and propagation through ice, with experimental verification now perhaps possible, would be of certain interest in this field. The ability to promote ice cracking, or for example sliding, could be a useful functionality if somehow this could implemented into a coating system to cause an interaction at the surface.

6.2. Conclusion

It is clear that accumulation aircraft icing is a significant safety and performance issue that has yet to be solved in aviation. Current solutions such as the application of deicing fluids are a costly and labour intensive form of reactive maintenance, and the approach is not environmentally friendly and provides no protection against ice in flight. A relatively new field of passive 'icephobic' coatings have emerged in the past 15 years, which looks to mitigate this issue by changing the interaction between ice and the aircraft surface to gain control over the ice growth or reduce the ice adhesion strength. However, initial approaches have critical design flaws, so novel strategies such as patterned coatings and surfaces have been developed in order to introduce new interactions at the interface. However, in literature it is often unclear how to best quantify the effectiveness and viability of these coatings against one another. The most straightforward and arguably most important metric to quantify is the ice adhesion strength, which in many cases is equated to the average critical shear stress defined by a simple $\tau_{ave} = F/A$ relationship, with the peak force *F* required to remove the ice from the interfacial area *A* recorded. Attempts at reliably testing the ice adhesion strength in the past have been riddled with issues. The reported scatter of ice adhesion strength on any one material in literature is huge, along with high standard deviations reported, typically anywhere from 10-15% for an excellent result to 30-40 % for an average result. This is partly due to the lack of standardization in ice adhesion testing. Without a known ice adhesion set-up to validate against, many of the approaches can differ significantly in their designs, which impact the validity and confidence in their results. It has been modelled and shown by other studies how sensitive the ice adhesion strength is to testing parameters which are often overlooked in the preliminary design stage, such as the pushing height and mould dimensions in the case of horizontal shear testing. Often the scatter in ice adhesion is deemed to be an 'inherent property' of testing ice. In this work, this idea is challenged, by analysing and unraveling the root causes of outliers in the data.

In order to achieve this, a functional, robust and versatile ice adhesion set-up was designed and built. Focus was placed on the preliminary research and design, with the importance of validation at a later stage influencing the design decisions during the design process. It was found that there are many objectively good and bad designs to test ice adhesion, but often there is a valuable lessons to be learned from analysing the approaches of others. The best features of these various approaches were integrated together as smoothly as possible into one set-up, whilst working within the constraints present and adhering closely to the outlined design requirements. The result was a prototype set-up that worked as designed from the initial testing, with many tweaks and adjustments made to improve the operational procedure as the project progressed.

In order to reliably interpret the results with a known confidence, the set-up was validated against a known set-up with almost identical set-up testing conditions. To achieve this, the data distributions were analysed with respect to the testing parameters. The ability to investigate the effect of the various testing parameters was intentional, and made possible due to the flexible design with validation in mind. It was found that there are a plethora of testing parameters that can have a significant effect on the results, but control of the surface temperature and relative humidity are the most critical. The thorough validation process in this project also outlined significant flaws and potential sources of deviation in the set-up, the largest of which was the temperature gradient across the testing surface. This was likely caused by a poor design choice in terms of the cooling chamber. The discovery was an excellent example of the importance of attention to detail and overall understanding of the set-up as designed and manufactured, including the sources of deviation. Therefore, the motivation for any future design improvements to the set-up can be focused and data-driven, with a clear goal and objective in mind to affect the data in a predicted manner. The ability to change a single parameter or customize an element in the design is a testament to the design process; flexibility was outlined at an early stage in order for the set-up to not too become rigid and over-constrained.

One of the most useful features of the testing procedure is the various sources of data that are collected, which are both qualitative and quantitative. This allows for the investigation and correlation of individual data points in the scatter. With fracture surfaces and force curves for reference, the causation for their location in the spread of data points can be thoroughly analysed, which is an incredibly powerful capability. This was especially interesting for investigation into the outliers in the dataset, as the causation of the outliers could typically be identified from the various data sources. With the

a significant sample size collected, and the explainable outliers removed,the set-up was successfully validated using a singular material AA-6082. With the only one unexplained outlier, the standard deviation with respect to the mean value is %σ = 14%. Removing this one data point for direct comparison with a similar set-up, and the spread tightens and σ reduces to 11%. Considering the high standard deviations in literature often with unexplained data points, and the clear room for improvement in the design of the set-up, this range of 11-14% is considered an excellent result. Not only is the set-up itself validated, but the utility of a well-thought out, thoroughly researched design methodology, and detailed experimental approach is validated for ice adhesion testing.

The preliminary results provided some interesting insights into ice adhesion, so the influence of material and topology on the failure mechanisms were investigated further. Across both aluminum and bare polymer substrates, there were four main failure mechanisms of the ice under quasi-static loading - adhesive failure, cohesive failure, mixed mode adhesive/cohesive failure, and sliding failure. On aluminium, the predominant failure was stress dominated, where the entire ice interface failed instantaneously. This could be in adhesive, mixed mode or cohesive modes, as sliding failures were possible but more prevalent on polymer substrates. It was estimated that for AA-6082, increased % ice area coverage correlates with the ice adhesion strength increased linearly. Mixed mode failures were the most common result, and therefore mixed mode failures typically failed closer the mean peak stress just below 900 kPa. The effect of changing the surface roughness and grain direction on AA-6082, had little effect on the ice adhesion strength, but it was proven that a high humidity set-up will drastically decrease the ice adhesion strength compared to a low humidity set-up, which once again brings into question the validity of results in literature without sufficient humidity control. If these set-ups are used to test and report low ice adhesion coatings surfaces, then the effectiveness and perceived improved results with the coatings will surely be falsely inflated, as the uncoated control material will fail at a deceptively lower peak stress.

It was also shown how in some cases, that despite being a set-up where stress dominated fractures are expected due to the small interface length of the ice, toughness dominated failures with crack propagation are also present and deemed valid results. The testing on polymers provided many examples of toughness dominated failures, with both slow and relatively quickly crack propagation, which shows the importance of analysing the data beyond just the peak force value. Interestingly for polymers, adhesive failures corresponded to tests with higher peak stresses, whereas the mixed mode failures required less force to initiate, which is the opposite to aluminium. Surface chemistry and roughness both contribute to ice adhesion strength on polymers. For chemically modified and patterned surfaces, the hydrophilic nature of the surfaces caused issues with leaking in the set-up, so how they react in terms of ice adhesion strength in still unknown.

To conclude, it is apparent that ice adhesion can be reliably and confidently quantified, provided that the design of the ice adhesion set-up is well-researched, robust and thoroughly validated. By correlating qualitative and quantitative data from various sources, it is possible to explain the mechanisms behind individual data points in a typical scatter plot. In this work, an ice adhesion set-up was successfully designed and validated, so that the preliminary results could be sufficiently analysed. With a reliable set-up now in place, the design can improved further to reduce sources of deviation and improve the consistency in the data. The set-up provides an excellent platform for further research, and the possible avenues of exploration into ice adhesion mechanics and phenomena are plentiful. In terms of ice adhesion testing, this truly is just the tip of the iceberg.

Appendix

Figure 3: 08-02, X4, polished, partial spill

Figure 4: 08-02, X3, polished, partial spill

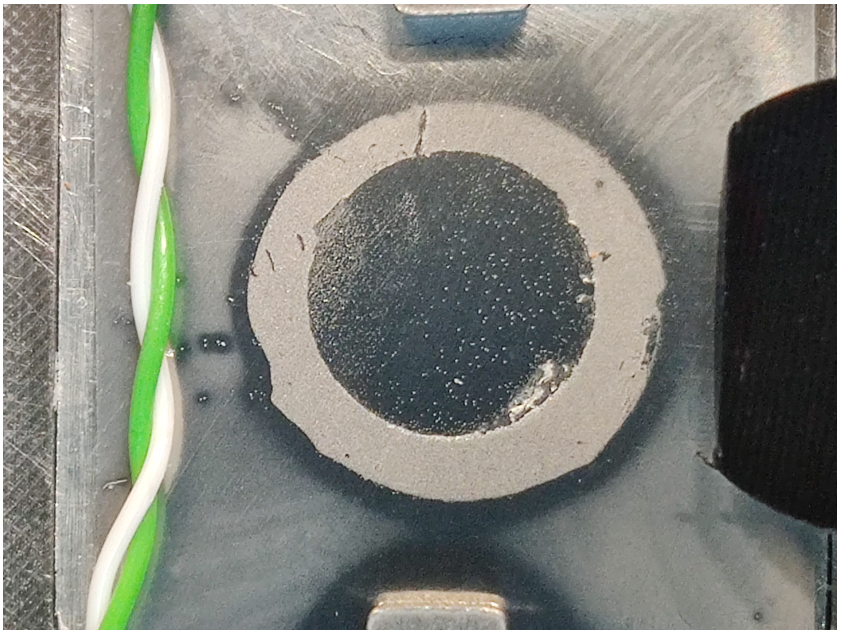

Figure 5: 8th Feb x14 Al polished fracture surface, high adhesion

Figure 6: Spilling under mould, which was a prevalent error on polymer substrates.

Figure 7: Hairline fracture on unpolished AA-608

References

1. Petty, K. & Floyd, C. D. A statistical review of aviation airframe icing accidents in the U.S. *Conference on Aviation, Range, and Aerospace Meteorology,* 623–628 (2004).
2. Cao, Y., Tan, W. & Wu, Z. Aircraft icing: An ongoing threat to aviation safety. *Aerospace Science and Technology* **75,** 353–385 (2018).
3. *In-Flight Icing* 2020. `https://skybrary.aero/articles/flight-icing`.
4. Huang, X. *et al.* A survey of icephobic coatings and their potential use in a hybrid coating/active ice protection system for aerospace applications. *Progress in Aerospace Sciences* **105,** 74–97 (2019).
5. Bharathidasan, T., Kumar, S. V., Bobji, M. S., Chakradhar, R. P. & Basu, B. J. Effect of wettability and surface roughness on ice-adhesion strength of hydrophilic, hydrophobic and superhydrophobic surfaces. *Applied Surface Science* **314,** 241–250 (Sept. 2014).
6. Zhang, J., Gu, C. & Tu, J. Robust Slippery Coating with Superior Corrosion Resistance and Anti-Icing Performance for AZ31B Mg Alloy Protection. *ACS Applied Materials and Interfaces* **9,** 11247–11257 (Mar. 2017).
7. Irajizad, P. *et al.* Stress-localized durable icephobic surfaces. *Materials Horizons* **6,** 758–766 (2019).
8. Boreyko, J. B. *et al.* Controlling condensation and frost growth with chemical micropatterns. *Scientific Reports* **6,** 19131 (2016).
9. Work, A. & Lian, Y. *A critical review of the measurement of ice adhesion to solid substrates* Apr. 2018.
10. Thomas Young. III. An essay on the cohesion of fluids. *Philosophical transactions of the Royal Society of London* **95,** 65–87 (1805).
11. Rame-Hart. *Information on Contact Angle* 2023.
12. Robert N, W. Surface Roughness and Contact Angle. *The Journal of Physical and Colloid Chemistry, 53(9), 1466–1467.* **53,** 1466–1467 (1949).
13. Vladsinger. *Cassie's law* 2023.
14. Lin, Y., Chen, H., Wang, G. & Liu, A. Recent Progress in Preparation and Anti-Icing Applications of Superhydrophobic Coatings. *Coatings* **8,** 208 (May 2018).
15. Rønneberg, S., Zhuo, Y., Laforte, C., He, J. & Zhang, Z. Interlaboratory study of ice adhesion using different techniques. *Coatings* **9** (Oct. 2019).
16. Vincent, A. *et al.* Experimental rig for ice accretion and adhesion strength measurement for air cycle machine system. *Cold Regions Science and Technology* **213** (Sept. 2023).
17. Stendardo, L. *et al.* Reframing ice adhesion mechanisms on a solid surface. *Applied Surface Science* **641** (Dec. 2023).
18. Wang, C., Zhang, W., Siva, A., Tiea, D. & Wynne, K. J. *A laboratory test for ice adhesion strength using commercial instrumentation* tech. rep. (2014).
19. Meuler, A. J. *et al. Relationships between Water Wettability and Ice Adhesion* tech. rep. (2010).
20. Laforte, C. *Icephobic Materials Centrifuge Adhesion Test* tech. rep. (2005).
21. Rønneberg, S., He, J. & Zhang, Z. The need for standards in low ice adhesion surface research: a critical review. *Journal of Adhesion Science and Technology* **34,** 319–347 (Feb. 2020).
22. Li, K. *et al.* Investigating the effects of solid surfaces on Ice nucleation. *Langmuir* **28,** 10749–10754 (July 2012).

23. Nath, S., Ahmadi, S. F. & Boreyko, J. B. *A Review of Condensation Frosting* Apr. 2017.
24. Jin, Y. *et al.* Inhibiting Condensation Freezing on Patterned Polyelectrolyte Coatings. *ACS Nano* **14,** 5000–5007 (Apr. 2020).
25. Wyslouzil, B. E. & Wölk, J. *Overview: Homogeneous nucleation from the vapor phase - The experimental science* Dec. 2016.
26. M, V. & A, W. Keimbildung in übersättigten gebilden. *Z. Phys. Chem., Stoechiom. Verwandtschaftsl* **119,** 277–301 (1926).
27. Varanasi, K. K., Hsu, M., Bhate, N., Yang, W. & Deng, T. Spatial control in the heterogeneous nucleation of water. *Applied Physics Letters* **95** (2009).
28. Varanasi, K. K., Deng, T., Smith, J. D., Hsu, M. & Bhate, N. Frost formation and ice adhesion on superhydrophobic surfaces. *Applied Physics Letters* **97** (Dec. 2010).
29. Kulinich, S. A. & Farzaneh, M. Ice adhesion on super-hydrophobic surfaces. *Applied Surface Science* **255,** 8153–8157 (June 2009).
30. Chen, J. *et al.* Superhydrophobic surfaces cannot reduce ice adhesion. *Applied Physics Letters* **101** (Sept. 2012).
31. Mulroe, M. D., Srijanto, B. R., Ahmadi, S. F., Collier, C. P. & Boreyko, J. B. Tuning Superhydrophobic Nanostructures to Enhance Jumping-Droplet Condensation. *ACS Nano* **11,** 8499–8510 (Aug. 2017).
32. Ensikat, H. J., Ditsche-Kuru, P., Neinhuis, C. & Barthlott, W. Superhydrophobicity in perfection: The outstanding properties of the lotus leaf. *Beilstein Journal of Nanotechnology* **2,** 152–161 (2011).
33. Jung, S., Tiwari, M. K. & Poulikakos, D. Frost halos from supercooled water droplets. *Proceedings of the National Academy of Sciences* **109,** 16073–16078 (2012).
34. Ahmadi, S. & Boreyko, J. B. in *Ice Adhesion: Mechanism, Measurement and Mitigation* 111–134 (Wiley, 2020).
35. Murphy, D. M. & Koop, T. *Review of the vapour pressures of ice and supercooled water for atmospheric applications* 2005.
36. Dooley, J. B. *Determination and Characterization of ice propagation mechanisms on surfaces undergoing dropwise condensation: A dissertation* PhD thesis (Texas A&M University, May 2010).
37. Nath, S., Ahmadi, S. & Boreyko, J. B. How Ice Bridges the Gap. *Soft Matter* **16** (2019).
38. Nath, S. & Boreyko, J. B. On Localized Vapor Pressure Gradients Governing Condensation and Frost Phenomena. *Langmuir* **32,** 8350–8365 (Aug. 2016).
39. Guadarrama-Cetina, J., Mongruel, A., González-Viñas, W. & Beysens, D. Frost formation with salt. *EPL* **110** (June 2015).
40. Yang, S. *et al.* Research on the icephobic properties of fluoropolymer-based materials. *Applied Surface Science* **257,** 4956–4962 (Mar. 2011).
41. Lohmann, R. *et al.* Are Fluoropolymers Really of Low Concern for Human and Environmental Health and Separate from Other PFAS? *Environmental Science and Technology* **54,** 12820–12828 (Oct. 2020).
42. Shen, Y. *et al.* Icephobic materials: Fundamentals, performance evaluation, and applications. *Progress in Materials Science* **103,** 509–557 (2019).
43. Parker, A. R. & Lawrence, C. R. Water capture by a desert beetle. *Nature* **414,** 33–34 (2001).
44. Liu, K., Du, J., Wu, J. & Jiang, L. Superhydrophobic gecko feet with high adhesive forces towards water and their bio-inspired materials. *Nanoscale* **4,** 768–772 (Feb. 2012).
45. Wood, M. J., Brock, G. & Kietzig, A. M. The penguin feather as inspiration for anti-icing surfaces. *Cold Regions Science and Technology* **213** (Sept. 2023).
46. Wood, M. J., Brock, G., Servio, P. & Kietzig, A. M. Leveraging Solidification Dynamics to Design Robust Ice-Shedding Surfaces. *ACS Applied Materials and Interfaces* **14,** 38379–38387 (Aug. 2022).

47. Hu, Z. *et al.* Regulating water adhesion on superhydrophobic TiO2 nanotube arrays. *Advanced Functional Materials* **24,** 6381–6388 (Oct. 2014).
48. Tian, J., Zhang, Y., Zhu, J., Yang, Z. & Gao, X. Robust nonsticky superhydrophobicity by the tapering of aligned ZnO nanorods. *ChemPhysChem* **15,** 858–861 (Apr. 2014).
49. Lai, Y. *et al.* Designing superhydrophobic porous nanostructures with tunable water adhesion. *Advanced Materials* **21,** 3799–3803 (2009).
50. Cui, W., Jiang, Y., Mielonen, K. & Pakkanen, T. A. The verification of icephobic performance on biomimetic superhydrophobic surfaces and the effect of wettability and surface energy. *Applied Surface Science* **466,** 503–514 (Feb. 2019).
51. Wong, T. S. *et al.* Bioinspired self-repairing slippery surfaces with pressure-stable omniphobicity. *Nature* **477,** 443–447 (Sept. 2011).
52. Heydarian, S., Jafari, R. & Momen, G. *Recent progress in the anti-icing performance of slippery liquid-infused surfaces* Feb. 2021.
53. Yeong, Y. H., Wang, C., Wynne, K. J. & Gupta, M. C. Oil-infused superhydrophobic silicone material for low ice adhesion with long-term infusion stability. *ACS Applied Materials and Interfaces* **8,** 32050–32059 (Nov. 2016).
54. Koop, T., Beiping, L., Athanasios, T. & Thomas, P. Water activity as the determinant for homogenous ice nucleation in aqueous solutions. *Nature* **406,** 611–614 (2000).
55. He, Z. *et al.* Tuning ice nucleation with counterions on polyelectrolyte brush surfaces. *Science Advances* **2.** ISSN: 23752548 (June 2016).
56. Peppou-Chapman, S., Hong, J. K., Waterhouse, A. & Neto, C. Life and death of liquid-infused surfaces: a review on the choice, analysis and fate of the infused liquid layer. *Chemical Society Reviews* **49,** 3688–3715 (2020).
57. Liu, B. *et al. Strategies for anti-icing: Low surface energy or liquid-infused?* 2016.
58. Wang, C., Fuller, T., Zhang, W. & Wynne, K. J. Thickness dependence of ice removal stress for a polydimethylsiloxane nanocomposite: Sylgard 184. *Langmuir* **30,** 12819–12826 (Nov. 2014).
59. Golovin, K. *et al.* Designing durable icephobic surfaces. *Science Advances* **2** (Mar. 2016).
60. Chaudhury, M. K. & Kim, K. H. Shear-induced adhesive failure of a rigid slab in contact with a thin confined film. *European Physical Journal E* **23,** 175–183 (June 2007).
61. Zeng, X. *et al.* Inspired by Stenocara Beetles: From Water Collection to High-Efficiency Water-in-Oil Emulsion Separation. *ACS Nano* **11,** 760–769 (Jan. 2017).
62. Ahmadi, S. F. *et al.* Passive Antifrosting Surfaces Using Microscopic Ice Patterns. *ACS Applied Materials & Interfaces* **10,** 32874–32884 (Sept. 2018).
63. Zuo, Z., Zhao, Y., Li, K., Zhang, H. & Yang, C. Suppressing condensation frosting using micropatterned ice walls. *Applied Thermal Engineering* **224** (Apr. 2023).
64. Fortin, G., Beisswenger, A. & Perron, J. *Centrifuge adhesion tests to evaluate icephobic coatings* in *AIAA Atmospheric and Space Environments Conference 2010* (2010).
65. Biro, R. A. *An examination of the anti-icing mechanisms of charged polymer coatings* tech. rep. (DTU Chemistry, 2022).
66. Chen, D., Gelenter, M. D., Hong, M., Cohen, R. E. & McKinley, G. H. Icephobic surfaces induced by interfacial nonfrozen water. *ACS Applied Materials and Interfaces* **9,** 4202–4214 (Feb. 2017).
67. Bleszynski, M. & Clark, E. Current Ice Adhesion Testing Methods and the Need for a Standard: A Concise Review. *Standards* **1,** 117–133 (Nov. 2021).
68. Golovin, K., Dhyani, A., Thouless, M. D. & Tuteja, A. *Low-interfacial toughness materials for effective large-scale deicing* tech. rep. (2019), 371–375.
69. Huré, M., Olivier, P. & Garcia, J. Effect of Cassie-Baxter versus Wenzel states on ice adhesion: A fracture toughness approach. *Cold Regions Science and Technology* **194** (Feb. 2022).
70. Zou, M. *et al.* Effects of surface roughness and energy on ice adhesion strength. *Applied Surface Science* **257,** 3786–3792 (Feb. 2011).

71. Dou, R. *et al.* Anti-icing Coating with an Aqueous Lubricating Layer. *ACS Applied Materials & Interfaces* **6,** 6998–7003 (May 2014).

72. He, Z., Vågenes, E. T., Delabahan, C., He, J. & Zhang, Z. Room Temperature Characteristics of Polymer-Based Low Ice Adhesion Surfaces. *Scientific Reports* **7** (Feb. 2017).

73. Wang, F. *et al.* Dynamic Anti-Icing Surfaces (DAIS). *Advanced Science* **8,** 2101163 (Nov. 2021).

74. Atman, C. J. *et al. Engineering design processes: A comparison of students and expert practitioners* in *Journal of Engineering Education* **96** (Wiley-Blackwell Publishing Ltd, 2007), 359–379.